Balanced Microwave Transmission Lines, Circuits, and Sensors

FERRAN MARTIN [1] **(Fellow, IEEE) AND FRANCISCO MEDINA** [2] **(Fellow, IEEE)**

(Invited Paper)

[1]CIMITEC, Departament d'Enginyeria Electrònica, Universitat Autònoma de Barcelona, 08193 Bellaterra, Spain
[2]Departamento de Electrónica y Electromagnetismo, Facultad de Física, Universidad de Sevilla, 41012 Sevilla, Spain

CORRESPONDING AUTHOR: Ferran Martín (e-mail: Ferran.Martin@uab.cat).

ABSTRACT This paper provides an overview of balanced (or differential-mode) structures operating at microwaves, including common-mode suppression filters, balanced filters and circuits with intrinsic common-mode suppression, and differential-mode sensors. The increasing interest for balanced structures within the framework of communication circuits and sensors, related to their major robustness against electromagnetic interference (EMI), noise, and environmental factors, is duly justified. Then the paper reports various approaches for the implementation of common-mode suppression filters, balanced filters and circuits (including narrowband and wideband filters, multi-band filters, power dividers, couplers and phase shifters), and differential-mode sensors (mainly devoted to the measurement of permittivity and related variables). Rather than providing a detailed analysis of the different considered implementations/approaches, the main goal of this review paper is to discuss, and compare in some cases, the main proposed strategies (pointed out in the up-to-date state-of-the-art) for optimizing the performance of the various differential-mode devices under study.

INDEX TERMS Absorptive common-mode filters, balanced circuits, balanced couplers, balanced microwave filters, balanced phase shifters, balanced power dividers, common-mode rejection ratio (CMRR), common-mode suppression, differential transmission lines, differential-mode sensors, even and odd mode, microstrip technology, MTT 70th Anniversary Special Issue, reflection-less filters.

I. INTRODUCTION

Balanced, or differential-mode, transmission lines, microwave circuits, and sensors have been the subject of an intensive research activity in recent years. Traditionally, balanced structures have been applied to the implementation of low-frequency analog systems and high-speed digital systems. The reason is that, as compared to single-ended (unbalanced) signals, differential-mode signals are robust against electromagnetic interference (EMI), noise, and crosstalk [1], [2], [3], [4], [5], [6]. Consequently, differential systems inherently provide good signal integrity and signal-to-noise ratio (SNR), as compared to the single-ended counterparts. Nevertheless, the implementation of differential-mode structures requires the

design and fabrication of balanced interconnects (transmission lines) and circuits, and this is not absent of a certain level of complexity. This explains that unbalanced circuits have dominated the design of RF and microwave communication systems for decades. However, with the recent technological advances, balanced structures and systems are progressively penetrating the RF/microwave area [7], [8], [9], and this justifies the huge activity of research in the field of balanced microwave circuits and systems in recent years (see [10] and references therein).

Despite the inherent advantages of balanced circuits over their single-ended counterparts, perfect balance cannot be achieved in real systems. Therefore, differential-mode to

common-mode conversion (i.e., cross-mode coupling) is unavoidable in practice, and constitutes a source of radiation and EMI problems in differential systems, that may degrade the integrity of the differential signals. Thus, the design of differential transmission lines and circuits with intrinsic common-mode suppression, yet keeping the integrity of the differential mode, are highly demanded. Within the framework of balanced microwave circuits, the main research effort has been focused on the design of differential filters with intrinsic common-mode suppression, where topologies that generate a differential-mode passband (or passbands, in multiband structures) with simultaneous common-mode rejection within that/those band/s have been reported [10]. This topic constitutes a significant part of the present review paper. Nevertheless, we also include a review of the so-called common-mode rejection filters, where typically, although not exclusively, defected ground structures (DGS), conveniently disposed in the ground plane and transparent to differential-mode signals, are applied to suppress the common mode in differential lines. With regard to balanced circuits, this paper also discusses some other devices, in particular, power dividers, couplers and phase shifters.

Concerning sensors, despite the fact that optical technologies dominate the market, microwaves exhibit a series of benefits that make microwave sensors, and specifically wireless sensors and radiofrequency identification (RFID) sensors, an enabling technology for the so-called Internet of Things (IoT) (see [11] and references therein). Among such advantages, microwaves are very sensitive to the dielectric properties of the medium to which they interact. Therefore, microwave sensors are canonical permittivity sensors. However, as far as the permittivity of a material correlates with many other variables, such as humidity, temperature, material composition, etc., microwave sensors can be applied to many diverse scenarios. Of special interest are the so-called planar microwave sensors [11], due to their low cost and profile, as well as to their compatibility with both additive (e.g., screen- or inkjet-printing) and subtractive (e.g., photoetching) fabrication processes. Moreover, planar sensors can be fabricated not only on rigid materials (e.g., commercial microwave substrates), but also by using flexible substrates, including polymers and organic substrates, such as paper. This opens the possibility of implementing conformal sensors, as well as environmentally friendly (green) sensors. Additionally, planar sensors are compatible with other technologies of interest for sensing, such as microfluidics (for liquid sensing) [12], textiles (for wearables) [13], micromachining, etc., and the associated electronics needed for signal generation, post-processing, and, eventually, communication purposes, can be integrated within the sensor substrate (thereby representing a cost reduction).

Most reported planar microwave sensors are single-ended structures, operating either in reflective- or in transmission-mode, and most of them are resonant [11], [14]. Their working principle is the variation in the resonance frequency and quality factor, or magnitude, of the notch, or peak, generated in a transmission line based structure loaded with at least one resonant element, when the resonator/s is/are under the influence of the so-called material under test (MUT). Nevertheless, resonant sensors that exploit the phase (rather than the frequency) variation of a resonator loaded, or terminated, line have also been reported [11], [15], [16]. The main limitation of these single-ended sensors (regardless on whether the output variable is either a frequency or a phase) is their cross-sensitivity to environmental factors (mainly temperature and humidity). Although more complex, differential-mode sensors constitute a solution to such problem, since environmental factors are seen as common-mode stimuli at the typical scales of the sensors (few centimeters or even less). Thus, a significant effort has been dedicated in recent years to investigate differential-mode structures useful for sensing [11], [17], and some of the reported implementations are reviewed in this paper.

The paper is organized as follows. Section II briefly presents the fundamentals of balanced transmission lines, and introduces the mixed-mode S-parameters. Section III is focused on the different approaches for the implementation of common-mode suppression filters. Balanced filters with intrinsic common-mode noise suppression, including narrowband, wideband and multiband differential-mode responses, are the subject of Section IV. In Section V, other balanced circuits are reported. The topic of differential-mode sensors is treated in Section VI. Finally, Section VII highlights the main conclusions of the work.

II. FUNDAMENTALS OF BALANCED TRANSMISSION LINES
A. TOPOLOGIES AND FUNDAMENTAL PROPAGATING MODES

In unbalanced transmission lines, one of the two conductors (or wires) is connected to the common ground, and the (single-ended) signal is referenced to that ground [see Fig. 1(a)]. In such lines, the conductors are fed by single-ended ports, in which there is an active terminal and a ground terminal (that is, one of the conductors is fed, whereas the other one is tied to ground potential) [11], [18]. Thus, one conductor transports the signal current and the other conductor, considered as reference, is the return current path. A microstrip transmission line [Fig. 2(a)] is a good example of a single-ended (unbalanced) line.

Differential, or balanced, transmission lines can be implemented by means of two or three conductors (wires), as depicted in Fig. 1(b) and (c), respectively. Coplanar strips [Fig. 2(b)] or slotlines are examples of two-wire balanced lines, whereas symmetric microstrip coupled lines [Fig. 2(c)] constitute a representative (and exhaustively used) type of three-wire differential transmission lines. In two-wire balanced lines, the signal in one line is referenced to the other. The conductors exhibit equal potential and impedance with respect to (the virtual) ground with 180° phase shift (balanced lines carry balanced currents). Nevertheless, it should be mentioned that the nature (balanced or unbalanced) of
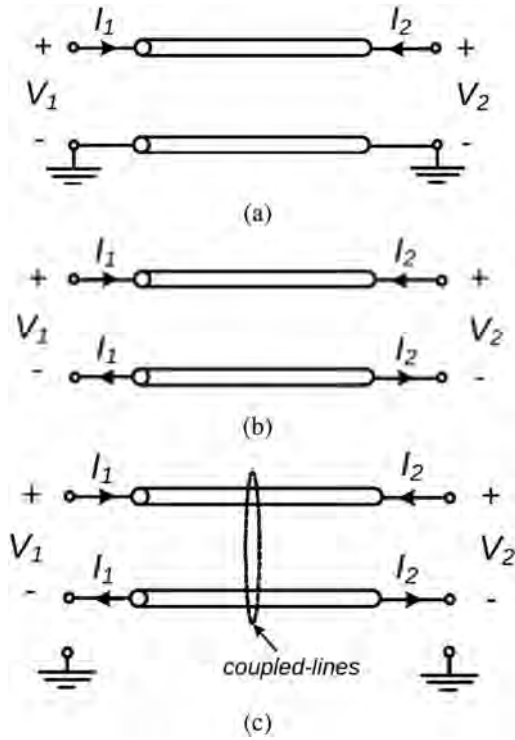
FIGURE 1. Schematic of a two-wire unbalanced line (a), two-wire balanced line (b) and three-wire balanced line (c). In (c) the coupling between the lines is not a requisite.
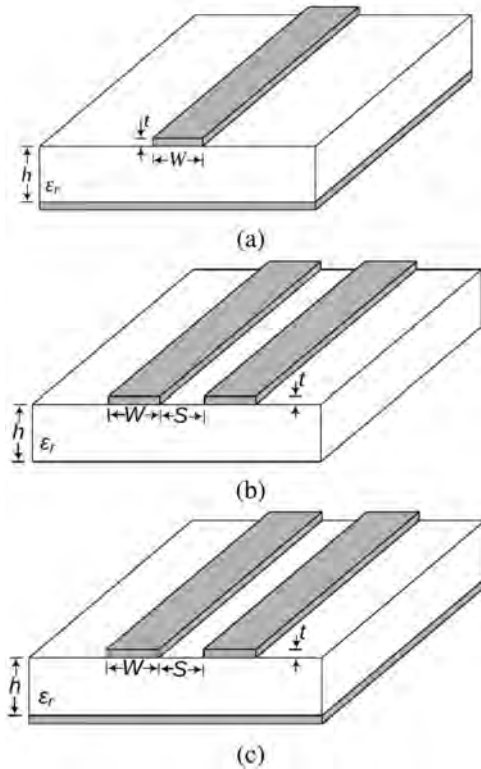

FIGURE 2. Examples of unbalanced and balanced lines. (a) Unbalanced microstrip line. (b) two-wire balanced transmission line consisting of coplanar strips (CPS). (c) three-wire balanced line based on microstrip coupled lines.

a two-wire transmission line is determined by the type of feeding (balanced or unbalanced), rather than by the physical structure [18].

Most reported balanced transmission lines include a third conductor acting as a ground plane (three-wire transmission lines), and the canonical implementation is the one depicted in Fig. 2(c), a pair of identical lines on top of a ground plane. Such configuration is usually referred to as microstrip coupled lines, though for the implementation of differential-mode transmission lines, electromagnetic coupling between the lines is not a requisite. Under perfect balance, the active conductors carry identical and opposite currents, since the impedance of each line to ground is identical. However, if the lines are not identical (line unbalance), the presence of the ground plane may unbalance the currents in the conductors.

Three-wire balanced lines (the most extensively used, due to the presence of the ground plane) support two fundamental propagating modes: the balanced (or differential) mode and the unbalanced (or common) mode (by contrast, two-wire balanced lines do not support the unbalanced mode). The differential mode is the fundamental mode in balanced lines, and it is an odd-type mode (according to the definition of such mode within the framework of electromagnetic symmetry properties), where the symmetry plane is an electric wall (and a virtual ground) [19], [20], [21]. By contrast, the symmetry plane for the common mode is a magnetic wall, and the nature of such mode is even (in the common mode, the active conductors carry identical currents in both magnitude and phase).

B. EVEN/ODD MODES VERSUS COMMON/DIFFERENTIAL MODES

In [11], subtle differences between the even/odd modes and the common/differential modes in differential lines, related to signal definitions, were pointed out (nevertheless, along this review paper, we will indistinctly refer to the balanced mode as odd or differential, and to the unbalanced mode as even or common). Fig. 3 depicts the currents and voltages for the odd and even modes in the individual lines of a three-wire transmission line, as well as their excitation by means of single-ended ports. The odd and even voltages are defined as [20],

$$V_o = \frac{1}{2}(V_1 - V_2) \tag{1a}$$

$$V_e = \frac{1}{2}(V_1 + V_2) \tag{1b}$$

whereas the odd and even currents are

$$I_o = \frac{1}{2}(I_1 - I_2) \tag{2a}$$
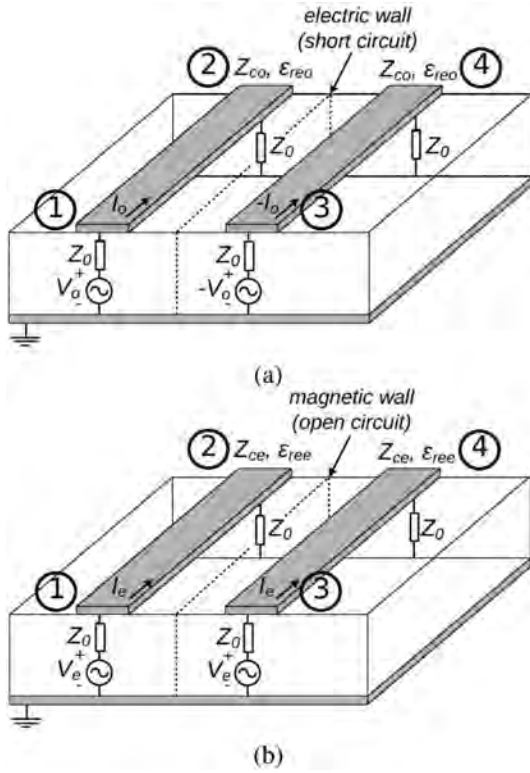
$$I_e = \frac{1}{2}(I_1 + I_2) \tag{2b}$$

FIGURE 3. Voltages and currents in a balanced line and generation of the odd (a) and even (b) modes. The single ended ports are indicated.

FIGURE 4. Voltages and currents in a balanced line and generation of the differential (a) and common (b) modes.

In expressions (1) and (2), V_1 (V_2) and I_1 (I_2) are the voltage and current, respectively, in line 1 (line 2) of the differential pair. Note that these voltages and currents are not those of Fig. 1, which refer to the ports, rather than to the lines. For a pure odd mode, it follows that $V_o = V_1 = -V_2$, $V_e = 0$, $I_o = I_1 = -I_2$, and $I_e = 0$, whereas $V_e = V_1 = V_2$, $V_o = 0$, $I_e = I_1 = I_2$, and $I_o = 0$ for the even mode. The characteristic impedances for the odd and even modes are

$$Z_{co} = \frac{V_o}{I_o} \tag{3a}$$

and

$$Z_{ce} = \frac{V_e}{I_e} \tag{3b}$$

respectively. If the lines are uncoupled, both impedances are identical, and coincide with the characteristic impedance of the isolated line.

The differential and common modes are indeed equivalent to the odd and even modes, respectively, the unique difference being related to signal definitions. That is, in the differential and common modes, it is considered that the two (input) single-ended ports are driven as a pair, called composite port [8], which can be decomposed in its differential and common mode portions [7] (see, Fig. 4). The differential voltage is defined as [7]
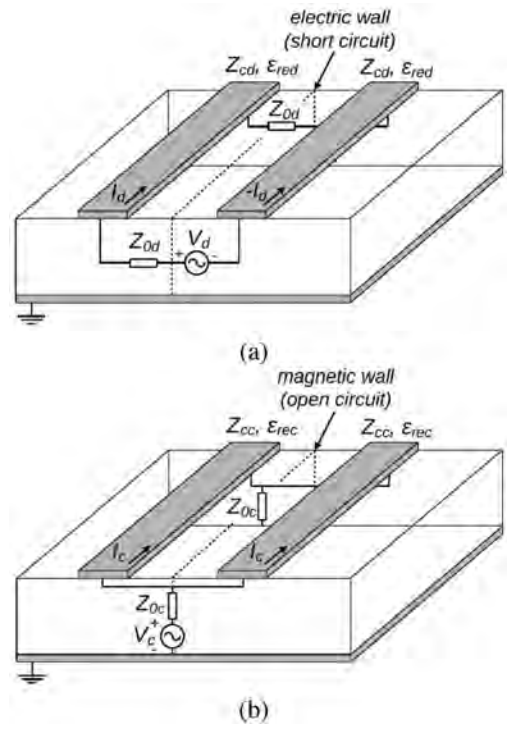
$$V_d = V_1 - V_2 \tag{4}$$

whereas the differential current is

$$I_d = \frac{1}{2}(I_1 - I_2) \tag{5}$$

Note that these are the natural definitions of the differential voltage and current, according to Fig. 4(a), since it is expected that the differential driving voltage source, V_d, generates identical currents of opposite signs in the single-ended ports. According to Fig. 4(b), the common-mode source will generate in-phase (identical) currents at both single-ended ports. Thus, in this case, the common-mode current is defined as

$$I_c = I_1 + I_2 \tag{6}$$

corresponding to the total current flowing in the lines, whereas the common-mode voltage is the average between the voltages in the lines, i.e.,

$$V_c = \frac{1}{2}(V_1 + V_2) \tag{7}$$

According to the previous definitions of voltages and currents for the even/odd modes and common/differential modes, the following relationships are found

$$V_d = 2V_o \tag{8a}$$

$$I_d = I_o \tag{8b}$$

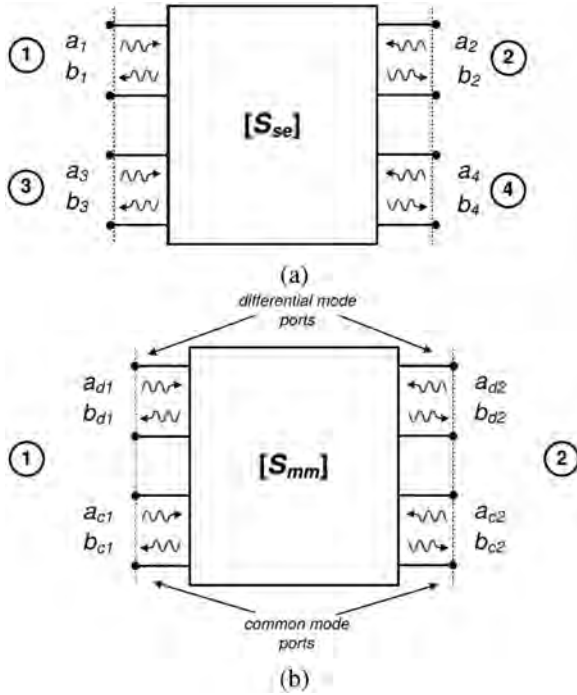$$V_c = V_e \tag{8c}$$

$$I_c = 2I_e \tag{8d}$$

FIGURE 5. (a) Single-ended four-port circuit described by the single-ended S-parameter matrix, and indication of the positive (a_i) and negative (b_i) normalized (single-ended) voltage waves. (b) conceptual diagram of the mixed-mode S-parameters in a differential two-port network, with indication of the normalized common-mode positive (a_{ci}), differential-mode positive (a_{di}), common-mode negative (b_{ci}), and differential-mode negative (b_{di}) voltage waves (b). The sub-index i indicates the port number.

The characteristic impedances of the odd and even modes are related to those of the differential (Z_{cd}) and common (Z_{cc}) modes according to

$$Z_{cd} = 2Z_{co} \qquad (9a)$$

$$Z_{cc} = Z_{ce}/2 \qquad (9b)$$

It is thus clear that the even/odd modes are equivalent to the common/differential modes. That is, an even-mode signal propagating in a line pair cannot be distinguished from a common-mode signal, and the same applies to an odd-/differential mode (the only difference concerns how the voltages and currents, and consequently the characteristic impedances, for the modes have been defined, as indicated before).

C. MIXED-MODE S-PARAMETERS

Three-wire balanced transmission lines can be described by standard (single-ended) order-4 S-parameter matrices [21], see Fig. 5(a). Nevertheless circuits that support the simultaneous propagation of differential and common modes (mixed-mode propagation), either balanced or not, are preferably

described by the so-called mixed-mode S-parameter matrix [7], [8], [11], [22], [23], i.e.,

$$\begin{pmatrix} b_{d1} \\ b_{d2} \\ b_{c1} \\ b_{c2} \end{pmatrix} = \begin{pmatrix} S_{11}^{dd} & S_{12}^{dd} & S_{11}^{dc} & S_{12}^{dc} \\ S_{21}^{dd} & S_{22}^{dd} & S_{21}^{dc} & S_{22}^{dc} \\ S_{11}^{cd} & S_{12}^{cd} & S_{11}^{cc} & S_{12}^{cc} \\ S_{21}^{cd} & S_{22}^{cd} & S_{21}^{cc} & S_{22}^{cc} \end{pmatrix} \begin{pmatrix} a_{d1} \\ a_{d2} \\ a_{c1} \\ a_{c2} \end{pmatrix} \qquad (10)$$

where it has been considered that the pairs of single-ended ports 1-3 and 2-4 are driven as pairs, i.e., as differential and common mode ports. This gives the conceptual diagram of mixed-mode S-parameters shown in Fig. 5(b). Note, however, that the four ports of Fig. 5(b) are conceptual tools only, rather than physically separated ports. The left- and right-hand side column vectors are the positive and negative, respectively, voltages waves at the composite ports 1 and 2 [see Fig. 5(b)], and the sub-index "d" or "c" is used to differentiate the differential and common modes. Such order-4 mixed mode S-parameter matrix, typically designated as $\mathbf{S}_{mm}$, can be expressed as [7], [8], [11]

$$\mathbf{S}_{mm} = \begin{pmatrix} \mathbf{S}^{dd} & \mathbf{S}^{dc} \\ \mathbf{S}^{cd} & \mathbf{S}^{cc} \end{pmatrix} \qquad (11)$$

where $\mathbf{S}^{dd}$ is the differential-mode order-2 S-parameter matrix, $\mathbf{S}^{cc}$ is the common-mode order-2 S-parameter matrix, and $\mathbf{S}^{cd}$ and $\mathbf{S}^{dc}$ are the so-called order-2 mode-conversion, or cross-mode, S-parameter matrices. In perfectly balanced lines, $\mathbf{S}^{dc}$ and $\mathbf{S}^{cd}$ should be null, since mode conversion is not possible under perfect symmetry. However, in real lines, certain level of imbalance is unavoidable and these matrices are not strictly null. On the other hand, in differential-mode sensors, imbalances are generated by the differential input variable, usually the differential permittivity, or difference between the permittivity of the so-called material under test (MUT) and a reference (REF) material, and the cross-mode transmission, S_{21}^{dc}, or reflection, S_{11}^{dc}, coefficients are typical output variables in such sensors [24], [25].

The relationship between the single-ended S-parameters and the mixed-mode S-parameters is [8], [11]:

$$S^{dd} = \frac{1}{2} \begin{pmatrix} S_{11}-S_{13}-S_{31}+S_{33} & S_{12}-S_{14}-S_{32}+S_{34} \\ S_{21}-S_{23}-S_{41}+S_{43} & S_{22}-S_{24}-S_{42}+S_{44} \end{pmatrix}$$
$$(12a)$$

$$S^{cc} = \frac{1}{2} \begin{pmatrix} S_{11}+S_{13}+S_{31}+S_{33} & S_{12}+S_{14}+S_{32}+S_{34} \\ S_{21}+S_{23}+S_{41}+S_{43} & S_{22}+S_{24}+S_{42}+S_{44} \end{pmatrix}$$
$$(12b)$$

$$S^{dc} = \frac{1}{2} \begin{pmatrix} S_{11}+S_{13}-S_{31}-S_{33} & S_{12}+S_{14}-S_{32}-S_{34} \\ S_{21}+S_{23}-S_{41}-S_{43} & S_{22}+S_{24}-S_{42}-S_{44} \end{pmatrix}$$
$$(12c)$$

$$S^{cd} = \frac{1}{2} \begin{pmatrix} S_{11}-S_{13}+S_{31}-S_{33} & S_{12}-S_{14}+S_{32}-S_{34} \\ S_{21}-S_{23}+S_{41}-S_{43} & S_{22}-S_{24}+S_{42}-S_{44} \end{pmatrix}$$
$$(12d)$$

Thus, the mixed mode S-parameters, in particular the differential- and common-mode S-parameters, can be inferred from the measurement of the single-ended S-parameters.

III. COMMON-MODE SUPPRESSION FILTERS

Common-mode suppression (or bandstop) filters are structures added to balanced lines (generally, although not exclusively, based on defected ground structures – DGS) in order to reject the common mode within a certain frequency band. Despite the fact that most reported implementations of balanced bandpass filters are able to inherently suppress the common mode in the differential-mode passband, the common mode rejection ratio (CMRR) in that band does not always reach the required values to efficiently suppress the common-mode noise. Thus, common-mode rejection filters can be applied to improve the CMRR in balanced bandpass filters by cascading them. Another application of common-mode bandstop filters concerns the suppression of undesired common-mode noise present in balanced lines acting as interconnects for high-speed digital circuits. Such common-mode noise is inevitable due to time-skew or amplitude imbalance between the differential lines, and may degrade the signal integrity and cause EMI emission [26]. Thus, common-mode bandstop filters exhibiting broad stop bands for the common mode, and all-pass responses with low insertion loss for the differential mode (from DC up to frequencies beyond those required in high-speed data transmission), are necessary.

This section succinctly reviews some up-to-date reported implementations of common-mode suppression filters. Most of them are based on DGSs, conveniently designed in order to achieve responses insensitive to the differential mode [27], [28], [29], [30], [31], [32], [33], [34], [35], [36]. Other common-mode rejection filters exploit the inherent rejection properties of periodic structures [37], [38], [39], [40], [41]. There are also approaches based on multilayer or low temperature co-fired ceramic (LTCC) technology [2], [42], [43], [44], [45], [46], [47], [48], [49]. It is shown in this section that glide symmetry can be applied to certain common-mode rejection filters in order to widen the common-mode stopband bandwidth [50]. Recently, common-mode dissipative (absorption) filters, where the power associated to the common mode is absorbed, rather than reflected, have also been reported (see, e.g., [51], [52], [53]). Finally, let us mention that, traditionally, common-mode chokes with high-permeability ferrite cores have been used to mitigate common-mode noise [54], [55], [56]. However, chokes exhibit a limited operating range and do not constitute a good solution in terms of size and cost, as compared to full-planar structures.

The key aspect for a successful common-mode bandstop filter is mode selectivity, that is, the filter must be able to efficiently suppress (either reflect or absorb) the common mode in the widest possible frequency band, and at the same time must be transparent to the differential mode. Certain (symmetric) planar resonators are useful for achieving mode suppression selectivity. Thus, let us next discuss this aspect, and then let
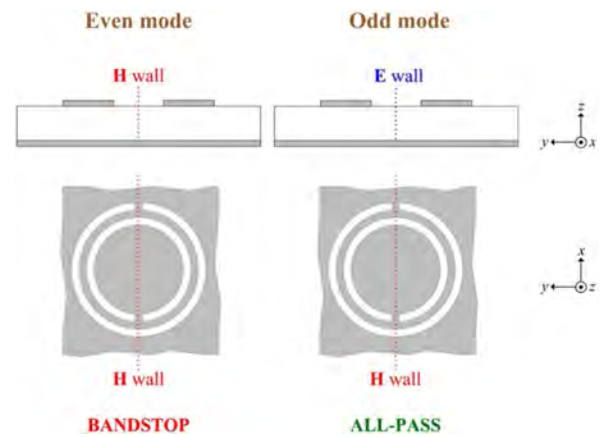

FIGURE 6. Illustration of selective mode suppression in microstrip differential lines by using CSRRs (etched in the ground plane). Note that bandstop and all-pass is in reference to a region in the vicinity of the fundamental CSRR resonance (further stop bands may appear for both modes at higher frequencies).

us report different considered strategies/implementations of common-mode bandstop filters.

A. SELECTIVE MODE SUPPRESSION

Selective mode suppression in balanced lines can be achieved by symmetrically loading the line with a planar resonant element, either a metallic or a slot (or DGS-based) resonator [32], [57], [58], [59], [60].

The key aspect for achieving selective mode suppression is the electromagnetic nature (either a magnetic or an electric wall) of the symmetry plane of the resonant element at the considered resonance frequency (typically the fundamental one). The axial symmetry plane of a balanced line is an electric wall for the differential mode and a magnetic wall for the common mode. Thus, it follows that by symmetrically loading the line pair with a resonant element exhibiting a magnetic wall at resonance, the common mode should be suppressed [57], [58] in the vicinity of that frequency, whereas the line should be transparent for the differential mode, provided both symmetry planes (the one of the line and the one of the resonator) are perfectly aligned. By contrast, if the considered resonator exhibits an electric wall at the considered resonance frequency, the line exhibits a stopband response for the differential mode and an all-pass response for the common mode (though this case lacks practical interest).

Among those planar resonant elements exhibiting a magnetic wall at the fundamental resonance, the complementary split ring resonator (CSRR), first reported in [61], and the dumbbell defect ground structure (DB-DGS) resonator [62] (including the folded version), are good examples. As it will be shown in the next subsection, these resonators have been used as efficient common-mode bandstop filters, since reasonable stopband bandwidths can be achieved by conveniently tailoring their topology. Fig. 6 illustrates the principle of (selective) common-mode suppression by considering a pair of balanced microstrip coupled lines loaded with a CSRR. Note

that CSRRs and DB-DGSs are slot resonators that should be etched in the ground plane, beneath the line pair, as depicted in Fig. 6. There are also metallic resonators that exhibit a magnetic wall at the fundamental resonance. For example, the so-called electric-LC (ELC) resonator [63] is a bisymmetric resonator that exhibits both a magnetic and an electric wall (orthogonally oriented) at the fundamental resonance. Thus, the ELC resonator is a potential candidate to suppress the common-mode by etching (or printing) it in the substrate side where the active lines are present. However, this strategy has the penalty of a wide transverse dimension of the line pair, since the metallic resonator should be symmetrically located between the lines of the differential pair.

B. COMMON-MODE FILTERS BASED ON DEFECTED GROUND PLANES

There are many strategies for selectively suppressing the common mode (keeping unaltered the differential mode) by means of slot-based structures etched in the ground plane, in particular, by using symmetric resonators, such as the DB-DGS and the CSRR.

In [27], a common-mode filter based on a differential microstrip line pair loaded with DB-DGS resonators was proposed [see Fig. 7(a)]. Such resonators open the return current path through the ground plane for the common mode, whereas the presence of such resonators has negligible effect on the differential-mode signals, since relatively small current density returns through the ground plane for such signals. Nevertheless, a more convincing explanation of the filtering behavior of such structures for the common mode can be given by taking into account the equivalent circuit model of the unit cell. By assuming that the coupling between adjacent DB-DGS resonators can be neglected, the line pair loaded with a DB-DGS can be described by means of the circuit shown in Fig. 7(b) [64]. In that circuit, L and C are the inductance and the capacitance, respectively, of the line corresponding to the length of the unit cell, L_c and C_c model the DB-DGS resonator, and M accounts for the mutual (magnetic) coupling between the lines and the resonator. Finally, L_m and C_m account for the magnetic and electric coupling, respectively, between the lines.

In view of the circuit model in Fig. 7(b), it is clear that the resonant element is magnetically driven for the common mode, since the lines carry current in the same direction for that mode. Thus, the injected common-mode signals are reflected back to the source in the vicinity of the resonance frequency. By contrast, the current in the lines flow in opposite directions for the differential mode, and the DB-DGS resonator cannot be excited for that mode. Fig. 7(c) depicts the frequency response of the considered DB-DGS-based common-mode filter (see details of the geometry and substrate parameters in [27]), including not only the common mode insertion loss (S_{cc} in the figure, the nomenclature used in the original source [27]), but also the differential mode insertion loss (S_{dd}), as well as the cross-mode insertion loss (S_{cd}). It can be seen that a significant common-mode rejection band in
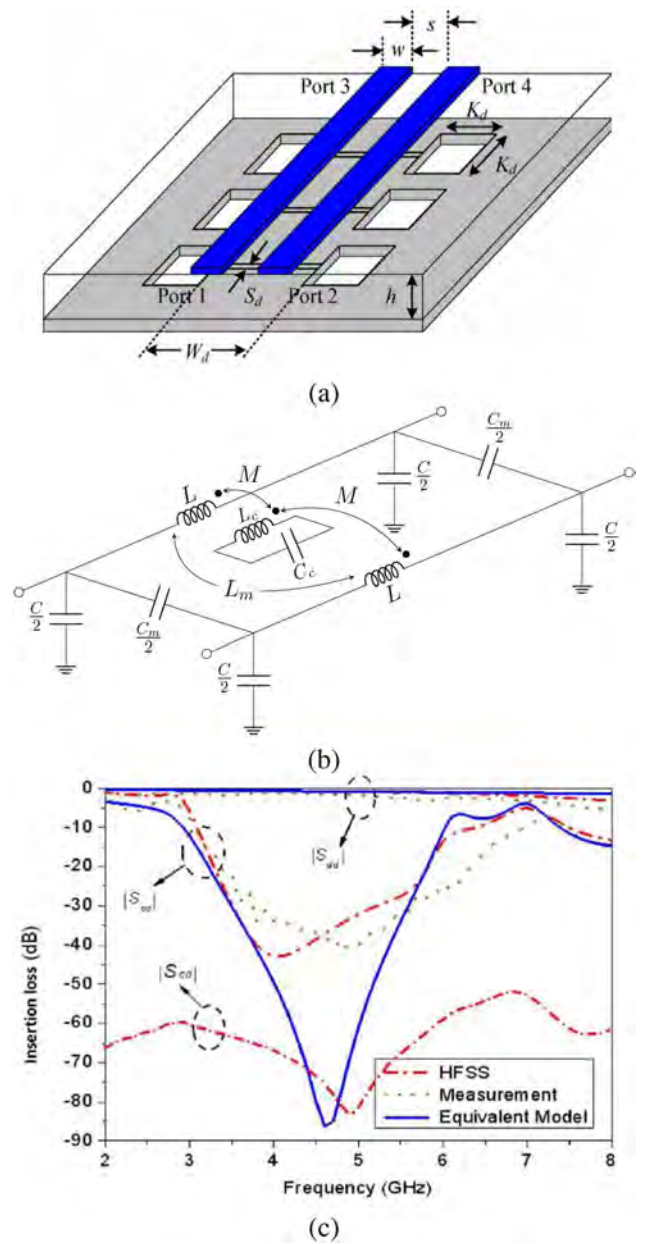

FIGURE 7. Perspective view of a common-mode bandstop filter consisting of a pair of microstrip lines loaded with DB-DGS resonators (a), lumped-element equivalent circuit model of the unit cell (b), and frequency response (insertion loss) (c). Reprinted from [27] with permission.

the vicinity of 4.5 GHz is generated, whereas the insertion loss for the differential mode is close to 0 dB, and mode conversion from the differential to the common mode is very small. In [27], it was demonstrated by means of measured differential eye diagrams that the integrity of the differential signals was preserved, despite the presence of the DB-DGS resonators (common-mode filter). Moreover, it was demonstrated in that paper the potential of the designed DB-DGS structure for the suppression of the common mode by inserting a delay structure in one of the lines, consequently causing a time skew, or line imbalance, and hence differential to common mode conversion.

The use of CSRRs for the implementation of common-mode filters was reported in [29], [30]. The capability of these resonators for the selective rejection of the common mode is clear, according to the illustration of Fig. 6. Nevertheless, the common-mode bandstop filters reported in [29], [30] are based on square-shaped CSRRs. Such geometry favors inter-resonator (electric) coupling, which in turn helps to widen somehow the common-mode rejection band, as reported in [30]. Fig. 8(a) depicts a specific implementation of a common-mode rejection filter based on three CSRRs. The rejection of the common mode in the vicinity of resonance and the transparency of the structure for the differential mode signals is clear in view of the equivalent circuit model of the unit cell, depicted in Fig. 8(b). In that model, L and C are the line inductance and capacitance of the unit cell, L_c and C_c describe the CSRR, L_m and C_m account for the electric and magnetic coupling, respectively, between the lines, C is the coupling capacitance between the lines and the CSRR, and, finally, C_R is the coupling capacitance between adjacent CSRRs. For the common mode, the equivalent circuit is inferred by eliminating half of the circuit, and leaving the resulting terminals open-circuited (equivalent to locating a magnetic wall in the symmetry plane), see Fig. 8(c). The resulting circuit exhibits a stop band in the vicinity of the resonance frequency of the CSRR, magnified by inter-resonator coupling through the generation of complex modes, as reported in [30]. By contrast, the equivalent circuit for the differential mode [see Fig. 8(d)], inferred by short-circuiting to ground the resulting terminals of the symmetry plane after eliminating half of the circuit, is the one corresponding to an ordinary line. Thus, the structure is transparent for the differential mode. Fig. 8(e) and (f) depict the differential-mode and common-mode responses, respectively. The differential mode insertion loss is very small within the considered frequency range, whereas the common mode insertion loss exhibits more than 40 dB rejection in a relatively broad frequency band. Thus, the functionality of this CSRR-based structure as an efficient common-mode bandstop filter is demonstrated. The details of the geometry, substrate parameters, as well as a recipe for the design of such common-mode filters can be found in [30]. Nevertheless, let us report the measured eye diagrams corresponding to the balanced line of Fig. 8 with and without the presence of CSRRs (Fig. 9). Both diagrams are roughly indistinguishable, which means that the integrity of the differential signals is preserved despite the presence of the common-mode filter.

Common-mode filters based on ground plane etching can also be implemented by means of central metallic patches connected to the ground plane through meandered inductors, as reported in [31]. The topology of these structures is depicted in Fig. 10(a). If the patches are separated a small distance, capacitive coupling between them arises, and the equivalent circuit model (unit cell) is the one shown in Fig. 10(b). The main difference in comparison with the circuit of Fig. 8(b) is the fact that the resonant tank $L_c - C_c$ in that circuit (describing the CSRR) is a pair of inductors (L_p) in the circuit of Fig. 10(b), corresponding to the meandered strips. It
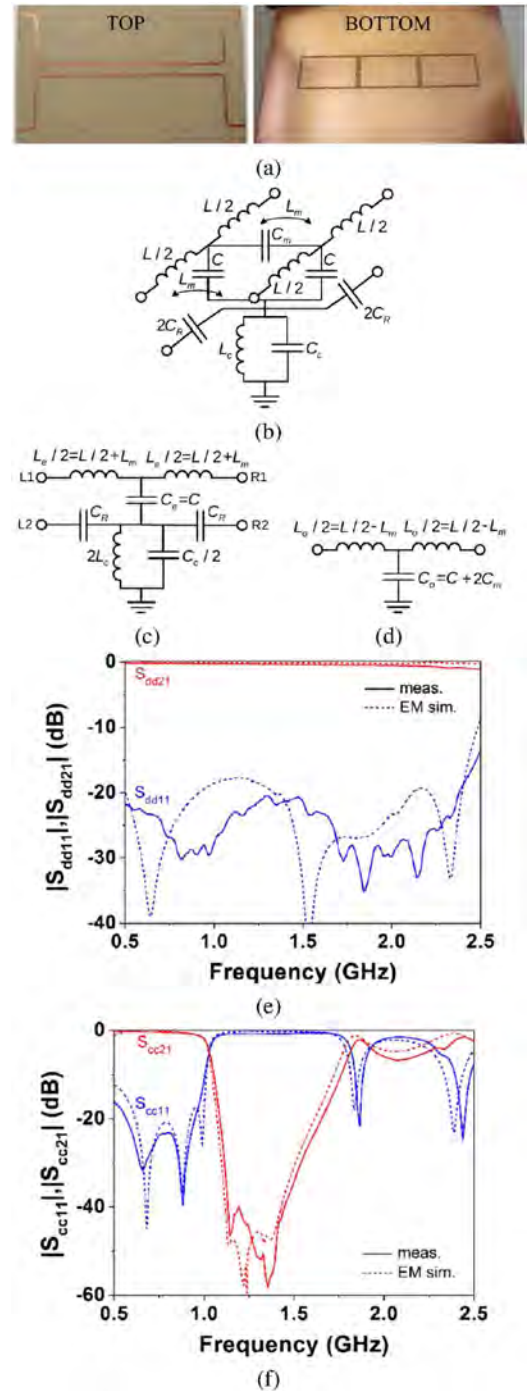

FIGURE 8. CSRR-based common-mode bandstop filter. (a) Photograph. (b) lumped element equivalent circuit model (unit cell). (c) common-mode equivalent circuit. (d) differential-mode equivalent circuit. (e) differential-mode response. (f) common-mode response. Reprinted from [30] with permission.

is also assumed in the circuit of Fig. 10(b) that the lines are uncoupled. Nevertheless, if the lines are close one to each other, their mutual coupling can be taken into account through a mutual capacitance, C_m, and a mutual inductance, L_m, similar to Fig. 8(b). The circuit models for the common and differential modes are depicted in Fig. 10(c) and (d),
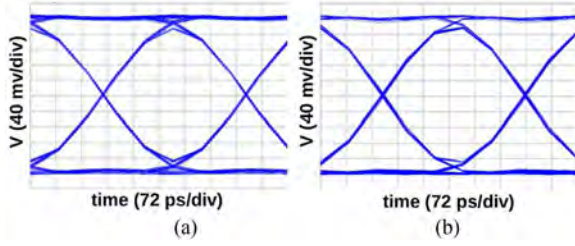
FIGURE 9. Measured differential eye diagram for the structure of Fig. 8 with (a) and without (b) CSRR. Reprinted from [30] with permission.

respectively. An all-pass structure results for the differential mode, whereas the common mode is expected to be filtered, as far as the equivalent circuit for such mode resembles the one of an elliptic low-pass filter (except by the presence of the coupling capacitances, C_s). The common-mode insertion loss corresponding to a four-stage structure is depicted in Fig. 10(e).

As it can be seen, in the common-mode bandstop filters reported so far there is a perfect topological symmetry with regard to the axial plane between the pair of lines. However, it has been recently reported that by considering glide-symmetric structures (meaning that the axial symmetry is disrupted), it is possible to improve the common-mode rejection bandwidth, yet preserving the integrity of differential-mode signals [50]. Indeed, the glide-symmetric common-mode filtering structures reported in [50] are inspired by the single-ended mushroom-type glide-symmetric bandstop filters previously reported in [65].

In [50], glide symmetry was applied to improve the common-mode filtering performance of both DGS and mushroom-type differential-mode transmission lines. Let us report in this section the results corresponding to the DGS-based structure. Fig. 11 shows the topologies of the different DGS common-mode filters reported in [50], one based on a perfectly symmetric configuration with regard to the axial plane AA' (fully symmetric), one non-symmetric (designated as conventional in [50]), and another one exhibiting glide symmetry. The measured common-mode transmission coefficients for the three structures are depicted in Fig. 12, where the superior performance of the glide-symmetric structure can be appreciated. Despite the fact that the glide-symmetric common-mode filter does not exhibit axial symmetry, the measured eye diagram is roughly undistinguishable from the one of the fully symmetric structure (see Fig. 13). Consequently, the differential-mode signals are not degraded in this glide-symmetric device, despite the absence of perfect symmetry.

Let us mention that, as argued in [50], and explained in detail in [65], by introducing glide symmetry, better common-mode rejection bandwidth and rejection level (and, consequently, common-mode rejection ratio, CMRR) are achieved by virtue of the enhanced coupling between the metallic patches of the DGS that results through glide symmetry. Such coupling is a key aspect in stopband bandwidth enhancement,
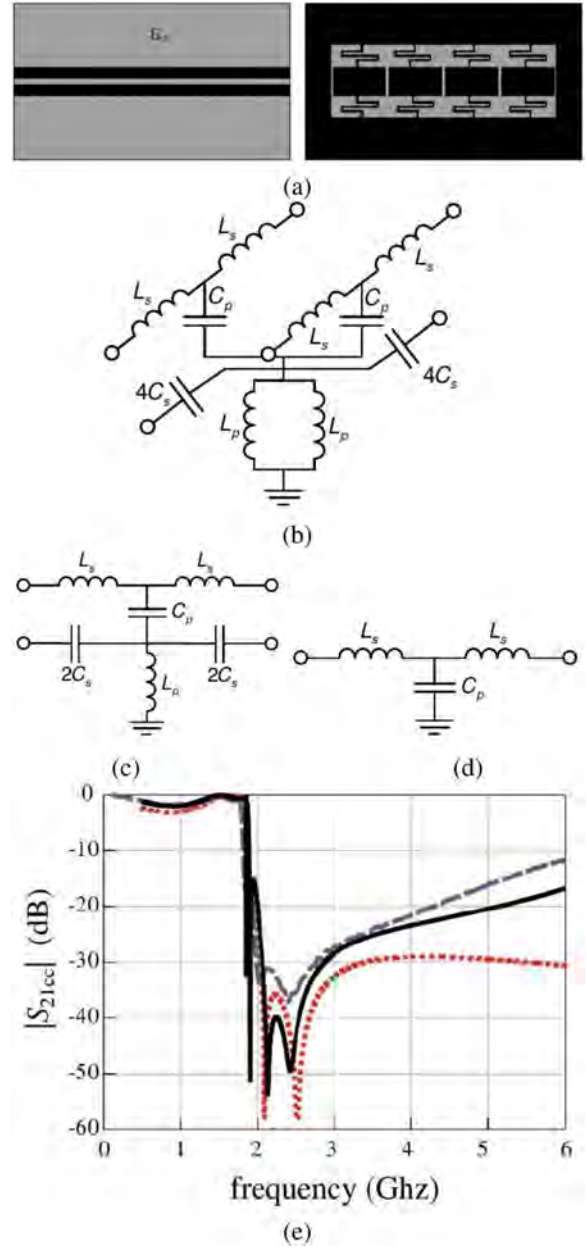

FIGURE 10. (a) Top (left) and bottom (right) views of the common-mode suppression filter based on metallic patches connected to the ground plane through meandered inductors. (b) lumped element equivalent circuit model (unit cell). (c) common-mode equivalent circuit; (d) differential-mode equivalent circuit. (e) common-mode response. Note that for the unit cells cascaded to the input and output ports, the capacitors C_s are connected to ground. In reference to (e), the full-wave simulation is depicted in solid black line, the measurement in blue dashed line, and the equivalent circuit response in red dotted line. Reprinted from [31] with permission.

as reported, e.g., in [10], and as revealed by the dispersion diagrams shown in [50] (not reproduced here). In such diagrams, it can be appreciated that the first stop band for the common mode signals (the one of interest) is significantly widened in the glide-symmetric structure (as compared to the one of the fully symmetric structure).
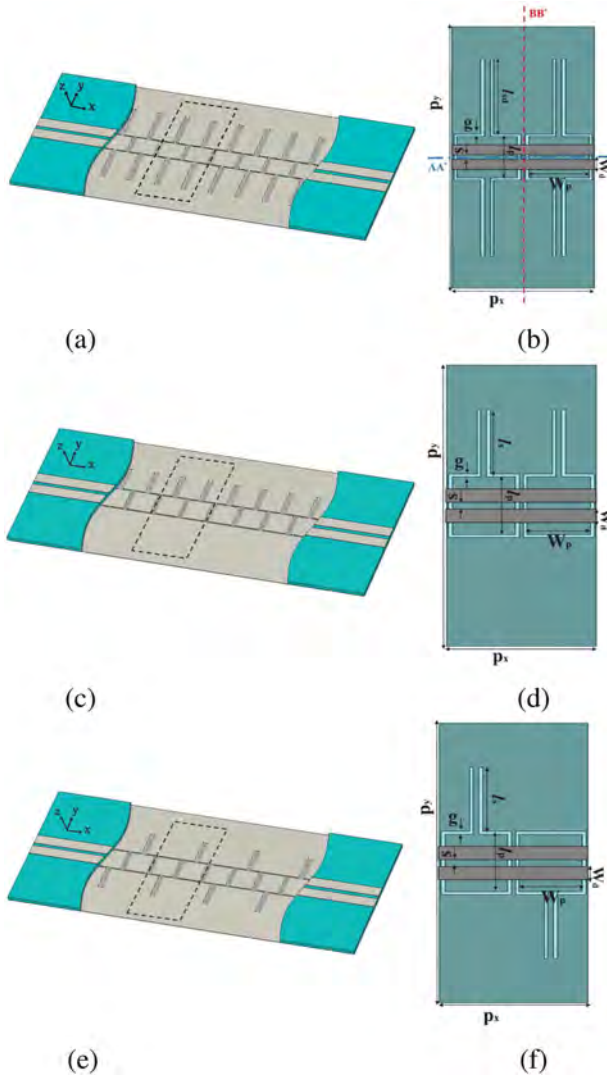
(a)   (b)

(c)   (d)

(e)   (f)

FIGURE 11. Differential lines loaded with DGSs and the corresponding unit cells. (a) Fully symmetric structure and (b) unit cell. (c) non-symmetric structure and (d) unit cell. (e) glide-symmetric structure and (f) unit cell. Reprinted from [50] with permission.
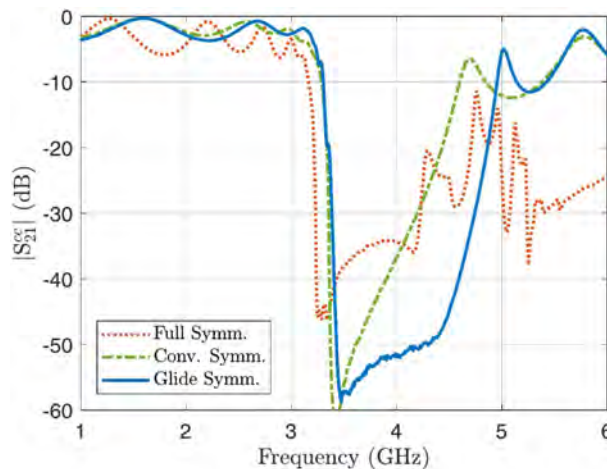

FIGURE 12. Measured common-mode responses of the common-mode filters of Fig. 11. Reprinted from [50] with permission.
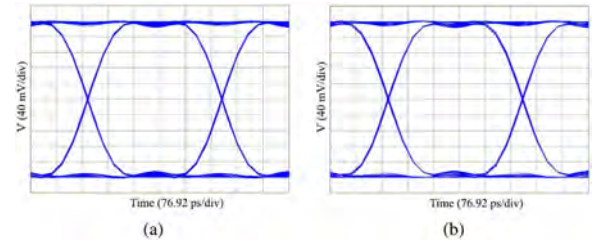

FIGURE 13. Measured eye diagram for the differential mode corresponding to the symmetric (a) and glide symmetric (b) DGS-based common-mode filters. Reprinted from [50] with permission.

C. COMMON-MODE FILTERS BASED ON ELECTROMAGNETIC BANDGAPS (EBGS)

After the previous representative set of DGS-based common-mode rejection filters, let us next briefly review a common-mode suppression strategy based on the inherent filtering properties of periodic structures, or electromagnetic bandgaps (EBGs). EBGs are periodic structures exhibiting stop bands at certain frequencies, due to the well-known Bragg effect [57], [66], [67] (in particular, the first stop band arises when the Bragg condition is fulfilled, i.e., when the period of the structure is half the wavelength). Thus, single-ended band-stop filters implemented by simply adding periodicity to a transmission line have been reported [68], [69], [70]. Such periodicity can be introduced by etching periodic patterns in the ground plane, or by periodically modulating the transverse geometry of the line (non-uniform transmission lines).

In [40], common-mode suppressed EBG-based differential lines implemented by continuously (and periodically) varying the separation and width of the lines were reported. The design strategy is very simple. In brief, it is necessary that the line geometry provides a periodic modulation of the common-mode characteristic impedance along the line (with a period determined by the required central frequency of the common-mode stop band), keeping unaltered the differential-mode impedance. Such differential-mode characteristic impedance must be set to $50\,\Omega$, in order to avoid mismatching reflections for that mode. From the substrate parameters (dielectric constant and thickness) the determination of the periodic line geometry providing a variation of the common-mode impedance within a certain range, maintaining invariable the differential-mode characteristic impedance, is feasible (e.g., by means of a transmission line calculator).

Fig. 14 depicts the EBG-based common-mode rejection filter reported in [40], together with the common-mode and differential-mode transmission coefficients. With four unit cells, a maximum rejection of 17 dB (measurement) at the central frequency of the common-mode stop band is achieved. This common-mode suppression strategy does not require ground plane etching, and the design of the common-mode bandstop filter is simple, as it is based on compact analytical expressions (derived in [40], [57]). Moreover, vias are not needed, and two metal levels suffice for filter implementation. However, it is not simple, in practice, to maintain the
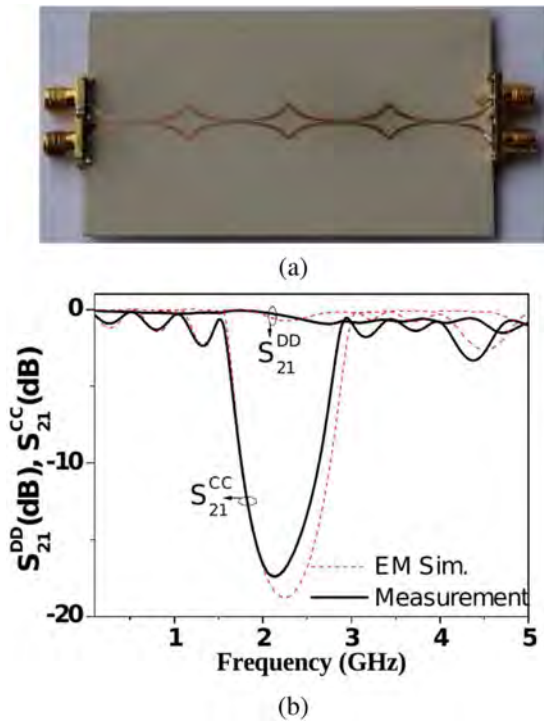
FIGURE 14. EBG-based common-mode filter. (a) Photograph. (b) transmission coefficient for the differential and common modes. Reprinted from [40] with permission.

FIGURE 15. Topology (a) and perspective view of the unit cell (b) of the mushroom-type common-mode rejection filter. Reprinted from [2] with permission.

differential-mode characteristic impedance to the nominal required value (50 Ω) along the whole structure, and this is the main cause of certain insertion loss for the differential mode, as it can be appreciated in Fig. 14. It is worth mentioning that widening the common-mode stop band is possible by implementing the device by means of a quasi-periodic structure. Since the central frequency of the common-mode stop band is determined by the period (according to the Bragg condition), it follows that by slightly varying the period along the structure (chirping), or by combining EBGs with different periodicity, the bandwidth can be substantially enhanced, as demonstrated in the EBG-based common-mode rejection filters reported in [40], [41].

Other common-mode rejection filters based on EBG periodic structures were reported in [37], [38], [39]. In [39], a two-dimensional DGS designated as uniplanar compact photonic bandgap (UP-PBG) ground plane by the authors was used in order to reject the common-mode over a very wide frequency band. The structure exhibits also a strong common-mode rejection level and it is compact, but, contrary to the EBG-based common-mode filter of Fig. 14, it needs ground plane etching. In [37], [38], common-mode filters based on EBGs were also presented. However, such filters need three metal levels, and are only able to suppress specific frequencies, as compared to the common-mode filters reported so far. In [71], a common-mode suppression filter based on a surface-mount technology (SMD) EBG structure is reported. In this proposal, the main advantage concerns the fact that
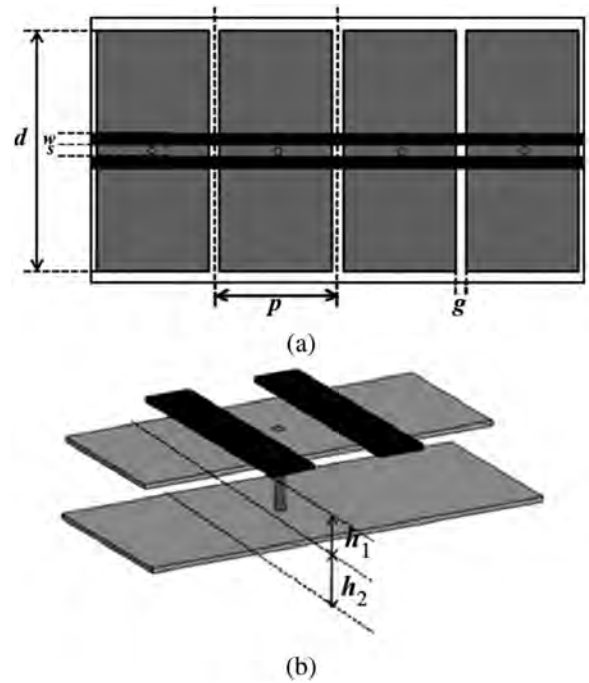
the printed circuit board (PCB), including the differential line pair, is separated from the common-mode filter (indeed, the common-mode filter is placed on top of the PCB as a surface-mount component). Thus, the common-mode filter can be easily removed and replaced with another one, if desired, designed to filter a different frequency (but maintaining the same footprint and external dimensions). The main drawback of the EBG-based common-mode filter of [71] is the limited bandwidth of the common-mode stop band.

D. COMMON-MODE FILTERS BASED ON MULTILAYER STRUCTURES

In the common-mode suppressed filter examples reported in the previous subsections, the structures use only two metal levels, one devoted to the line pair, and the other one to the ground plane, either etched or not. Nevertheless, there are various implementations of common-mode rejection filters based on three or more metal levels [2], [43], [44], [45], [46], [47], [48], [49], [50], [72]. Of particular interest are those common-mode filters based on the so-called mushroom-type structures [2], [49], [50], [72] to be discussed in the present subsection. Essentially, these filters consist of a pair of lines (upper metal level) on top of metallic patches (intermediate metal level) connected to the ground plane (bottom metallic level) through inductive vias (see Fig. 15). The lumped element equivalent circuit model of this structure is identical to the one of the CSRR-based common mode bandstop filter of Fig. 8. The main difference is that the ground plane is kept unaltered in the mushroom-type structure, although at the
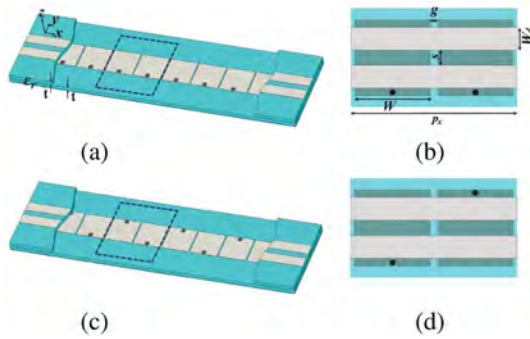
FIGURE 16. Differential lines loaded with grounded mushrooms. (a) Conventional structure and (b) unit cell. (c) glide-symmetric structure and (d) unit cell. Reprinted from [50] with permission.

expense of an additional metal level and the use of inductive vias.

As reported in [50], applying glide symmetry to mushroom-type common-mode filters provides a path to enhance the common-mode stopband performance (bandwidth and rejection level). Thus, we report in this subsection the mushroom-type common-mode glide-symmetric rejection filters of [50]. Glide symmetry is achieved by simply alternating the position of the vias, as depicted in Fig. 16. Actually, this figure includes the glide-symmetric structure, as well as the conventional structure, where the vias are located at the same position. Note that for the conventional structure, the position of the vias is not central, contrary to Fig. 15. Nevertheless, this does not represent a penalty in regard to the integrity of the differential-mode signal (and the integrity of the differential signals is also preserved for the glide symmetric structure).

Fig. 17 depicts the simulated and measured responses for both the conventional and glide-symmetric mushroom-type common-mode rejection filters. It can be appreciated the superior common-mode stopband performance of the glide-symmetric common-mode filter, with a wider stopband bandwidth and common-mode suppression level. For both filters, the insertion loss for the differential mode is very small, indicating that the structure is roughly transparent for that mode.

It is also worth-mentioning the mushroom-type structure reported in [72], fully symmetric but exhibiting a very broad common-mode stop band by virtue of the four transmission zeros generated for that mode. Such transmission zeros are achieved by enhancing the electrical length of the line pair over the mushroom patches by means of meanders, similar to [33], [43], [73]. Under these conditions, the circuit model needs to be described by a combination of distributed and lumped elements, resulting in a complex condition for the transmission zeros. Such condition depends on the various electrical parameters of the circuit model (characteristic impedances, electrical lengths, and inductance of the via), which can be tailored in order to enhance the common-mode rejection bandwidth, as detailed in [72]. Fig. 18 depicts the common-mode filter with four transmission zeros reported
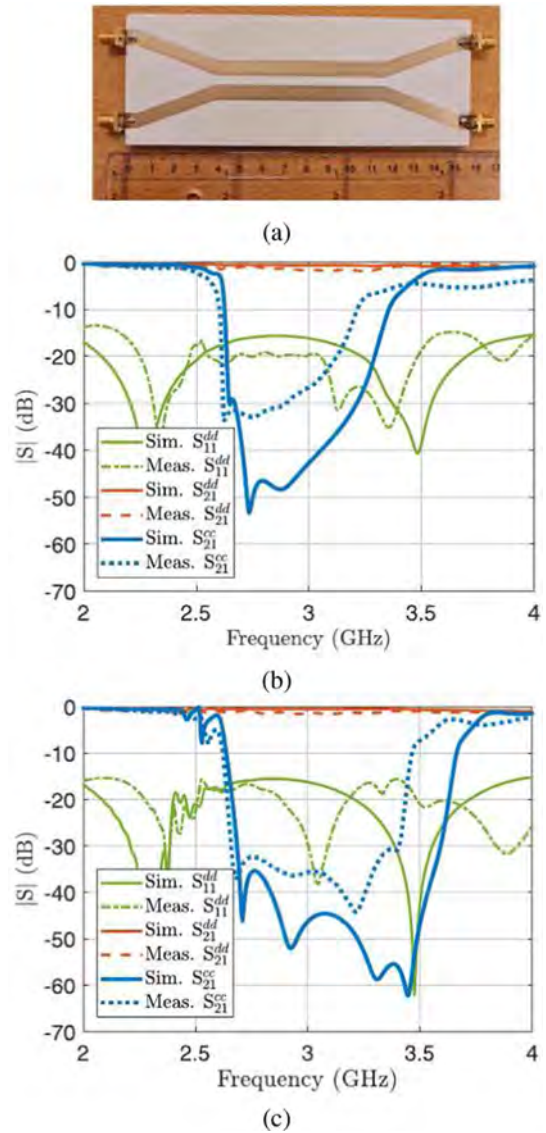
FIGURE 17. Photograph (top view) of the mushroom-type common-mode rejection filters (with 10 unit cells) (a), and responses for the conventional (b) and glide-symmetric (c) structures. Reprinted from [50] with permission.

in [72], as well as the common-mode and differential-mode responses. A very broad common-mode stop-band bandwidth of 123 % (considering the cutoff at -10 dB) results, with low insertion loss for the differential mode. The eye diagrams, not shown here but reported in [72], are indicative of the signal integrity for the differential mode.

E. ABSORPTIVE COMMON-MODE FILTERS (A-CMFS)

In the common-mode rejection filters reported so far, the common mode is reflected back to the source in a certain frequency band. Thus, these filters can be designated as reflective common-mode filters (R-CMF). Clearly, in R-CMFs, the common-mode noise is not dissipated. Therefore, the reflected common-mode noise can be driven through the whole
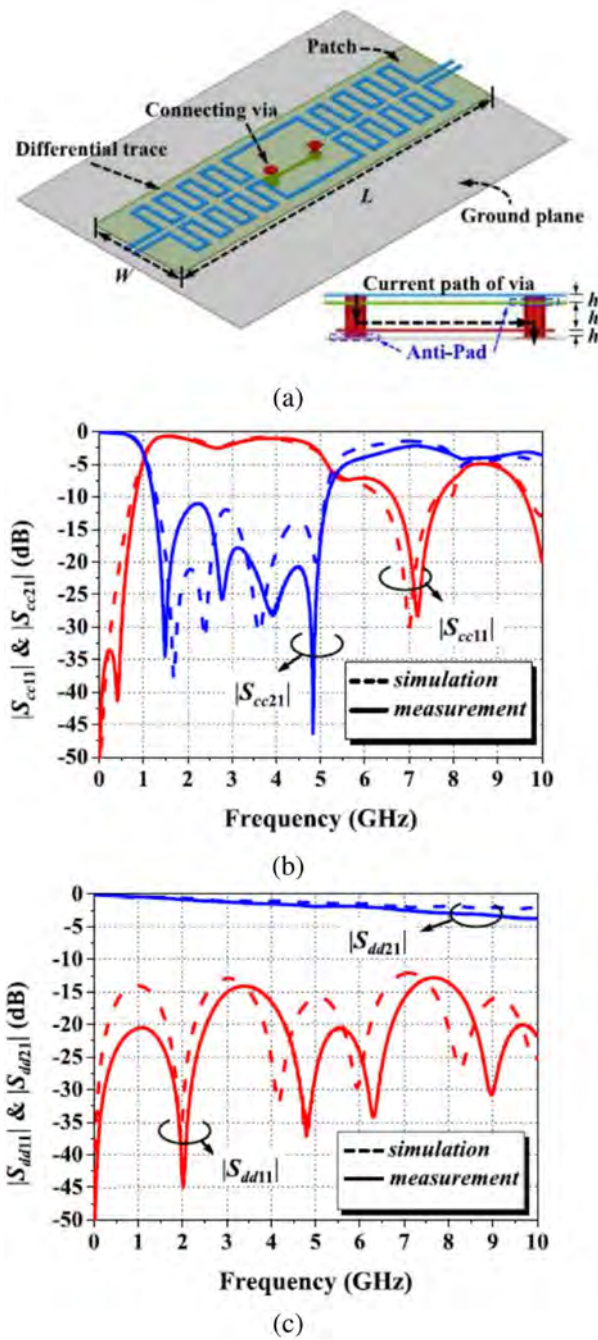
FIGURE 18. Perspective view of the mushroom-type common-mode rejection filter with four transmission zeros (a), and responses for the common mode (b) and differential mode (c). Reprinted from [72] with permission.

system and be the cause of unexpected radiation. To alleviate this problem, the so-called absorptive common-mode filters (A-CMFs) have been proposed in the last decade [51], [52], [53], [74], [75], [76], [77], [78], [79], [80], [81], [82], [83], [84], [85]. Such A-CMFs can absorb (or dissipate) the common-mode noise utilizing resistors or lossy materials, thereby preventing common-mode noise reflection, and hence, undesired radiation.

Certain implementations of A-CMFs use an R-CMF in order to block the common-mode noise, and an additional dissipative circuit placed at one side for common-mode noise absorption. Therefore, these techniques based on an R-CMF blocking module and a common-mode noise dissipative module only synthesize unidirectional A-CMFs. For this reason, these structures have been designated as unidirectional A-CMFs, and examples can be found in [74], [75], [76], [77], [79], [83]. By contrast, there are other A-CMF architectures able to dissipate the common-mode noise regardless on the circuit side from where it is injected (bidirectional A-CMFs [51], [52], [53], [78], [81], [82]). The dissipative element in an A-CMF is usually a resistor, or a set of resistors. Nevertheless, there are A-CMF implementations that exploit the inherent losses of certain planar resonators, for example, CSRRs [84], or gap coupled resonators [75].

The design of A-CMFs is not simple, since the considered implementations should be able to be transparent for the differential mode (all-pass structures for that mode), and simultaneously block and dissipate the common mode over the widest possible frequency band. It is not possible to discuss all the reported implementations of A-CMFs in a review paper focused on the general topic of balanced lines, circuits, and sensors. Thus, let us report two representative examples of A-CMFs, one of them unidirectional, and the other one bidirectional.

Concerning the unidirectional case example, the considered prototype is the one reported in [83]. Although this prototype A-CMF exhibits a limited common-mode suppression and absorption band in the vicinity of 2.4 GHz (it is intended to eliminate the EMI in the Wi-Fi 2.4 GHz band), it has been chosen because it is based on a single stage, and, therefore, the resulting device footprint is very small. It is also remarkable that the device uses only two metallic levels. Moreover, the design of this A-CMF is relatively simple and follows guidelines given by formulas derived in [83] (but not reproduced here). The schematic of the structure of [83] is depicted in Fig. 19(a). It consists of a differential pair (with single-ended characteristic impedance Z_1 and electrical length θ_1) cascoding two transmission lines (with characteristic impedance Z_2 and electrical length θ_2), terminated with a resistor, R. The resistor is located on the symmetrical plane of the circuit, drawn with dash line, as shown in Fig. 19(a). Fig. 19(b) and (c) depict the equivalent circuit model for the differential and common mode, respectively. The structure is transparent for the differential mode, whereas, according to the circuit of Fig. 19(c), the structure is able to block and absorb common mode signals (noise) at certain frequencies. The reason is that there are combinations of circuit parameters providing $S_{21} = 0$ and $S_{11} = 0$, the necessary conditions for achieving common-mode suppression (blocking) and absorption simultaneously (thus note that an additional condition as compared to R-CMFs is necessary in A-CMFs, i.e., $S_{11} = 0$).

In [83], the structure of Fig. 19(a) was synthesized by considering a pair of lines cascoded to a meandered slotline. The layout and the photograph of the fabricated A-CMF are
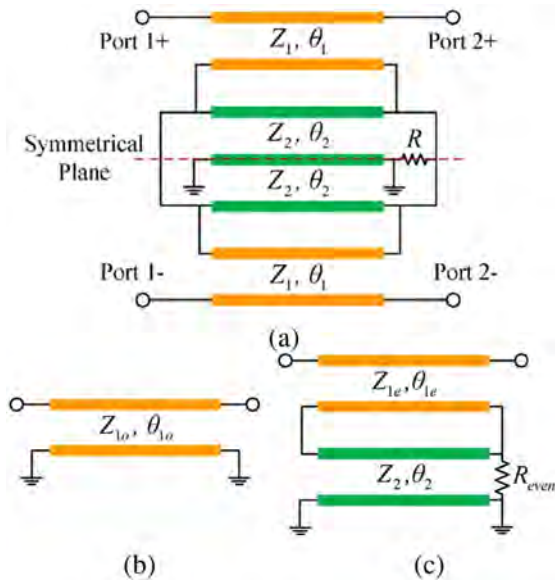
FIGURE 19. (a) Proposed circuit, composed of a differential pair, cascoded transmission lines, and a resistor, to synthesize an A-CMFs. (b) Odd-mode equivalent circuit. (c) Even-mode equivalent circuit. Reprinted from [83] with permission.

shown in Fig. 20. Such figure includes also the frequency response of the common-mode filter, where it can be appreciated that the differential mode exhibits very small insertion loss, whereas the common-mode is significantly absorbed in the vicinity of 2.4 GHz. The measured results show that $|S_{cc21}|$ is lower than -10 dB from 2.33 to 2.67 GHz and $|S_{cc11}|$ is less than -10 dB from 2.11 to 2.8 GHz. This corresponds to a common-mode noise absorption efficiency above 80 % between 2.33 to 2.67 GHz, where both $|S_{cc21}|$ and $|S_{cc11}|$ are less than -10 dB [83]. The measured eye diagrams (not shown here but reported in [83]) are indicative of the good signal integrity for the differential mode.

A bidirectional version of the previous A-CMF was reported in [81] by the same authors. To achieve bidirectional common-mode absorption, the structure was equipped with two resistors, rather than one, terminating the pair of meandered slotlines, in a symmetric configuration with regard to the bisecting plane between the input and output ports (see further details in [83]). The performance of this bidirectional A-CMF is similar to the one of the unidirectional counterpart.

To end this subsection, let us briefly report the bidirectional A-CMF reported in [82], with small size and very broad common-mode suppression and absorption bandwidth. This A-CMF is inspired by the R-CMF based on DB-DGS resonators of Fig. 7. The main difference is the presence of resistors in the central plane of the DB-DGS resonators (or axial plane of the structure), see Fig. 21, except for the central DB-DGS, which is resistor free. With these resistors, the resulting resonators are lossy components, able to absorb the common mode. It can be appreciated in Fig. 21 that the resistor-loaded DB-DGS resonators are not identical, a strategy to enhance the common-mode suppression and absorption. Nevertheless, the structure is symmetric with regard
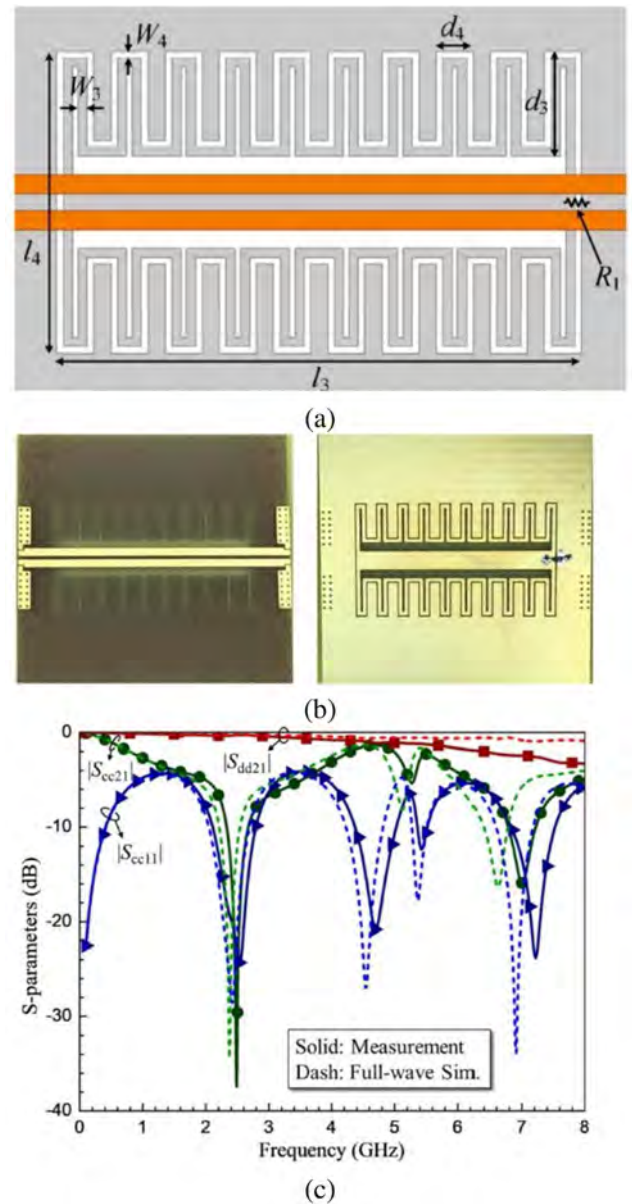
FIGURE 20. Layout (a) and photograph (b) of the upper (left) and lower (right) metal levels corresponding to the synthesized A-CMF of Fig. 19(a). (c) frequency response. Reprinted from [83] with permission.

to the bisecting plane between the input and output ports in order to achieve common-mode absorption bidirectionallity. Another important aspect is the fact that the filter is implemented in stripline, rather than microstrip, technology, as revealed by the three metal levels employed in the design (see Fig. 21).

The specific designed A-CMF device in [82] is shown in Fig. 22, whereas the frequency responses are depicted in Fig. 23. The differential-mode insertion loss is small, whereas for the common mode, both the insertion and return loss are significant, regardless of the considered input port, indicating that the common mode is efficiently, and bidirectionally, suppressed and absorbed (the reported common-mode noise
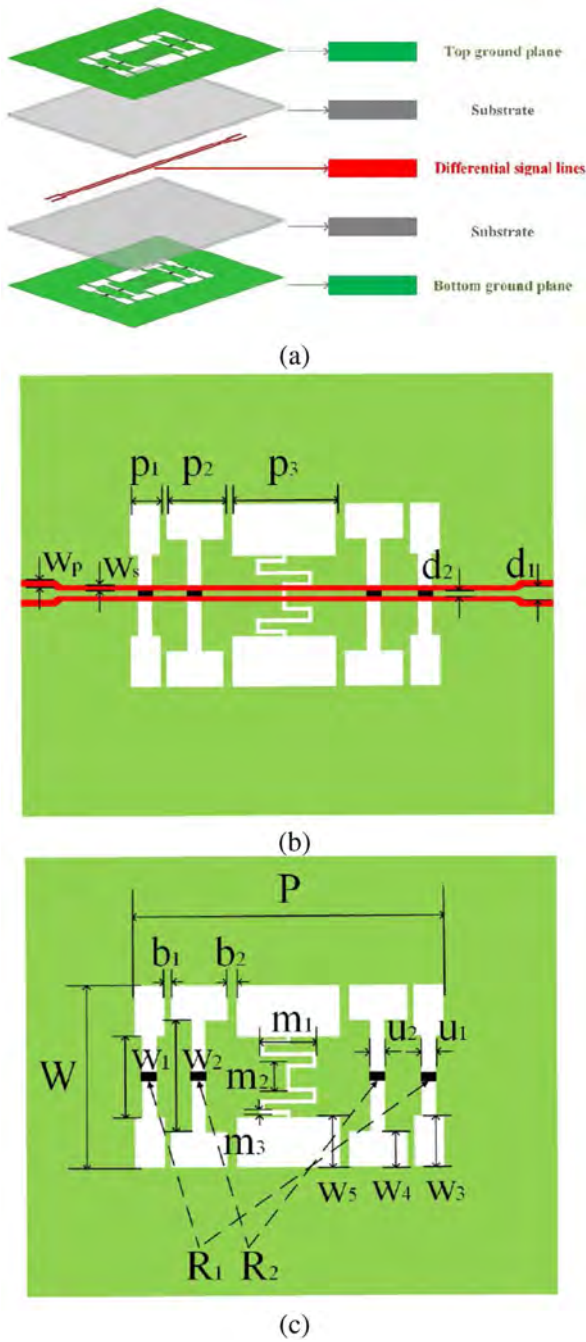
FIGURE 21. Configuration of the A-CMF based on DB-DGS resonators. (a) Layer stack-up. (b) Differential signal lines. (c) Top and bottom ground planes. Reprinted from [82] with permission.

FIGURE 22. Layout (a) and photograph (b) of the DGS-based stripline A-CMF of Fig. 21. Reprinted from [82] with permission.

absorption fractional bandwidth (FBW) is as high as 147% [82]).

F. COMPARISON OF COMMON-MODE REJECTION FILTERS

Table 1 compares the different common-mode bandstop filters reported in this section in terms of size (relative to the wavelength at the central frequency of the common-mode stop band), number of metallic layers, FBW, CMRR,
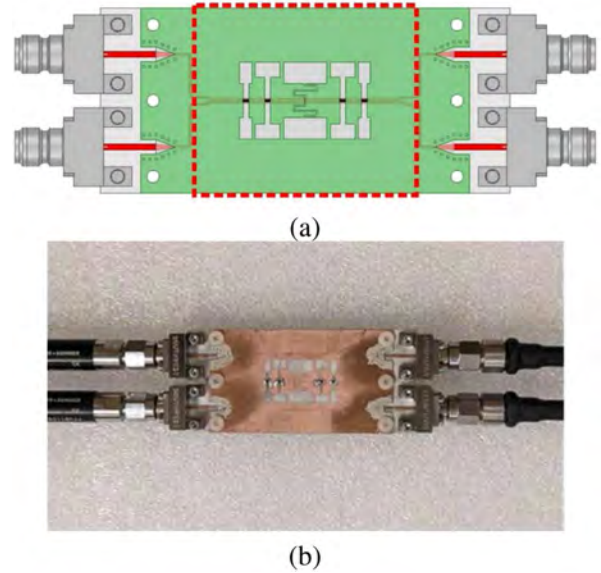
and common-mode (CM) absorption. The fractional bandwidth for the reflective mode filters is usually referred to the frequency span where the common-mode insertion loss is at least 10 dB, whereas for the absorptive common-mode filters, it is given by the bandwidth where the common-mode absorption factor is at least 80 %, or 90 % in most cases. Concerning the last column, it provides the CMRR for the reflective-mode filters (in dB), and the common-mode absorption (in %) for the absorptive common-mode bandstop filters (nevertheless, this information is not given in all the references). Let us mention that, in some cases, the considered fabrication technology is not PCB, and the number of layers is replaced with the considered technology, as indicated.

In view of the table, among those reflective-type common-mode filters implemented in PCB technology, those reported in [31], [35], [36] exhibit a good combination of common-mode rejection and fractional bandwidth. The filter of [42] is also very competitive, but it was fabricated in LTCC technology. Concerning the absorptive-type common-mode filters, a fractional bandwidth above 100 % was achieved in the implementations of refs. [51], [52], [79], [80], [82], [85], in some cases with very good common-mode absorption. Several of these filters are bidirectional. It is remarkable the common-mode filter presented in [51], which is bidirectional and very small, though it utilizes 3 metal levels. Although not indicated in the table, the differential-mode performance, i.e., the insertion loss in the frequency region of interest and the signal integrity (as estimated from the measured eye diagrams, reported in many cases), is in general good.

IV. BALANCED FILTERS WITH COMMON-MODE SUPPRESSION

The previous section has been focused on common-mode rejection filters, that is, differential lines able to suppress (either
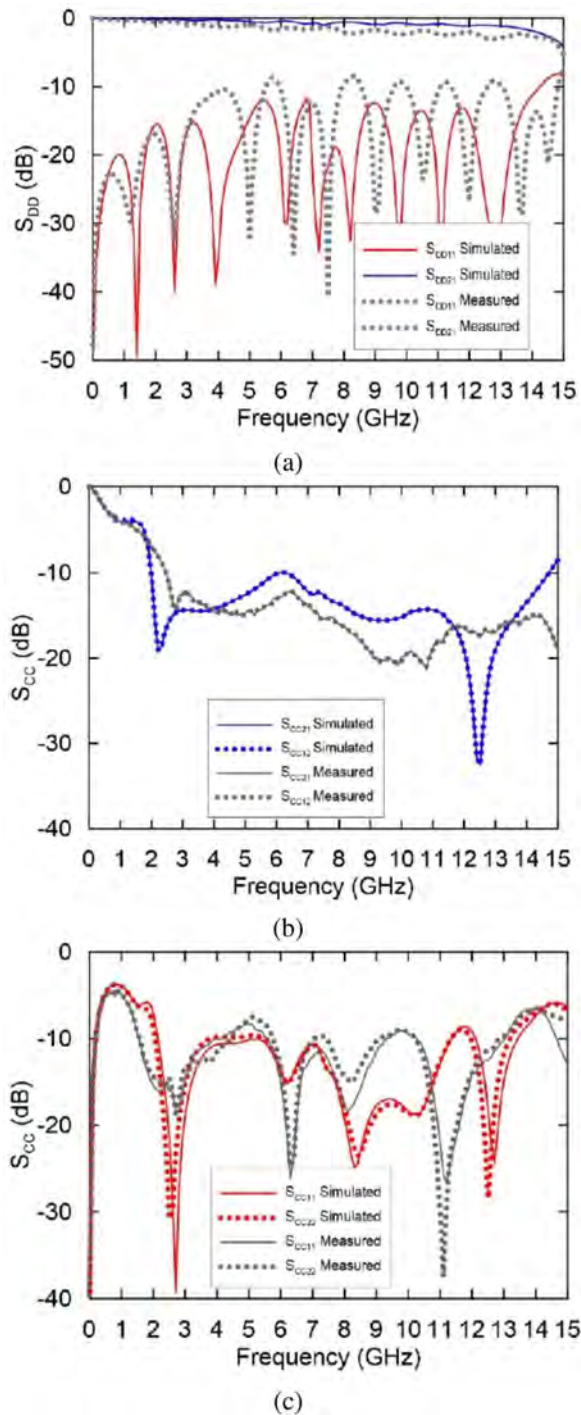
FIGURE 23. Frequency response of the A-CMF of Fig. 22. (a) differential mode. (b) common-mode transmission coefficients. (c) common-mode reflection coefficients. Reprinted from [82] with permission.

TABLE 1. Comparison of Common-Mode Filters

Ref.	Type[a]	Lay.[b]	Area (λ^2)	FBW (%)	CMRR(dB)/CM Absorption (%)
[2]	R	4	0.0416	60	> 40 / —
[27]	R	2	0.3572	70	> 35 / —
[28]	R	2	0.1936	87	> 15 / —
[29]	R	2	0.0602	54	> 30 / —
[30]	R	2	0.0832	51	> 40 / —
[31]	R	2	0.0704	100	> 20 / —
[33]	R	2	0.0400	130	> 12 / —
[34]	R	2	—	95	> 25 / —
[35]	R	2	—	130	> 12 / —
[36]	R	2	0.0350	73.5	> 40 / —
[37]	R	3	—	40	> 10 / —
[38]	R	3	—	18	> 15 / —
[39]	R	2	—	83	> 40 / —
[40]	R	1	0.5966	67	> 25 / —
[41]	R	1	1.7360	80	> 30 / —
[42]	R	LTCC	—	150	> 25 / —
[43]	R	4	0.0144	104	> 10 / —
[44]	R	3	—	73	> 35 / —
[45]	R	2	—	28	> 30 / —
[46]	R	LTCC	0.0038	42/18	> 10 / —
[47]	R	3	0.0003	100	> 12 / —
[48]	R	3	0.0817	27	> 25 / —
[49]	R	3	0.0260	72	> 20 / —
[50]	R	2	0.2535	46	> 50 / —
[51]	A-B	3	0.0025	111	— / > 80
[52]	A-B	IPD	—	128	— / > 90
[53]	A-B	4	0.0050	12	— / > 95
[71]	R	5	—	13	> 10 / —
[72]	R	3	0.0427	123	> 11 / —
[73]	R	3D-IC	0.0050	20	> 10 / —
[74]	A-B	4	—	25	— / > 95
[75]	A-U	4	—	5	— / > 95
[76]	A-U	4	0.0020	73	— / > 95
[77]	A-B	2	0.1400	50	— / —
[78]	A-B	2	0.0510	76	— / > 90
[79]	A-U	2	0.0120	104	— / > 95
[80]	A-B	2	0.0260	139	— / > 95
[81]	A-B	2	0.0317	15	— / —
[82]	A-B	3	0.0110	147	— / —
[83]	A-U	2	0.0360	14	— / —
[84]	A-B	2	—	27.4	— / > 80
[85]	A-U	3	0.0600	138	— / > 95

[a] R: reflective; A-B: absorptive bidirectional; A-U: absorptive unidirectional.
[b] LTCC: low-temperature co-fired ceramic; IPD: integrated passive device process; 3D-IC: three-dimensional integrated circuit.

order to control the transmission response (filtering) of the differential signals. By contrast in differential-mode (or balanced) filters, the key aspect is to generate a certain response (typically a bandpass-type) for the differential mode, and for that purpose, specific topologies are required, many times inspired by those of the single-ended counterparts.

Balanced filters are of interest in modern communication systems, and, similar to balanced lines (or interconnects), implementations simultaneously suppressing the common mode over the differential-mode passband are highly demanded. Ideally, balanced filters should intrinsically (and efficiently) suppress the common-mode (the CMRR within

block, or block and dissipate) the common mode in a certain frequency band. Ideally, these common-mode filters are transparent (all-pass) for the differential signals. In practice, certain level of signal attenuation is unavoidable, and such differential signals are filtered (reflected) above a certain (3-dB) cutoff frequency (usually located substantially beyond the region of interest). However, common-mode filters are not designed in

the differential-mode pass band is a good performance indicator in such filters). Cascading a common-mode filter to the differential filter provides a path for CMRR improvement [31], but this is not the preferred option in terms of overall filter size. Thus, a significant effort has been dedicated in the last 20 years to the design of balanced filters with intrinsic common-mode suppression. This topic has been exhaustively covered in the recent book [10], co-edited by the authors of the present review paper. In that book [10], the most significant implementations of the up-to-date state-of-the-art in balanced microwave filters, contributed by different (highly reputed) researchers, were presented. For this main reason, and because such book was published recently (2018), we will not treat the topic of common-mode suppressed balanced filters at the same depth level as common-mode filters in the present paper (it would be impossible on account of the huge number of contributions in the available literature). We will just report the main filter types, design strategies, and few implementations, with special emphasis on recent contributions (nevertheless, for an in-depth study, the authors recommend the book [10] and references therein).

Concerning the differential-mode filter response, balanced filters with intrinsic common-mode suppression can be divided between narrowband filters, wideband and ultra wideband (UWB) filters, and multiband filters, the categorization adopted in [10]. In all cases, the design strategies are based on topologies able to provide the required response for the differential mode, with the maximum possible attenuation level and stopband bandwidth for the common mode. Though most reported balanced filters in [10] and references therein intrinsically reflect (block) the common mode within a certain frequency band, many recent implementations have been focused on the dissipation, rather than reflection, of that mode (the interest is justified by the reasons in reference to the absorptive common-mode filters of the previous section). Let us next review (briefly, as justified) some of the reported common-mode suppressed (or dissipated) balanced filters, categorized as indicated above.

A. WIDEBAND AND UWB BALANCED FILTERS

There are many approaches for the implementation of balanced bandpass filters exhibiting broad transmission bands for the differential mode and, simultaneously, rejecting the common mode in that band. One of the earliest strategies utilizes branch-line-like structures. The seminal and canonical topology was presented in [86] but there are many other reported wideband and UWB balanced filters inspired by this branch-line topology (see, e.g., [87], [88], [89], [90], [91] and [10, chapter 4]). It has also been recently demonstrated that, with this type of balanced filters, it is possible to absorb, rather than reflect, the common mode in the region of interest. As an example of this type of wideband filters, Fig. 24 depicts the schematic and photograph of a specific device, exhibiting a broad differential-mode transmission band and common-mode noise absorption [92]. For the differential mode, the axial symmetry plane is an electric wall, and the
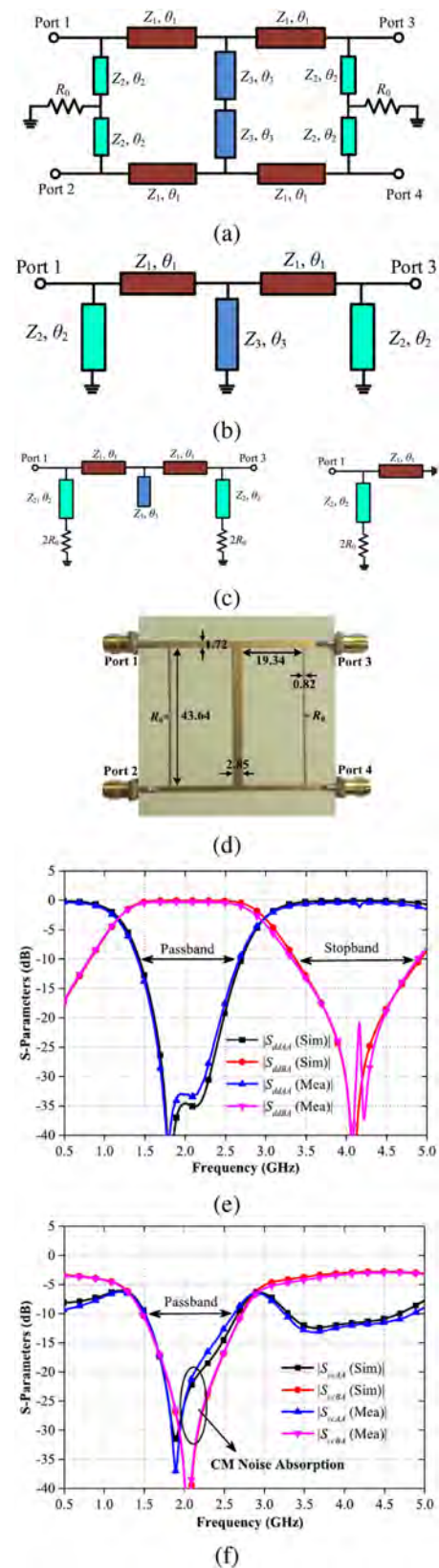

FIGURE 24. Balanced filter with common-mode noise absorption based on the branch-line topology. (a) circuit schematic. (b) circuit schematic for the differential mode. (c) circuit schematic for the common mode (left) and simplified circuit (right). (d) photograph. (e) differential mode response. (f) common-mode response. Reprinted from [92] with permission.

resistors are virtually grounded. The resulting schematic for this mode, with all the line sections and stubs exhibiting an electrical length of $\theta_1 = \theta_2 = \theta_3 = 90°$ at the central filter frequency, corresponds to the well-known topology of single-ended wideband branch-line bandpass filters [93], [94]. By contrast, for the common mode, with a magnetic wall at the axial symmetry plane, the resulting circuit schematic, also depicted in Fig. 24, provides a transmission zero at the central filter frequency (note that the central stub, with impedance and electrical length Z_3 and θ_3, respectively, is virtually open at its termination). Moreover, the common mode is absorbed at that frequency, provided the resistor satisfies $R_0 = Z_2^2/2Z_0$. The details of the different circuit parameters (line and stub impedances) is given and justified in [92]. The frequency response of this filter is also included in Fig. 24, where it can be appreciated the capability of the structure to efficiently absorb the common mode. The measured common-mode transmission coefficient is $|S_{ccBA}| = -38.13$ dB, whereas the common-mode reflection coefficient is $|S_{ccAA}| = -25.38$ dB. This indicates that the common-mode noise is absorbed and converted into heat by the resistors.

Another strategy, similar to the one discussed in the precedent paragraph, was reported in [95], [96], [97], [98], [99], [100] and [10, chapter 9]. Topologically, the common-mode suppressed balanced filters of [95], [96], [97] are similar to those based on the branch-line-like topology. However, rather than shunt stubs, such filters use (instead) mirrored stepped-impedance resonators (SIRs). Fig. 25 depicts a typical layout of these filters (for order-5), as well as the circuit schematic, and the circuit schematic for the differential and common modes. For the differential mode, the resulting circuit is similar (but not identical) to the canonical circuit of a band-pass filter, consisting of shunt-connected parallel resonators coupled through admittance inverters. The difference is the presence of the inductances designated as L_{ei}, where i denotes the stage. Nevertheless, the presence of this inductance provides a transmission zero above the differential-mode passband, which improves the filter selectivity for that mode. For the common mode, additional transmission zeros caused by the series resonators $L_{ci} - C_{ci}$ result. Thus, by conveniently distributing these zeros within the differential-mode passband, an efficient common-mode suppression in that band can be achieved. Fig. 26 depicts a prototype order-7 common-mode suppressed balanced filter implemented by means of mirrored SIRs as an illustrative example, as well as the differential and common-mode responses [97]. The common mode is significantly suppressed over a wide band, with a CMRR of 50 dB at the central filter frequency (3 GHz). In other implementations, the distributed inverters were replaced with semi-lumped components with the result of very compact filters [98], [99], [100], an advantageous aspect over those filters reported in [95], [96], [97] (Fig. 27 depicts a specific implementation [100]).

Wideband and UWB balanced filters based on coupled line sections (in some cases combined with other structures) have also been reported [101], [102], [103], [104], [105], [106],
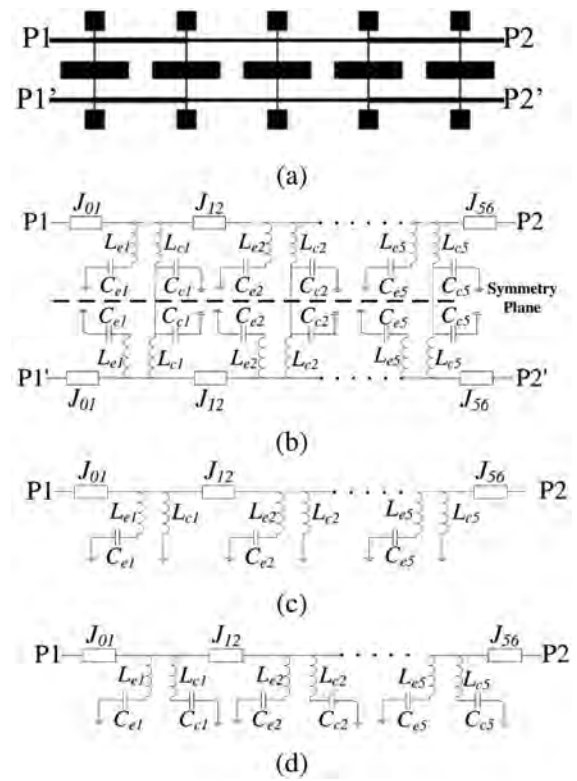

FIGURE 25. Typical topology of a wideband balanced filter with common-mode suppression based on mirrored SIRs (a), circuit schematic (b), circuit model for the differential mode (c), and circuit model for the common mode (d).

[107], [108], [109], [110], [111], and [10, chapters 5 and 6]. One of the canonical circuit schematics for such filters is depicted in Fig. 28 [102], where all the line sections and coupled lines exhibit an electrical length of $90°$ at the central filter frequency, f_0. The circuit schematic for the differential mode, also shown in the picture, exhibits a band pass response in the vicinity of the design frequency, f_0, with a transmission zero at $2f_0$, due to the short-circuited stubs (with an electrical length of $180°$ at $2f_0$). By contrast, the circuit schematic for the common mode [Fig. 28(c)], behaves as a bandstop filter with four transmission zeros, as discussed in [112]. Such stopband behavior can be explained as due to the interference between the two signal paths. The coupling factor of the coupled lines, as well as the characteristic admittances of both the coupled lines and the transmission line sections, determine the stopband characteristics of the common mode, as reported in [102]. As a representative illustrative example of this type of balanced filters, Fig. 29 depicts the photograph and the response of the prototype reported in [102], which is not the one exhibiting the optimum performance, but obeys to the topology of Fig. 28. Other balanced filters based on coupled lines combined with T-shaped structures, ring resonators, etc., can be found in the literature [103], [104], [105], [106], [107], [108], [109], [110], [111].

In the previously cited implementations of common-mode suppressed balanced bandpass filters, the ground plane was
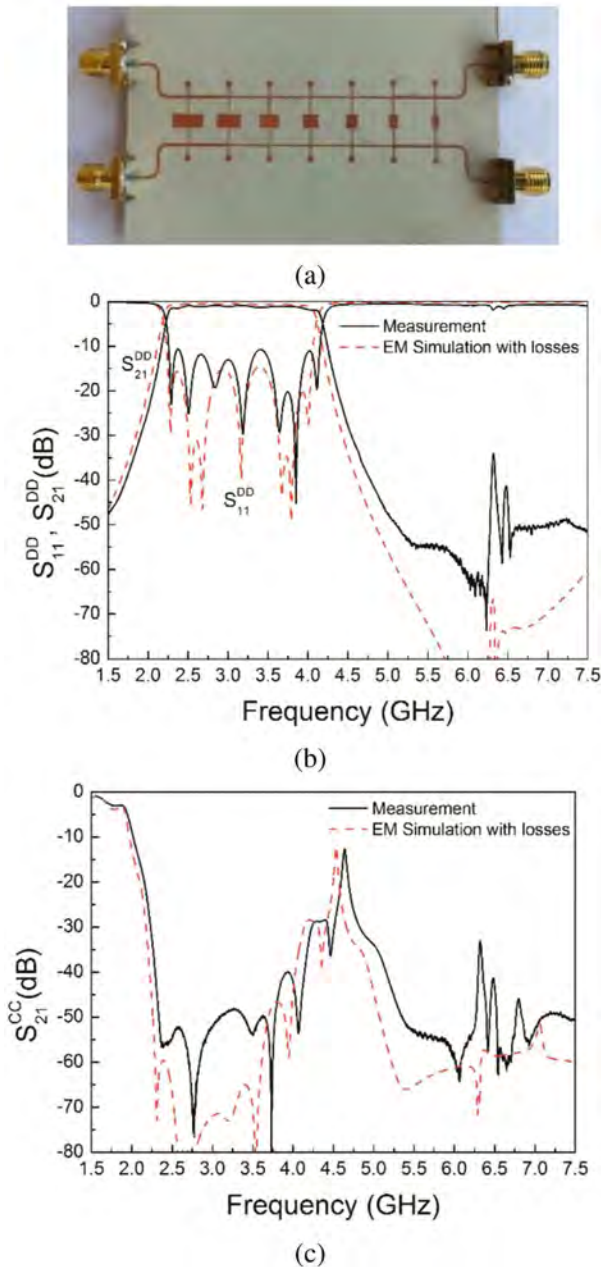
FIGURE 26. Photograph of an order-7 balanced filter based on mirrored SIRs (a) and response for the differential (b) and common (c) modes. Reprinted from [97] with permission.

FIGURE 27. Photograph of an order-5 balanced filter based on mirrored SIRs and interdigital series resonators (a) and response for the differential (b) and common (c) modes. Reprinted from [100] with permission.

kept unaltered. Nevertheless, considering defect ground structures (DGSs) and slot resonators provides an alternative approach for achieving wideband differential-mode responses with intrinsic common-mode suppression (see [113], [114], [115], [116], [117], [118], [119], [120], [121], [122], [123], [124] and [10, chapters 7, 10 and 11][10]). Many filters have been implemented by considering microstrip to slotline transitions. A canonical configuration (designated as differential microstrip to slotline transition) is shown in Fig. 30 [119]. According to this topology, the common mode cannot be transmitted, since the axial symmetry plane is a magnetic

wall for that mode, and the slot resonator cannot be excited. By contrast, such symmetry plane is an electric wall for the differential mode, and the slot resonator can be excited (note that according to the position of the differential microstrip to slot line transitions, the first two resonant modes can be excited).

Other more complex configurations of slotline resonators, i.e., combined with other elements, such as the strip-loaded slotline resonator [122], have been proposed in order to improve the filter performance. It is also remarkable the use of different defect ground structures for the implementation of common-mode suppressed bandpass filters, such as

(a)

(b)   (c)

FIGURE 28. Schematic of the canonical common-mode suppressed balanced filter based on coupled lines (a) and equivalent circuits for the differential (b) and common (c) modes. Reprinted from [102] with permission.
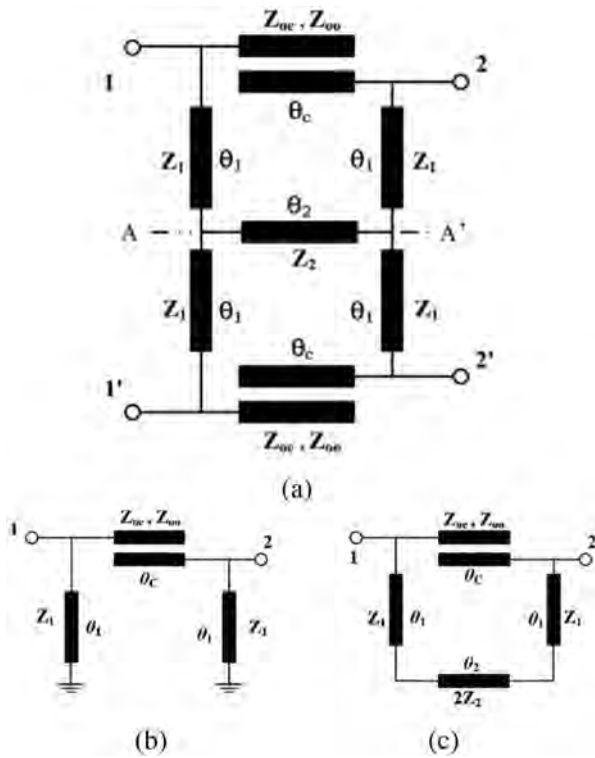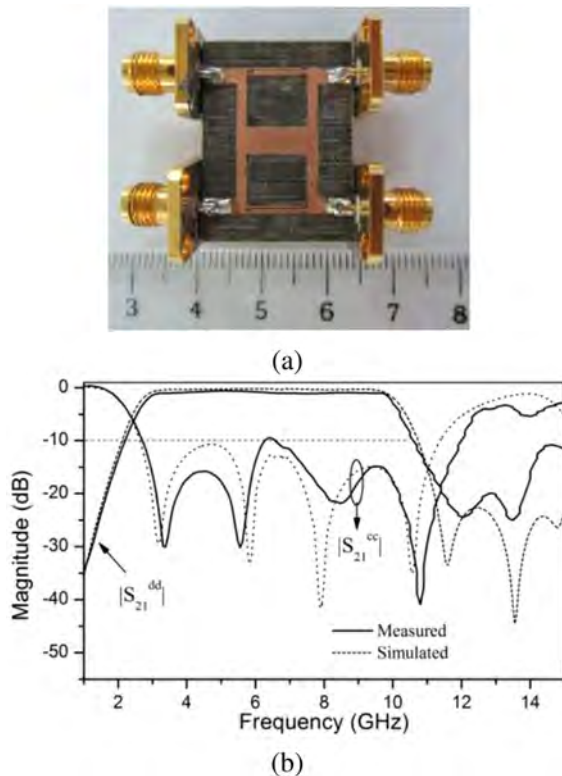

(a)

(b)

FIGURE 29. Photograph of a balanced filter based on the circuit schematic of Fig. 28 (a) and transmission coefficient for the differential and common modes (b). Reprinted from [102] with permission.
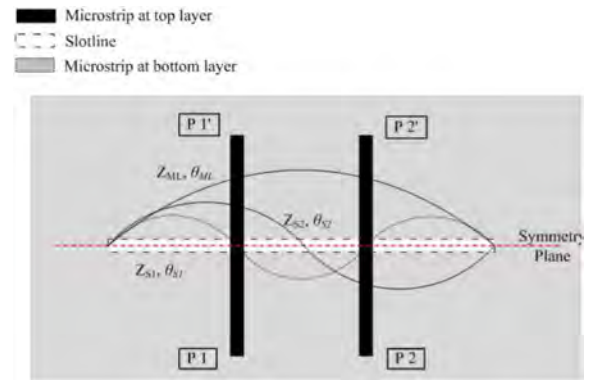

FIGURE 30. Top view of the canonical configuration of a balanced bandpass filter with intrinsic common-mode suppression based on a slot resonator excited by differential microstrip to slotline transitions. Reprinted from [119] with permission.

dumbbell-shaped defect ground structures (DB-DGSs) [113] and topologies based on the complementary split ring resonator, among others (see [117], [118] and [10, chapter 10]). As an illustrative example of a DGS-based balanced filter, let us report the wideband balanced filter implemented by means of a strip-loaded quadruple-mode slotline resonator reported in [122], see Fig. 31.

Another approach for the implementation of wideband balanced filters with intrinsic common-mode rejection exploits signal interference techniques [125], [126], [127], [128], [129]. The reported devices use Marchand baluns, phase shifters, and other circuit elements necessary to generate the convenient phases for the transmission of the differential mode with simultaneous cancelation of the common mode. The design of these filters is relatively simple, but their size tends to be significant, as compared to other implementations of wideband balanced filters. Recently, wideband balanced filters based on coplanar stripline resonators with substantial CMRR in the differential-mode passband have been reported [130], [131], [132], [133], [134] (in the device presented in [130] the common mode is absorbed).

B. NARROWBAND AND MULTIBAND BALANCED FILTERS AND DIPLEXERS

Concerning the implementation of balanced filters with narrow differential-mode pass bands, most implementations are based on coupled resonator topologies (see [135], [136], [137], [138], [139], [140], [141], [142], [143], [144], [145], [146], [147], [148], [149], [150], [151], [152], [153], [154], and [10, chapter 12]) It is sometimes difficult to differentiate between narrowband and wideband filters (either balanced or single-ended), since the frontier is rather diffuse (depending on the sources, the narrowband designation requires fractional bandwidths below 10 %, whereas in others, filters with fractional bandwidths as high as 20 % are considered to belong to the narrowband category). For this reason, some balanced filters reported in [10, chapter 12] (and references therein), dedicated to narrowband balanced filters, are considered to
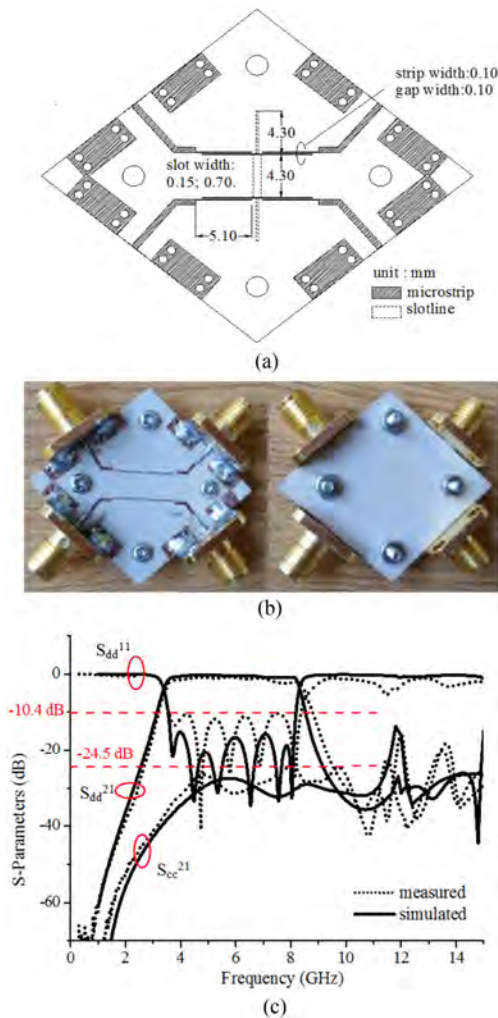
FIGURE 31. Top view layout (a), photograph including the top (left) and bottom (right) views (b), and response (c) of the wideband common-mode suppressed balanced bandpass filter implemented by means of a strip-loaded quadruple-mode slotline resonator. Reprinted from [122] with permission.

FIGURE 32. Layout (a) and frequency response (b) of the dual-band balanced filter based on magnetically coupled embedded resonators. Reprinted from [166] with permission.

be wideband filters in this review paper. Nevertheless, for the synthesis of very narrow differential-mode responses, typically with fractional bandwidths around 1 % and below, dielectric resonators have been used [155], [156], [157]. Narrowband balanced filters in groove-gap waveguide technology have also been reported [158].

Many efforts have also been dedicated to the implementation of multiband balanced filters (see [130], [159], [160], [161], [162], [163], [164], [165], [166], [167], [168], [169], [170], [171], [172] and [10, chapters 13 and 14]). In some cases, such filters have been implemented with topologies based on coupled embedded resonators (able to generate two transmission bands for the differential mode), and the working principle is similar to that of the single-ended counterparts. Let us next demonstrate the potential of coupled embedded resonators for the implementation of dual-band differential-mode bandpass filters with intrinsic common-mode suppression through an illustrative example. The considered device

was published in [166], and it consists of two magnetically coupled embedded resonators that, at the same time, are capacitively coupled to the external feeding lines [see Fig. 32(a)]. Note that this embedded open loop resonator consist of a folded stepped impedance resonator (FSIR) in which the low impedance region is replaced with another small FSIR (i.e. the small FSIR is embedded into the original and larger FSIR). With an adequate geometry, it is possible to control the position of the two first odd-mode resonances, i.e., those that determine the central frequency of the two differential-mode passbands. These frequencies do not coincide with the even mode resonances of the embedded coupled resonators, and therefore, the common-mode is suppressed at the central frequencies of the differential-mode passbands. Moreover, by virtue of the magnetic coupling between the resonators, their coupling for the (first) even mode resonance is very soft (the currents in the resonators are a minimum in the region of the symmetry plane AA'). This means that the common mode must (necessarily) be significantly reflected even at such frequency. The expected result is thus a broad common-mode

suppressed band. Fig. 32(b) depicts the frequency response of the device, where the dual-band functionality for the differential mode, as well as the broadband (and strong) common mode rejection can be appreciated (details on the geometry, substrate parameters, as well as design process of the filter of Fig. 32, can be found in [166]).

Balanced diplexers [173], [174], [175], [176], [177], [178], [179], [180], [181], [182], [183], [184], usually based on topologies similar to those of narrowband balanced filters, and reconfigurable/tunable balanced filters [185], [186], [187], have also been the subject of an intensive research activity in recent years.

C. REFLECTION-LESS BALANCED FILTERS

To end this section devoted to balanced filters, let us mention that a significant effort has been dedicated recently to the implementation of reflection-less structures, where either the common-mode (in the differential mode passband) or the differential mode (outside the differential-mode passband), or both modes simultaneously, are absorbed [92], [130], [172], [188], [189], [190], [191], [192], [193], [194], [195], [196]. Many different strategies for absorbing the common and/or the differential mode in the required frequency bands have been reported. Indeed, some of such strategies have been discussed (see, e.g., the device of Fig. 24, where power dissipation is insensitive to the differential mode, but not to the common mode). Let us report in this section an illustrative example of a reflection-less balanced bandpass filter able to absorb both the differential and the common modes, regardless of the considered input port (two-port, or bidirectional, reflection-less balanced bandpass filter). The filter schematic is depicted in Fig. 33(a). It is based on a coupled ring resonator and utilizes loading absorptive stubs at the input/output ports and at the ends of the coupled-lines. By means of these absorptive stubs, the balanced filter can realize input-/two-port wideband common-mode and differential-mode reflection-less performance from DC, as well as wide filtering band and all-stop common-mode suppression.

The circuit schematics of the filter for differential and common mode excitations are depicted in Fig. 33(b) and (c), respectively. Taking into account that the electrical lengths of the coupled lines and stubs are $\theta = 90°$ at the central filter frequency, f_0, it is obvious that for DC and for frequencies satisfying $2nf_0$ (with $n = 0, 1, 2, \ldots$), significant absorption for the differential mode is expected. However, for f_0 and the odd harmonics $(2n + 1)f_0$, the differential-mode circuit exhibits a band pass behavior (the resistors are seen as an open at such frequencies). By contrast, absorption at all these frequencies is expected for the common mode. Thus, wideband common mode absorption for the filter results. These features are corroborated by the filter response, depicted in Fig. 34, which includes the photograph and layout of the physical implementation (substrate characteristics, dimensions, and further details about this reflection-less balanced bandpass filter can be found in [196]).
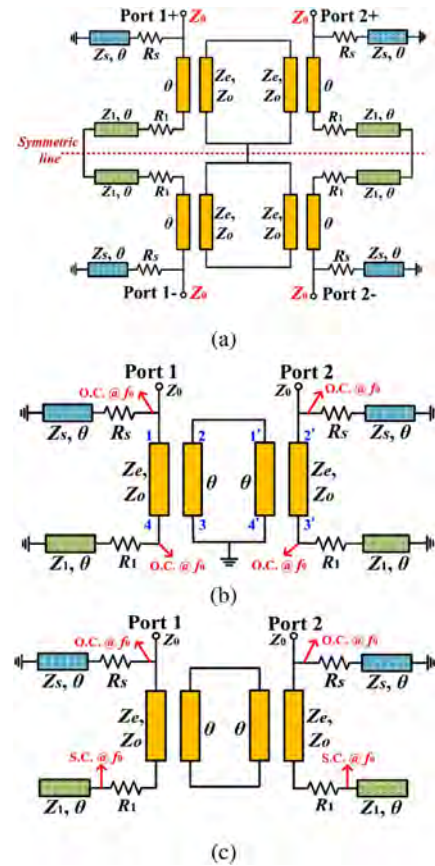
FIGURE 33. Circuit schematic of the two-port (bidirectional) reflection-less balanced bandpass filter with both differential and common mode absorption based on a coupled ring resonator (a) and equivalent circuit for the differential (b) and common (c) modes. Reprinted from [196] with permission.

V. OTHER PASSIVE BALANCED CIRCUITS

Previous sections have been mainly focused on a variety of differential microwave filtering devices, whose importance as building blocks in any microwave communication system is obvious. Due to this reason, the literature about filters has dominated the landscape of the research carried out around passive balanced microwave circuitry (see, for instance, [10], [197] and references therein). However, there are other important and ubiquitous passive components that are also of primordial importance to implement fully balanced RF/microwave front ends. In particular, the balanced versions of power distribution components, such as power dividers (PD) or directional couplers (DC) have attracted the interest of many researchers, specially during the last few years. Thus, the authors of [197] have recently published a review paper [198] focused on the study of balanced-to-unbalanced (BTU) four- and five-port filtering power dividers (FPD). At the moment of writing this paper, a significant number of contributions on balanced-to-balanced (BTB) or BTU power dividers and directional couplers is available in the literature about differential microwave passive devices. This section will present an overview of this work, with emphasis on the

FIGURE 34. Topology and photograph of the filter based on the schematic of Fig. 33(a) and frequency response for the differential (b) and common (c) mode. Reprinted from [196] with permission.
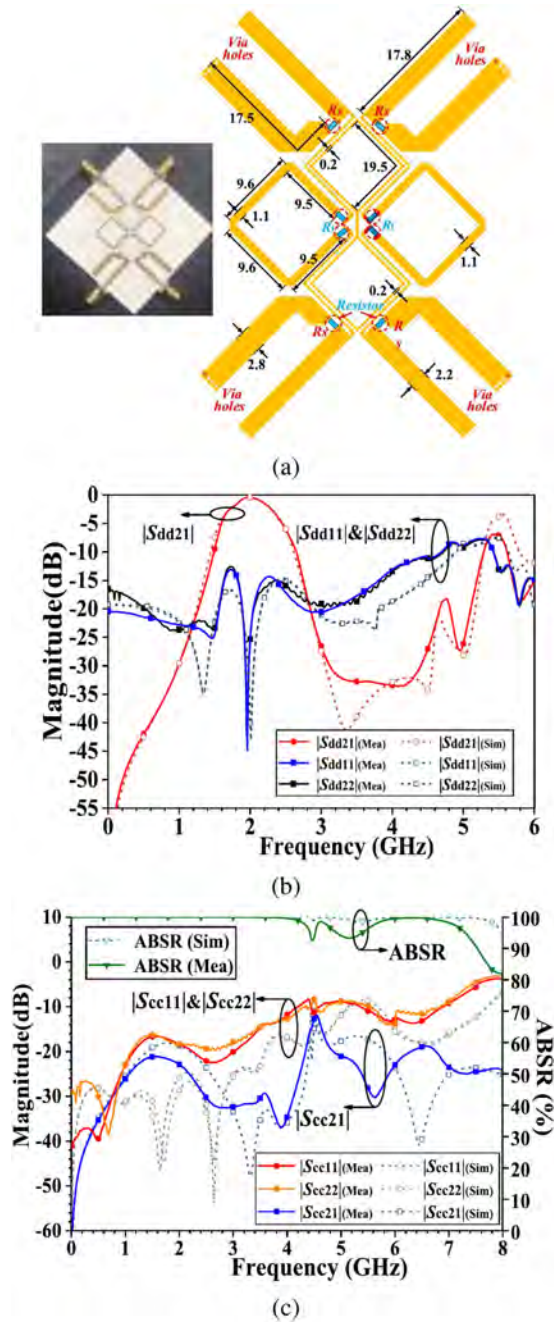

FIGURE 35. Circuit model of the balanced-to-balanced power divider/combiner proposed in [201]. Reprinted from [201] with permission.

common-mode absorption (in addition to reflection) will be briefly considered.

A. BALANCED-TO-BALANCED POWER DIVIDERS

A straightforward manner to build a three-port BTB divider/combiner would consist on adding baluns to each of the three ports of a single-ended divider/combiner. However, smaller size and lower losses are expected if a differential-mode divider whose ports are fully balanced is designed, combining power divider and balun functions in a single circuit. Although some previous attempts can be found in the literature, one of the first proposals of a differential power divider was reported in [200], although isolation between output ports was not considered in that work. The first available solution working as a true BTB PD (i.e., fulfilling all the theoretical constraints required for its ideal operation) can be found in [201]. The device proposed in [201] has three differential ports (named A, B and C, corresponding to six single-ended ports), and it is based on an appropriate interconnection of ideal microstrip transmission line sections and resistors having the topology shown in Fig. 35 (differential port A is formed by the pair of single-ended ports 1 and 4, B by 2 and 3, and C by 5 and 6). The power entering through port A is equally split into ports B and C (equal power division is then assumed). Due to the reciprocity and symmetry properties of the proposed circuit, its electrical response can be described by means of two 3 x 3 scattering matrices. The elements of such matrices are related through a set of analytical equations obtained after enforcing the set of constraint rules leading to the ideal performance for the differential signal (perfect matching at the three ports, perfect isolation between ports B and C and equal power division). The constraints for the common-mode signal (perfect reflection of the common-mode signal and vanishing mode conversion) should also be enforced. The details of these rules and the corresponding associated equations are described in depth in [201]. Since the circuit in Fig. 35 has a horizontal symmetry plane, even/odd

material not covered in previous review papers. Thus, for instance, in [198] the reader can find additional information about BTU devices, which will not be treated here. Nevertheless, note that BTU dividers are also relevant to the design of BTB devices since, for example, they can be combined with single-ended dividers to implement 1 to 2^n way BTB power dividers, as explained in [199]. In any case, this section will mainly focus on BTB power dividers and BTB directional couplers. Designs that incorporate other functionalities (such as filtering) will also be considered. Devices providing
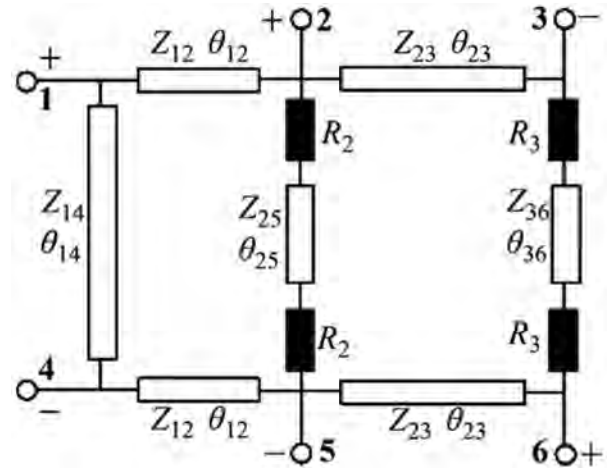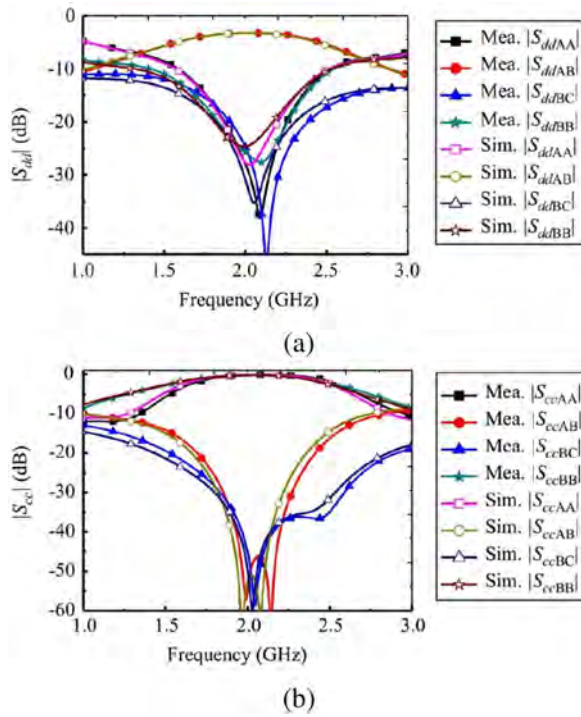
FIGURE 36. Simulated and measured differential (a) and common-mode (b) scattering parameters for the prototype reported in [201]. Reprinted from [201] with permission.

FIGURE 37. Diagram (a) and topology (b) of the arbitrary power division BTB power divider proposed in [202]. Reprinted from [202] with permission.

FIGURE 38. Layout of the BTB power divider proposed in [204]. (a) 3D view and (b) top view. Reprinted from [204] with permission.

mode analysis can be applied and, finally, the constraint rules establish the form required for the 3 x 3 scattering matrices of the even- and odd-mode equivalent circuits in order the whole device to behave as an ideal BTB power divider/combiner. Indeed, the form of those matrices suggests the topology of the proposed circuit. The analytical restrictions are strictly valid at the central frequency of operation (for which the electrical lengths $\theta_{14} = \theta_{25} = \theta_{36} = \pi$; see Fig. 35). At such frequency the theoretical scattering matrix corresponds to a perfectly matched power divider/combiner for the differential signal, with perfect isolation between ports B and C under DM excitation. Total reflection and perfect isolation between balanced ports for CM excitation are also obtained. However, a detailed study concerning the bandwidth of operation of the relevant parameters (for certain prescribed levels of the figures of merit) is necessary. This study is also reported in [201]. In Fig. 36 some of the results reported in [201] for the fabricated prototype are shown. Cross-mode scattering parameters are also provided in the original paper. For the fabricated prototype a measured FBW ($|S_{ddAA}|$, $|S_{cdAA}|$, $|S_{dcAB}|$ below -15 dB) of 20.8% (25% for the simulated data) is achieved.

Note that the circuit proposed in [201] was suitable for equal power division. However, an arbitrary power division ratio is required in many applications. In this way, for instance, a BTB Gysel power divider with arbitrary power division ratio was introduced in [202] by the same authors. Once again, the design method is developed analytically, enforcing the pertinent constraint rules for the required operation. The

proposed topology is the one shown in Fig. 37. The authors conclude that the maximum realizable power division ratio is 1:4.69 (the characteristic impedance of the transmission lines is considered to be limited to the range 20-120 Ω). Unequal BTB power dividers with wideband common-mode suppression over a large bandwidth, good isolation and high values of power ratio between output ports can be implemented by

using two ideal double-sided parallel-strip line (DSPSL) 180° phase inverters with isolation resistors, as explained in [203].

A differential Wilkinson type power divider with relatively small size and enhanced bandwidth for matching and isolation can be implemented by arranging two identical single-ended dividers in a back-to-back configuration by introducing rectangular apertures and slots in the shared ground plane [204]. The proposed structure is depicted in Fig. 38. Under DM operation, the rectangular aperture and the U-shaped slot etched in the common ground plane behave as a virtual perfect electric conductor, in such a way that the DM response does not differ from the one of each of the single-ended dividers obtained assuming a solid ground plane. However, the CM response is strongly affected by the presence of such aperture and slot. The dimensions of the elements etched in the ground plane are optimized through a parametric study to achieve good CM suppression as well as good isolation. The authors report a return loss (RL) level better than 15 dB over a 85 % FBW. Isolation better than 20 dB is achieved over 44 % FBW for the differential mode and 55 % for the common mode. CM suppression better than 20 dB is also reached over 44 % FBW. Besides, mode conversion remains below −20 dB for the whole considered frequency band.

B. FILTERING BALANCED-TO-BALANCED POWER DIVIDERS

Balanced power dividers can be designed to incorporate filtering properties (a functionality different from power division), without the need of adding balanced filter stages. Obviously, the co-design of the BTB divider and filter reduces the overall size of the circuit and the loss level. To the authors knowledge, the first proposal of a BTB filtering power divider (FPD) can be found in [205]. In particular, the structure is a BTB Gysel power divider with bandpass filtering response. The coupling scheme of the structure is shown in Fig. 39, as well as the schematic implementation suggested by the authors. Note that the ring can be regarded as formed by four microstrip resonators coupled through shorted stubs. Using some circuit equivalences valid when the characteristic impedance of the shorting stubs is half of the characteristic impedance of the ring, standard filter design methods can be applied to simultaneously obtain the power division and the filtering functions. According to [205] the main limitation of the proposed structure is the achievable DM bandwidth. Taking into account several considerations about minimum and maximum bandwidths (for given required levels of isolation, mode conversion or suppression as well as realizable characteristic impedances), the authors conclude that a range from 3 % to 12 % FBW can be covered with the proposed structure. Two prototypes are fabricated and measured, one of which uses uniform transmission lines whereas the other, for miniaturization purposes, makes use of stub loading (i.e., the transmission line sections are replaced with equivalent slow-wave structures). A photograph of the miniaturized version (about 50 % smaller than the original implementation) is depicted in Fig. 40. The measured and simulated results reported in [205] agree very well for the two fabricated prototypes. However,
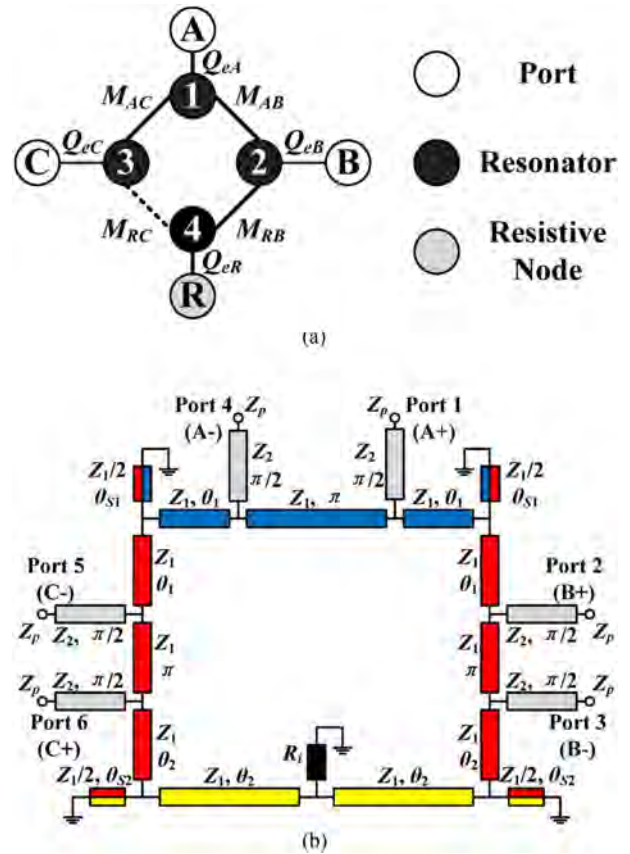
FIGURE 39. Coupling scheme (a) of the bandpass filtering BTB Gysel divider proposed in [205] and schematics (b) of its implementation. Resonator 1 is represented in blue, resonators 2 and 3 in red, and resonator 4 in yellow. Reprinted from [205] with permission.
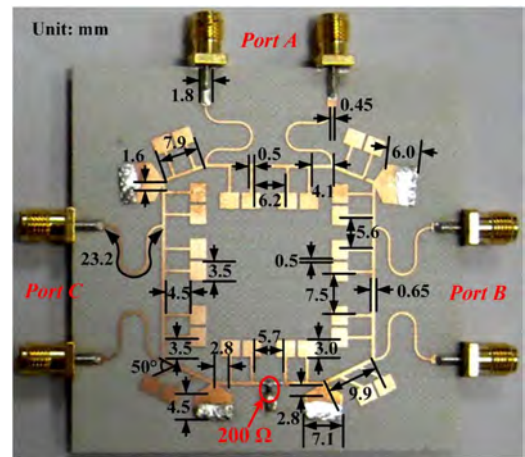
FIGURE 40. Photograph of the stub-loaded bandpass filtering BTB Gysel power divider in [205]. Reprinted from [205] with permission.

the rejection bands of the miniaturized prototype for common-mode noise and mode conversion are 21 % smaller when compared to the original structure based on uniform transmission lines. Nevertheless, in-band losses are only slightly higher for the miniaturized version (0.13 dB).
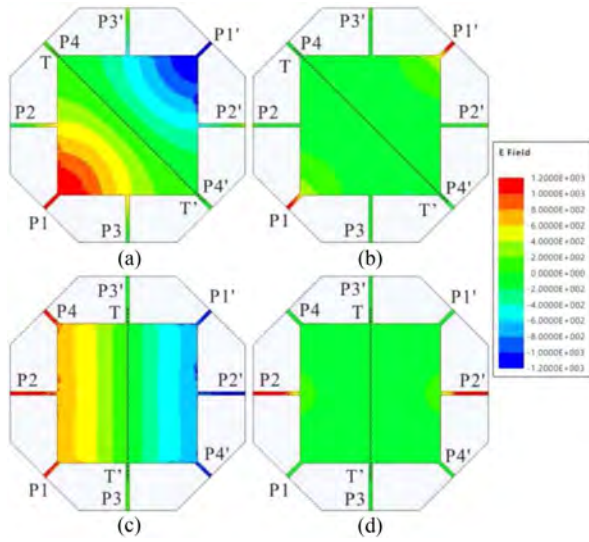
FIGURE 41. Simulated electric field distributions on the prototype at the center working frequency under distinctive excitation schemes according to [208]. (a) DM excitation on ports 1 and 1′. (b) CM excitation on ports 1 and 1′. (c) DM excitation on ports 2 and 2′. (d) CM excitation on ports 2 and 2′. Reprinted from [208] with permission.

FIGURE 42. Layout of the second-order balanced-to-balanced filtering power divider [208]. Reprinted from [208] with permission.

Note that the configuration used in [205] involves resonators working on second-order resonance. This fact leads to an increase of the circuit size. To solve this problem, a modified version of the implementation in [205] was proposed in [206], where short-stub-loaded resonators (SSLR) were used instead (remind that the dominant resonant frequency of SSLR is the even-mode resonant frequency). This simple modification yields a smaller structure (when compared with [205]) with excellent CM suppression (>60 dB over a wide frequency band around the central frequency). Unfortunately, insertion losses are worse than those reported in [205]. Finally, let us mention, as another interesting and recent example of BTB Gysel FPD with arbitrary power division, the circuit reported in [207].

A different strategy to implement BTB FPD makes use of patch resonators [208] (in particular, square patch resonators were used in that paper). Advantages of using patch resonators (when compared with microstrip line resonators) are the expected lower losses and the better power handling capabilities. The working principle of this device is strongly based on the analysis of the mode field distributions in the patch. Due to the degeneracy of the patch TM_{nm} and TM_{mn} modes, they can be simultaneously excited. Under the weight 1:1, four mixed modes are obtained corresponding to 4 combinations whose field distributions have relevant symmetry properties concerning the purpose of implementing the kind of devices that we are considering. In Fig. 41 the basic geometry of the power divider is schematically shown. The square resonator has 8 symmetrically distributed ports where 1 and 1′ form the balanced input port. Ports 2 and 2′ and 3 and 3′ are the balanced output ports. Finally, ports 4 and 4′ are terminated with the appropriate impedance to yield perfect isolation and matching. The represented field patterns for different DM and
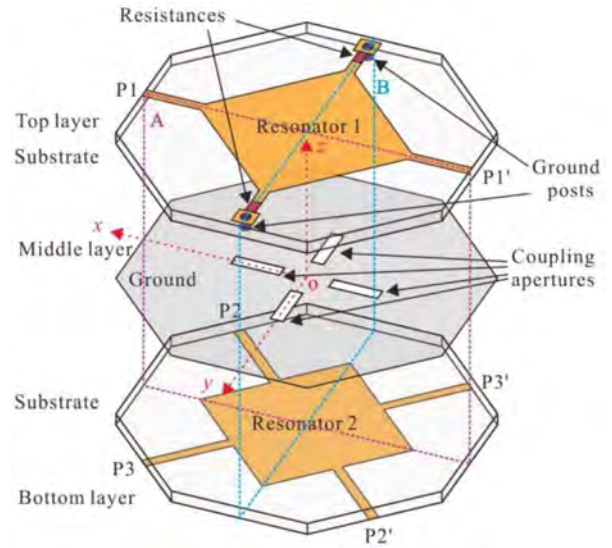
CM excitations (see Fig. 41) intuitively explain the working principle leading to equal power division for DM excitation and perfect CM suppression, as well as perfect isolation at the central frequency of operation (detailed explanations are given in [208]). If two of these square patches are mounted as shown in Fig. 42, in a back-to-back configuration with four slots in the ground plane to control the coupling between the resonators, the filtering BTB PD can be implemented. This structure was fabricated and measured with excellent in-band performance [208]. However, there was still place to improve the out-of-band rejection by properly modifying the feeding of the top square resonator, in such a way that the differential harmonic passband associated with mode 4 is eliminated. A similar structure, but this time based on the use of circular patches, has recently been used [209] to design a BTB FPD with arbitrary power division. Even more recently, circular patches and similar concepts have been utilized to implement a BTB PD with dual-band filtering characteristics [210].

High-selectivity and isolation for a BTB FPD can be achieved as suggested in [211], where a combined microstrip-slotline circuitry is employed (see the layout in Fig. 43). Ultra-wide band power division response is obtained by means of a uniform impedance slot T-junction. Symmetrical L-shaped microstrip/slotline transitions together with stub-loaded resonators are used to obtain a good filtering bandpass response, with two transmission zeros (TZ) used to improve the filter selectivity. Finally, the three ports are fed through a balanced microstrip/slot transition involving a U-shaped microstrip structure coupled to a stepped-impedance slot. This structure provides wideband transmission from the microstrip to the slotline under DM operation, while, at the same time, due to its symmetry properties and the nature of the slot mode, CM is intrinsically blocked (the slotline cannot be excited by the CM fields). This kind of microstrip/slot transitions were

TABLE 2. Comparison of Several Balanced-to-Balanced Filtering Power Dividers

Ref.	f_0 (GHz)	FBW (%)	RL (dB)	IL (dB)	In-band DM Isolation (dB)	CM rejection (dB) / (dB) / frec. range (GHz)	CM DM conv. (dB) f range (GHz)	Size ($\lambda_g \times \lambda_g$)
[205] (I)	2.02	8.4	12.6	0.73	>19	>20 / (1.32-2.68)	>20 / (1.24-2.67)	0.97 × 0.87
[205] (II)	2.01	7.7	15.8	0.86	>27.4	>20 / (1.39-2.45)	>20 / (1.35-2.47)	0.67 × 0.63
[206]	2.395	7.0	21	2.21	>20	>60 / (0-3.24)	>30 / —	0.46 × 0.40
[208] (I)	1.8	18.2	>20	1.08	>29.5	>52 / (0-3.25)	>44 / (0-5 GHz)	0.55 × 0.55
[208] (II)	1.8	11.7	>20	1.02	>32.1	>55 / (0-3.35)	>45.5 / (0-5 GHz)	0.55 × 0.55
[209]	1.86	10	>10	0.93	>27.4	>54.4 / (in-band)	>38.4 (0-5 GHz)	0.9 × 0.8
[211] (I)	2.76	15.9	>25	0.6	>18	>43 / (0.6-8.0)	—	0.60 × 0.45
[211] (II)	3.0	23.3	>15	0.8	>20	>43 / (0.6-8.0)	—	0.60 × 0.45
[216]	3.0	49.31	10	0.9-1.0	>20 (0-4.23 GHz)	>15 / (2.39-3.16)	>20 / (0-6 GHz)	1.0 × 0.63
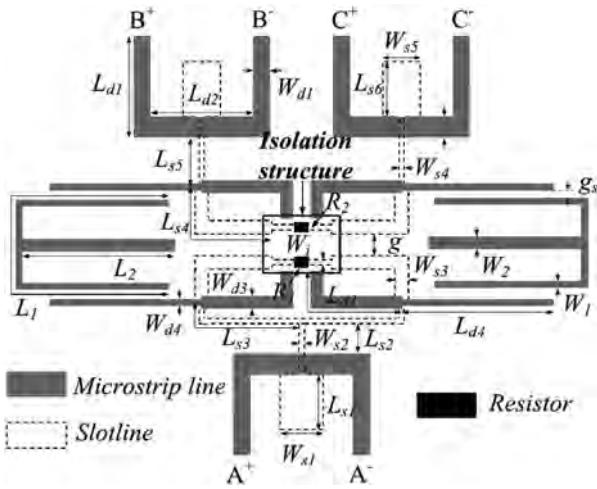
FIGURE 43. Layout of the second-order BTB in phase FPD reported in [211]. Reprinted from [211] with permission.

studied, and their CM rejection properties exploited, in [122], [212], [213], just to mention a few examples. They have frequently been used in the implementation of balanced structures. For instance, apart from the discussed example [211], the three balanced ports of a BTB FPD with dual-band frequency response described in [214] use the same type of transition (although they are followed by other components to provide the dual-band response, of course). Another example of this strategy can be found in [215]).

The literature still offers other paths to design BTB FPD. For instance, the design proposed in [216] reports on a balanced power divider with wideband filtering characteristics. The device is composed of coupled-line sections, $\lambda/4$ transformers and isolation resistors. Port-loaded coupled-line stubs introduce TZs improving the selectivity (differential response). For common-mode excitation the proposed circuit behaves as a bandstop filter, with >12 dB rejection level over 141 % bandwidth. As a final example, let us mention that metamaterial concepts have also been applied in this context. Thus, for example, differential-mode composite right-left handed (CRLH) transmission lines have been successfully applied to design differential power splitters with filtering response and common-mode rejection in [217]. In order to have an idea about typical achieved performances of filtering BTB power dividers, Table 2 summarizes some relevant figures of merit for several of the designs discussed in this subsection. In some cases, two different designs are reported in the same reference (labeled as I and II). All the compared circuits have a bandpass filtering response with center frequencies in the range 1.8 GHz to 3.0 GHz. Most of the examples correspond to relatively narrowband filtering responses, except the last one [216] whose FBW is close to 50%. The reported IL exclude the intrinsic 3 dB corresponding to the lossless operation of the equal-power dividers. The in-band DM isolation between the output ports is satisfactory in all cases. Excellent CM rejection levels are reported in [206], [208], [209], [211] over a wide range of frequencies, and the designs reported in [208] stand out due to their excellent DM - CM conversion.

C. BALANCED DIRECTIONAL COUPLERS

Directional couplers (DC) are other class of basic power divider component for high-frequency circuits. They have been used for decades and implemented using very different technologies (waveguide, microwave integrated and monolithic circuitry, substrate integrated waveguide, etc.). In principle, to realize quadrature differential signals, a single-ended quadrature coupler followed by a balun could be used. However, obviously, differential couplers would make unnecessary baluns, resulting in more compact and less lossy solutions. Thus, a significant effort has been devoted in recent years to develop balanced versions of these circuits too. To the best of our knowledge, the first quadrature differential coupler was based on a set of four edge- and broadside-coupled microstrip lines and implemented monolithically in a coplanar configuration [218] (see Fig. 44). All the input-output differential lines are 50-Ω coplanar strip (CPS) transmission lines. The four coupled microstrip lines, which have all the same width, behave as the differential version of a typical proximity coupler. The authors apply an approximate even-odd mode analysis to estimate the critical dimensions, although a full-wave optimization is required to calculate the final coupler dimensions. The total length of the coupler is reduced using a slow-wave version of the coupled lines (periodically corrugated strips). The simulated and measured data in [218] were reasonably good over a wide frequency band in the millimeter-wave region (15-45 GHz). In this subsection an overview of more
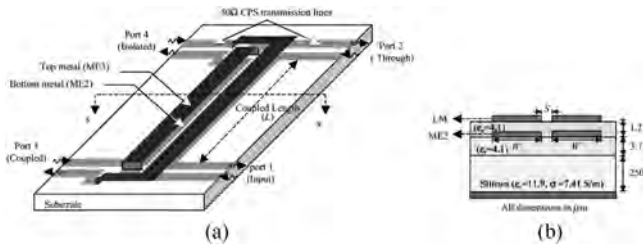
FIGURE 44. (a) Monolithic implementation of the wideband differential coupler in [218]. (b) Cross section through the coupler at location xx shown in (a). Reprinted from [218] with permission.

recent implementations of the balanced version of this well known device will be presented.

1) COUPLED-LINE BALANCED COUPLERS

Proximity balanced DC of the type reported in [218] (coupled-line couplers) can be designed using analytical expressions if the system of four identical coupled microstrips are symmetrically placed between two ground planes, in such a way that the whole structure has two symmetry planes (vertical and horizontal), as it is described in [219]. These symmetries are reflected in the structure of the per unit length (p.u.l.) capacitance and inductance matrices of the coupled section. This greatly simplifies the calculations. Indeed, only four capacitances, corresponding to the four orthogonal TEM modes supported by the structure (even-differential, odd-differential, even-common, and odd-common), each corresponding to a single strip line with vertical and horizontal symmetry planes behaving as electric or magnetic walls, are required. These parameters and the length of the coupled section completely determine the scattering parameters of the structure, which can be arranged in a 8×8 matrix (single-ended excitation) or into a 4×4 matrix for differential (or common) excitation. At the central frequency of operation (for which the length of the coupled section is $\lambda/4$), the four differential ports are required to be matched. Besides, the power entering through one of the ports (port 1) is derived to other two ports (ports 2 and 3) being the fourth port isolated. Once established the desired coupling factor (i.e. the information about how much power is transferred to the through, 2, and coupled, 3, ports) standard theory of stripline coupled-line couplers can be applied to obtain the widths and separation gaps for the four identical coupled strips. Two designs (with 3 dB and 8 dB coupling factors) are presented in [219]. Due to the symmetry of the structure, mode conversion is extremely weak. The measured return loss for differential-mode operation is well above 30 dB for the two designs, and the measured directivity (isolation minus coupling in dB) is also very good (around 26 dB at the central frequency for the 8 dB coupler). However, common-mode rejection is not contemplated in this design.

The bandwidth of coupled-line couplers can be significantly extended using cascaded coupled-line sections, as it is well known for the case of single-ended versions of this
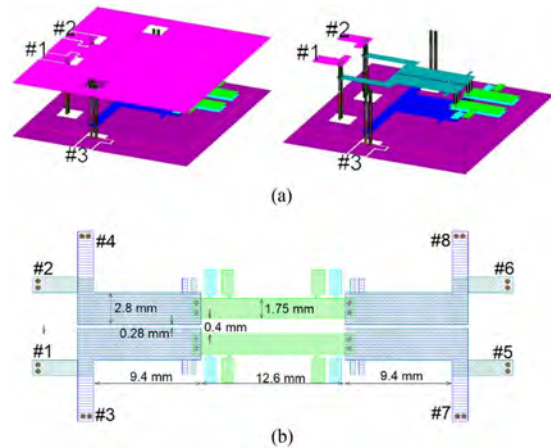
FIGURE 45. (a) 3-D view of one half of the directional coupler described in [220] with and without the top metallized layer. (b) Top view of the entire coupled-line coupler. Reprinted from [220] with permission.

class of devices. For the balanced version, this is demonstrated in [220], where two weakly coupled sections and a central tightly coupled one are cascaded and interconnected to increase the bandwidth of a single section design (only the differential mode is considered in the study). The interconnection between successive sections is carried out using buried vias. The need for buried vias comes from the fact that coupled strips are printed at different levels to obtain the required coupling for each of the involved sections (the geometry of half of the three-section structure proposed in [220] is reproduced in Fig. 45 for clarity). A method to alleviate this technological difficulty is to allow the width of the coupled strips printed at the two different levels to be different. Thus, in [221] the authors describe a manner of implementing coupled-line sections with different coupling levels using the same metallization layer, thus avoiding the buried vias. Note that in the previously mentioned coupled-line DCs, CMRR is not explicitly considered. In [222] this problem is addressed by adding a simple section that provides good common-mode rejection to a balanced coupled-line structure based on coplanar-waveguide transmission lines, instead of microstrip lines. The structure uses a single substrate with two-side metalization. Due to the existence of two planes of symmetry, the design is relatively simple. The penalty is a larger size of the overall circuit due to the addition of the CM rejection section.

Let us close this brief overview on balanced coupled-line DC mentioning the non-symmetric and non-homogeneous implementation reported in [223]. In the structure proposed in [223] the width of the metal strips and their separations, in the top and bottom sides of the supporting substrate, are different (i.e., in the top side there are two strips having width w_1 separated a distance s_1 and in the bottom side there are two strips of width w_2 separated a distance s_2; an additional dielectric or air layer separates this structure of the ground plane). The inhomogeneity of the dielectric introduces a well-known deleterious effect on the electrical response. Due to this reason, a detailed study on the incorporation of

FIGURE 46. Circuit model (a) and microstrip layout (b) of the balanced branch-line coupler proposed in [225]. The 180° lines are folded for miniaturization purposes. Reprinted from [225] with permission.
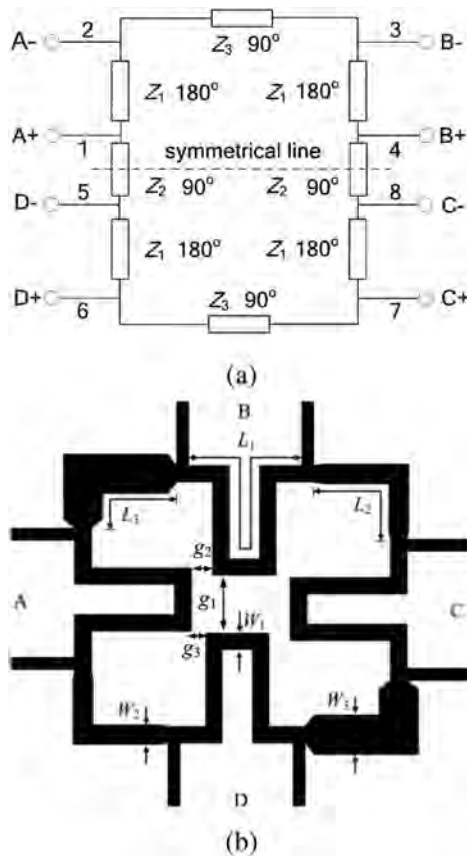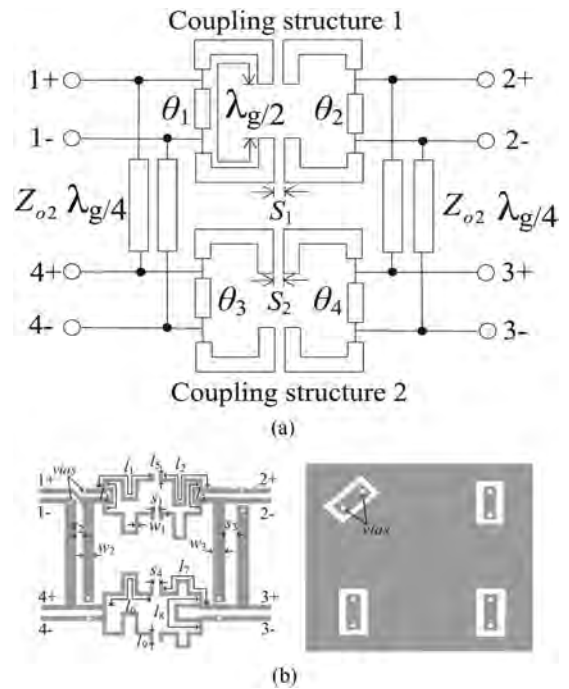

FIGURE 47. Circuit model (a) of the filtering branch-line coupler proposed in [226] and its microstrip layout (b). Reprinted from [226] with permission.

compensating elements is reported in [223]. The proposed structure is fabricated using a combination of laminate and additive manufacturing technologies. The measured data reveal a satisfactory performance thanks to the compensation of the difference between electric and magnetic coupling. Other compensation methods employed to improve the directivity of singled-ended differential couplers can also be used for differential versions [224].

2) BALANCED BRANCH-LINE AND RAT-RACE COUPLERS

Branch-line and rat-race are among the most widely used microwave couplers. They involve the interconnection of four $\lambda/4$ transmission line sections (branch-line) or three $\lambda/4$ sections plus one $3\lambda/4$ section (rat-race) forming a ring. Both devices have 4 accessible ports. Once again, a balanced design prevents the necessity of adding baluns, in such a way that, in the last few years, many balanced versions of those popular devices have been proposed. In consequence, a meaningful variety of balanced branch-line and rat-race couplers are available nowadays. Let us start with the design described in [225], where a balanced branch-line coupler with arbitrary power division ratio is proposed. The circuit model and the corresponding microstrip layout are depicted in Fig. 46. Due to the presence of the symmetry plane (see Fig. 46(a)) the

even/odd mode analysis can be applied to facilitate the calculation of the scattering matrix elements. If the excitation balanced port is A, ports B and C are the output ports, D being the isolated port. An arbitrary power division ratio for ports B and C ($k = |S_{ddBA}|^2/|S_{ddCA}|^2$) can be imposed. Adding the conditions of perfect matching for the four differential ports, isolation between ports A-D and B-C, perfect reflection of the common mode, and absence of mode conversion, it is relatively straightforward to obtain the structure of the scattering matrix [225]. The relations between the elements of the scattering matrix and the line characteristic impedances are finally obtained with the help of the aforementioned even/odd mode formalism. Finally, a parametric analysis is used in [225] to determine Z_1 (see Fig. 46) in order to maximize the operation bandwidth (Z_2 and Z_3 are determined by k and Z_0). The authors report measured data for three prototypes (having $k = 1, 2, 4$). The nominal values of k are experimentally reproduced with less than 1 % of error. The matching and isolation bandwidths (for 15 dB level) for the worst case ($k = 1$) are 4.3 % and 5.1 %. Much wider bandwidths can be achieved by using the dual-stage version of this design, as it is demonstrated in [225] through HFSS simulations.

Balanced branch-line couplers that incorporate filtering functions are also of practical interest, since they combine two functions in a single device. One of the first implementations of this type of circuit was introduced in [226]. The schematics of the circuit and its microstrip layout are shown in Fig. 47. The first step is to design a conventional branch-line coupler but substituting the $\lambda/4$ transmission
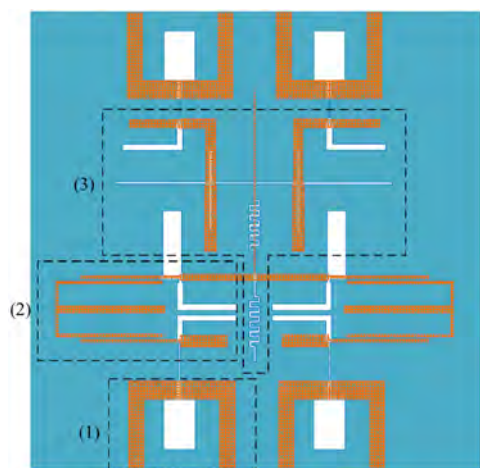
FIGURE 48. Configuration of the BFDC described in [229]. The top side microstrip structure is represented in brown color, the white regions being slots etched in the ground plane. The three main building blocks providing high CMRR (1), filtering and selectivity (2), and enhanced isolation (3) are highlighted (regions limited by dashed lines). Reprinted from [229] with permission.

line sections with coupled-line sections of the same electrical length. Under differential-mode excitation, the equivalent circuit corresponds to a single-ended version. However, the obtained device has poor common-mode rejection. In order to improve CMRR, the horizontal coupled lines are replaced by the coupled-line-fed coupling structures shown in Fig. 47 (coupling structures 1 and 2). These modified sections provide both common-mode suppression and the desired filtering function for the differential-mode signal. The half-wavelength transmission lines used in [225], [226] can be replaced with broadband 180° phase inverters [227] implemented in DSPSL technology, thus leading to a more compact design. The fabricated prototypes [227] exhibit excellent electrical performance concerning differential-mode matching level and broadband common-mode suppression. Besides, as an additional advantage, dual-band and triple-band operation is feasible. Other dual-band implementations have been proposed in the literature more recently [228].

A different type of balanced filtering directional coupler (BFDC) has been implemented combining microstrip and slotline circuitry. A recent example of this approach can be found in [229] (a schematic representation of the layout is depicted in Fig. 48). In that paper a U-shaped microstrip/slotline transition is used at each of the four ports to obtain high CMRR. This type of transition feed structures are used at the input and output ports of many balanced designs to make the DM response independent of the CM one and to achieve good CM suppression. In [229] two stub-loaded resonators are employed to introduce the filtering response, whose selectivity is enhanced by adding L-junction slotlines. Odd-even mode phase velocity compensation structures are also included in the ground plane, in the form of U-shaped bending slotline geometries, with the purpose of improving isolation.

Another interesting BFDC based on slotline structures, providing similar functionalities, and exploiting similar ideas (for instance, U-shaped microstrip/slotline transitions to enhance the CM rejection response), can be found in [230]. In that paper self-packaged substrate integrated suspended slotline (SISSL) technology is used and two out-of-band transmission zeros (TZs) are introduced and controlled using a three-line cross-finger-coupled resonant structure. This structure enhances the selectivity of the DM passband. The authors add parallel branches and asymmetric capacitive branches to each branch line with the aim of flattening the coupling response. SISSL technology was also used in [231] to design a BFDC. In that paper a simple branch-line coupler based on SISSL was designed (taking into consideration the differences with the conventional branch-line microstrip coupler), and the structure was connected to the four balanced microstrip ports using the already mentioned U-shaped microstrip/slotline transitions, which inherently suppress the common-mode transmission. The measured designs reported very good CM rejection over a wide frequency band, as well as good filtering characteristics. The design process is relatively simple in comparison with other alternative implementations of this kind of balanced circuits. Another simple implementation based on branch slotline structures can be found in [232]. The intrinsic differential nature of the slotline is also employed in the design of wideband BTB differential couplers (branch-line and rat-race) [233] making use of the so-called multimode star junction [234]. This junction leads to size reduction and wideband common-mode suppression. However, the differential signal of the slotline ports must be extracted using a suitable slotline-to-differential microstrip transition, thus enlarging the size of the circuit. In any case, it is an interesting and original solution providing very wide bandwidths for CM rejection ($>375\%$) and DM-to-CM conversion ($>150\%$) (a threshold of 15 dB has been considered to establish these values).

Rat-race couplers in its balanced version have also been studied in recent years. Although in [235] a differential rat-race coupler was introduced in the context of the design of a double-balanced mixer, no attention was paid to important issues, such as CM suppression. The detailed analysis and the design of more sophisticated versions of balanced rat-race couplers has been accomplished more recently. Thus, for instance, in [236] a BTB rat-race circuit where CM suppression is achieved using a defected ground structure is described in detail. The layout of the microstrip side and the defected ground slotline side are shown in Fig. 49. The device exhibits the expected rat-race response for the DM and good CM suppression over a 11% FBW. An interesting paper reporting on the implementation of several classes of six-port balanced rat-race couplers with wideband common-mode suppression can be found in [237]. DSPSL technology is employed in that paper, thus allowing easy substitution of $\lambda/2$ transmission line sections with DSPSL-based phase inverters. The derived advantages are wideband operation and common-mode suppression, size reduction and lower in-band losses. Besides, the
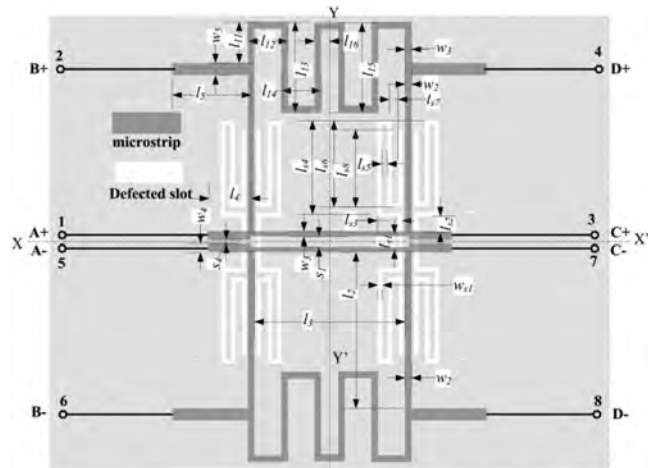
FIGURE 49. Balanced-to-balanced rat-race coupling network proposed in [236]. Reprinted from [236] with permission.

six-port structure can be used as a differential-mode circuit or as a single-ended-to-balanced device (multiple functionality). The proposed device can also provide arbitrary power division ratio. Two demonstrators designed for a central frequency of 0.9 GHz are presented in [237] (for equal and non-equal power division). Very good performance in terms of bandwidth operation and common-mode suppression were reported.

D. BALANCED POWER DIVIDERS AND COUPLERS WITH COMMON-MODE ABSORPTION

As it has been treated in previous sections devoted to filtering devices, the suppression of the common-mode in balanced structures is usually carried out imposing strong reflection of such component of the input signal. However, partial or total absorption of the common-mode signal has been proposed as a better solution [51]. This strategy has also been employed in the case of BTB PD. Several examples using different approaches can be found, for instance, in [239], [240], [241]. Thus, [240] incorporates appropriate constraint rules including the common-mode absorption requirement, and a relatively simple circuit satisfying such rules is proposed. The solution presented in [241] is specially interesting since leads to extremely wideband common-mode suppression bandwidth for both balanced-to-balanced and balanced-to-unbalanced structures (200 %, $|S_{cc}^{21}|$ better than -15 dB). Besides, absorption >85% is achieved over 116 % bandwidth for BTU power dividers and 71.2 % for BTB PD. The layout (3D view, front-side and back-side views) of the BTB power divider design is shown in Fig. 50.

To close this section devoted to balanced power dividers and couplers, let us mention that tunable and reconfigurable versions of these devices have also been subject of attention. For this topic the reader is referred to a recent review paper that covers the literature in depth and detail [242].
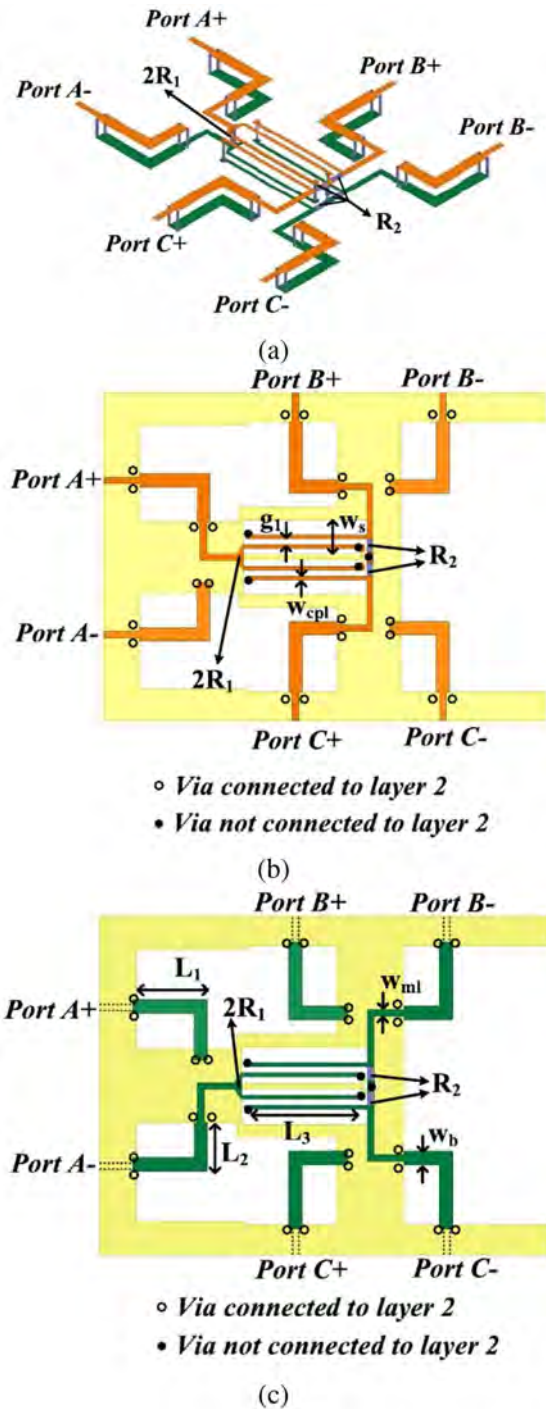
FIGURE 50. 3D representation (a), front-side (b) and back-side (c) views of one of the structures proposed in [241] (B-B PD) achieving an excellent wideband reflection and absorption response for the CM operation. Reprinted from [241] with permission.

E. BALANCED PASSIVE PHASE SHIFTERS

In order to finish this section let us devote a few words to the balanced version of passive phase shifters, whose study has also been object of some attention in the recent literature. Only a few references will be included here. Balanced digital phase shifters were proposed some time ago [243] (additional

classical references can be found in this paper), but no attention was paid to common-mode performance. Common-mode suppression has been considered more recently in this class of devices. Thus, for instance, in [244] the authors propose a balanced phase shifter based on a coupled line loaded with a transmission line connected to the central point of the coupled line section plus the reference line. The proposed circuit provides RL > 15 dB for a FBW of 80%, 88% and 98% depending on the implemented phase shift ($90° \pm 5.5°$, $60° \pm 4.2°$, $30° \pm 2.5°$). The phase shift bandwidth for the mentioned values are, respectively 93%, 88% and 81%. Finally, CM suppresion of more than 10 dB is achieved over FBW of 77%, 70% and 68% for each of the chosen phase shifts. A wideband phase shifter with common-mode suppression and filtering properties is described in [245]. In this design the main branch and the reference branch of the phase shifter incorporate similar filtering structures, based on coupled lines and a multimode T-shaped resonator. As a consequence of the design of the two branches, the structure provides, simultaneously, differential-mode passband and common-mode suppression (for both, the main and the reference lines). Filter synthesis methods are applied to obtain the filtering response of the DM and a step-by-step design method is reported by the authors. Another advantage of the solution proposed in [245] is its simple fabrication in single-layer PCB technology. The same authors proposed a different design leading to a very wide shift range ($30°$ to $180°$) with excellent phase deviation and common-mode suppression over large FBW. Synthesized, simulated and measured data agree very well and the structures are implemented in a single-layer PCB. To finalize this subsection, let us mention that microstrip/slotline designs have also been suggested to implement balanced phase shifters. A very recent example can be found in [246], where a Schiffman design is proposed. In that paper the authors make use of the U-shaped microstrip/slotline structures mentioned in previous sections, in such a way that only the DM response has to be considered. Thanks to the use of the U-shaped structures in all the ports of the device, CM is strongly suppressed in the whole frequency range of operation (> 40 dB).

VI. BALANCED MICROWAVE SENSORS

In this section, the focus is on balanced, or differential-mode, microwave sensors. Such sensors consist of two independent (single-ended) sensors, one devoted to the so-called reference (REF) material, or measurand (i.e., the input variable), and the other one devoted to the material (or measurand) under test (MUT) [11]. The main relevant advantage of balanced sensors over their single-ended counterparts is their major robustness against cross-sensitivities related to ambient factors, such as temperature, humidity, or atmospheric pressure. At the typical scale of the sensors, environmental factors are seen as common-mode stimuli by differential sensors. Consequently, the effects of ambient factors, or other common-mode undesired stimuli, are minimized in differential-mode sensors.
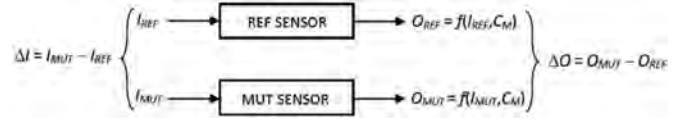

FIGURE 51. Sketch of the differential-mode sensor concept.

A. THE DIFFERENTIAL-MODE SENSOR CONCEPT

In a differential-mode measurement, the differential variable to be measured is the difference between the measurand in the REF sensor, I_{REF}, and the measurand in the MUT sensor, I_{MUT}. Thus, the differential input variable is $\Delta I = I_{MUT} - I_{REF}$. The differential output variable is simply the difference between the output variables of each independent sensor, in response to the respective input variable, i.e., $\Delta O = O_{MUT} - O_{REF}$ (see Fig. 51). As mentioned, the key aspect of balanced sensors is their capability to suppress the effects of common-mode signals, or variables. However, this aspect requires further analysis, since absolute cancelation of cross-sensitivities related to common-mode variables is not possible, in general [11]. Let us consider that the output variable of the REF and MUT sensors is also sensitive to an external common-mode variable, designated as C_M, and let us define the transfer function of the sensors as

$$\Delta O = O_{MUT} - O_{REF} = f(I_{MUT}, C_M) - f(I_{REF}, C_M) \tag{13}$$

If $I_{MUT} \neq I_{REF}$, the sensor response is

$$\Delta O = f(I_{MUT}, C_M) - f(I_{REF}, C_M) \neq f(I_{MUT}, C_M = 0)$$
$$- f(I_{REF}, C_M = 0) \tag{14}$$

where the right-hand side member is the expected sensor response without the presence of the external common-mode stimulus. According to expression (14), the effects of cross-sensitivities to common-mode signals cannot be completely suppressed. However, it is reasonable to consider that such common-mode signals generate a small variation in the output variables of both sensors, as compared to the effects generated by the input variable of interest. Under such "small-signal" conditions, the response of each independent sensor can be approximated by

$$O_{MUT} = f(I_{MUT}, C_M) = f(I_{MUT}, C_M = 0) +$$
$$+ \left[\frac{df(I_{MUT}, C_M)}{dC_M} \right]_{C_M=0} C_M \tag{15a}$$

$$O_{REF} = f(I_{REF}, C_M) = f(I_{REF}, C_M = 0) +$$
$$+ \left[\frac{df(I_{REF}, C_M)}{dC_M} \right]_{C_M=0} C_M \tag{15b}$$

Thus, the differential output variable is found to be

$$\Delta O = O_{MUT} - O_{REF} = f(I_{MUT}, C_M) - f(I_{REF}, C_M)$$
$$= f(I_{MUT}, C_M = 0) - f(I_{REF}, C_M = 0)$$

$$+ \left(\left[\frac{df(I_{MUT}, C_M)}{dC_M} \right]_{C_M=0} \right) - \left(\left[\frac{df(I_{REF}, C_M)}{dC_M} \right]_{C_M=0} \right) \tag{16}$$

The derivatives in the right-hand side member of (16) are not, in general, identical, unless $I_{MUT} = I_{REF}$. However, it is expected that the difference between these derivative terms is small (especially if the MUT and REF measurands do not differ so much). Therefore, the differential output variable can be approximated by

$$\Delta O = f(I_{MUT}, C_M) - f(I_{REF}, C_M) \approx f(I_{MUT}, C_M = 0)$$
$$- f(I_{REF}, C_M = 0) \tag{17}$$

Hence, to a first order approximation, the effects of cross-sensitivities to common-mode external signals can be neglected in differential-mode sensors. By contrast, in the single-ended counterparts, the presence of the external signal C_M generates a difference in the output variable O_{MUT} (with regard to the expected value) given by the last term in (15a).

B. TYPES AND SOME REPRESENTATIVE EXAMPLES OF BALANCED MICROWAVE SENSORS

There are many different types of differential-mode sensors, but a relevant categorization divides them between non-resonant and resonant sensors [11]. In non-resonant differential sensors, the phase difference in a pair of sensing transmission lines (one devoted to the REF sample or measurand, and the other one to the MUT), or more specifically, the difference between the phases of the transmission coefficients of such lines, is the considered output variable. The sensing lines can be ordinary lines (typically meandered) [17], [247], [248] or artificial lines, e.g., composite right/left handed (CRLH) lines [249], slow-wave transmission lines [250], or electro-inductive-wave (EIW) [251] transmission lines, among others. The main advantage of artificial transmission line based differential sensors over those implemented by means of ordinary lines is the possibility of achieving an enhanced sensitivity with a reduced sensing region, by virtue of the potentially high dispersion of artificial lines [57]. For example, it is remarkable the huge sensitivity achieved in the sensor reported in [249], where the device is based on a pair of CRLH lines. However, the use of artificial lines is not exempt of certain design complexity. Moreover, artificial lines, especially EIW lines, are prone to detuning effects caused by fabrication related tolerances and inaccuracies in the values of substrate parameters (dielectric constant and thickness) [251]. It should be mentioned that, despite the fact that phase variation is the working principle of these differential non-resonant sensors, in many cases, phase to magnitude conversion has been implemented [17], [249], [252]. For that purpose, additional elements to the sensing lines, e.g., couplers, or dividers/combiners, are required.

Concerning differential-mode resonant sensors, the sensing element is typically a pair of transmission lines loaded with a planar resonator, either a metallic or a slot resonator [24],
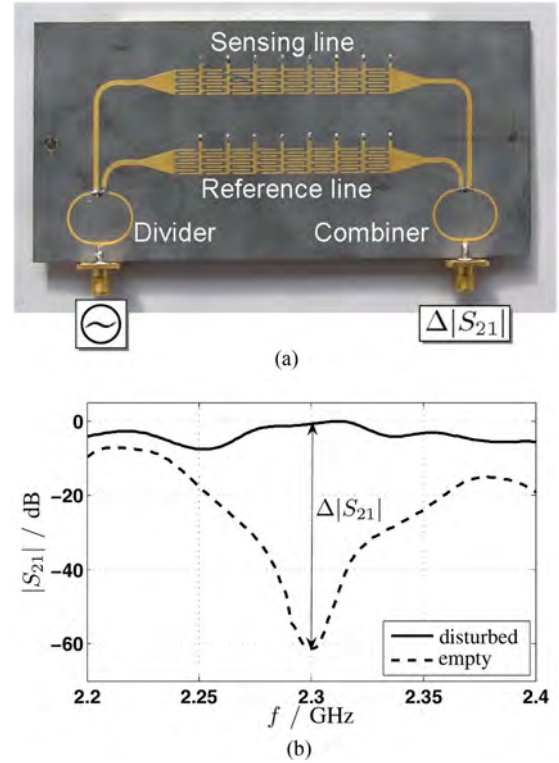

FIGURE 52. Photograph of the CRLH transmission line based differential-mode sensor (a) and comparison between the transmission coefficients for the empty case (unloaded sensing line) and for the sensing line loaded with a MUT (b). Reprinted from [249] with permission.

[25], [253], [254], [255], [256], [257], [258], [259], [260], [261], [262], [263], [264]. In these sensors, the canonical output variable is the differential resonance frequency between the pair of resonator-loaded lines. Sometimes, the differential resonance magnitude is used as an additional output variable (for example, in measurements of the complex permittivity of materials). Nevertheless, in many reported implementations, the cross-mode transmission coefficient has been the considered output variable in balanced resonant sensors (e.g., in [24], [25], [253]). According to expressions (12), if the lines are uncoupled, the cross-mode transmission coefficient is simply:

$$S_{21}^{cd} = S_{21}^{dc} = S_{21} - S_{43} \tag{18}$$

In many reported balanced resonant sensors, the maximum in the magnitude of the cross-mode transmission coefficient and, eventually, the frequency of such maximum, have been the considered output variables.

Let us next report three representative examples of balanced microwave sensors, two of them non-resonant, and one of them resonant. The first non-resonant sensor, reported in [249], consists of a pair of CRLH lines, as depicted in Fig. 52. In this sensor, phase to magnitude conversion is implemented by means of a Wilkinson power divider and a combiner. The input signal is divided between the two CRLH lines. However, the lines connecting the divider/combiner with the feeding points of the CRLH lines are different.

Particularly, the feeding lines of the sensing CRLH line are half-wavelength longer than the ones of the reference CRLH line. Therefore, the signals at the input ports of the combiner are out of phase (line imbalance). Because of this, the magnitude of the transmission coefficient of the resulting two-port structure, or the amplitude of the output signal, is expected to be roughly null, provided the CRLH lines are perfectly imbalanced. However, loading the sensing line with a MUT alters the perfect imbalance (180° phase difference) between the signals present at the input ports of the combiner. The reason is the phase variation experienced by the CRLH sensing line due to the presence of the MUT on top of it. The consequence is the presence of a certain signal level at the output port of the structure (i.e., $S_{21} \neq 0$), related to ε_{MUT}.

Fig. 52(b) depicts the frequency response of the sensor for two cases, i.e., with unloaded (empty) sensing line, and with the sensing line loaded with a MUT [disturbed case, in reference to Fig. 52(b)]. The combination of CRLH line characteristics and ε_{MUT} was determined in [249] in order to obtain the maximum possible transmission coefficient when the MUT is on top of the sensing line (this occurs provided the signals at the input ports of the combiner are in-phase). The output dynamic range at the operating frequency, $f_0 = 2.3$ GHz, is roughly 60 dB. Further details on this structure can be found in [249].

The second case example, also a non-resonant differential sensor, consists of a pair of ordinary (meandered) lines [17]. In this case, phase to magnitude conversion was also applied and achieved by means of a pair of rat-race hybrid couplers. The photograph of the sensor is depicted in Fig. 53, where it can be appreciated the presence of fluidic channels. Thus, the sensor is devoted to the characterization of liquid samples, particularly, to the measurement of the concentration of isopropanol in deionized (DI) water (hence, the REF liquid is DI water). As demonstrated in [17], with the configuration of Fig. 53, the transmission coefficient between the input and the output port ($S_{1'2}$, following the port designation of [17]), is proportional to the cross-mode transmission coefficient of the pair of sensing lines, i.e.,

$$S_{1'2} = -S_{21}^{cd} \tag{19}$$

In [17], the magnitude of such transmission coefficient at the operating frequency ($f_0 = 6$ GHz) was used as output variable. For measuring purposes, the REF liquid (pure DI water) was injected in the REF channel of line A, and subsequently different mixtures of isopropanol in DI water were injected in the MUT channel (line B), starting with a null volume fraction (corresponding to the REF liquid), and progressively increasing the volume fraction of isopropanol. The responses for the different mixtures are depicted in Fig. 53(b). The sensor was able to resolve concentrations of isopropanol in DI water as small as 1 %. The dependence of the transmission coefficient at f_0 as a function of the isopropanol content is depicted in Fig. 53(c). It should be mentioned that, in order to avoid liquid absorption by the substrate, a dry film with thickness 50 μm and dielectric constant 3.6 was deposited on the upper side
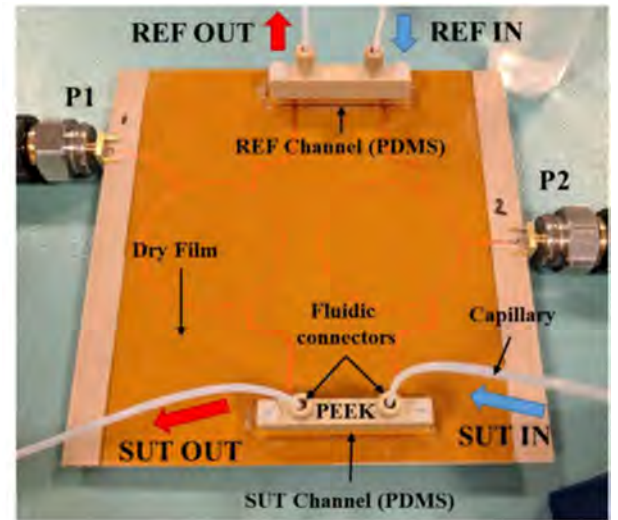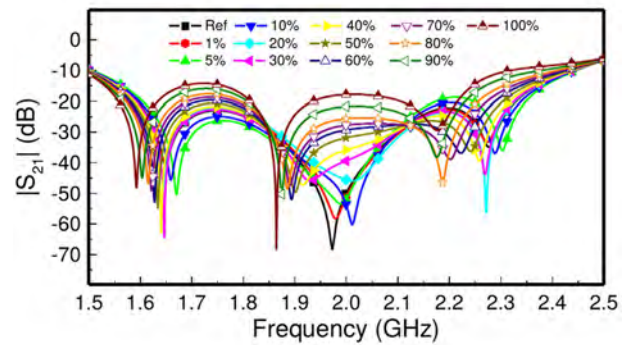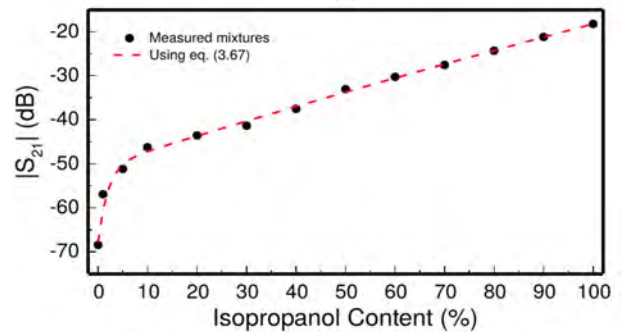
FIGURE 53. (a) Photograph of the differential-mode fluidic sensor based on a pair of meandered lines (present below the channels) and equipped with a pair of couplers for phase to magnitude conversion. (b) Measured transmission coefficient that results by loading line A with the REF liquid (DI water) and line B with MUT samples corresponding to the indicated volume fractions of isopropanol in DI water. (c) Value of the transmission coefficient (dB) at f_0 as a function of the isopropanol content. Reprinted from [17] with permission.

of the substrate. In this sensor, the maximum sensitivity is roughly 12 dB/%. Let us mention that such high sensitivity was achieved by adjusting the electrical length of the pair of lines at the design frequency to a multiple of 180°, as specified in [17] (particularly, the length was set to 540° in the sensing

lines of the device shown in Fig. 53). Further details of device dimensions and substrate parameters can be found in [17].

The third, and last, example is a differential-mode resonant sensor based on a pair of lines loaded with a split ring resonator (SRR) and applied to the measurement of electrolyte concentration in diluted aqueous solutions [253]. The layout of the sensor is depicted in Fig. 54(a), whereas the photograph of the fabricated device is depicted in Fig. 54(b) (the details of substrate parameters and sensor dimensions can be found in [253]). The fluidic channels are conveniently located to ensure that the liquid under test (LUT) and REF liquids are in contact with the gaps of the SRRs, the more sensitive regions of the resonators, due to the high fringing fields in such regions. The validation of the sensor of Fig. 54 was carried out in [253] by considering solutions of DI water with different types of electrolytes, particularly, NaCl, KCl and $CaCl_2$. Here we report the first set of experiments, consisting in the measurement of the cross-mode reflection coefficient after injection of DI water solutions with different concentrations of NaCl in the LUT channel, and pure DI water in the REF channel. The results are shown in Fig. 54(c). Concentrations of NaCl as small as 0.25 g/L can be resolved with the proposed sensor. Fig. 54(d) depicts the dependence of the maximum value of the cross-mode transmission coefficient, $|S_{21}^{cd}|_{max}$ with the concentration of NaCl, [NaCl]. Actually, a pair of measurements was carried out in [253], in order to ensure that the results are repetitive [such measurements are distinguished by the labels 1 and 2 in Fig. 54(d)]. The sensitivity for small NaCl concentrations is very high, and it progressively decreases as [NaCl] increases. The maximum value of the sensitivity is found to be 0.033 $(g/L)^{-1}$, a competitive value.

There are many differential-mode microwave sensors reported in the literature, and their applications are very diverse. Consequently, a faithful comparison, including all the differential sensors reported in references [17], [18], [19], [20], [21], [22], [23], [24], [247], [248], [249], [250], [251], [252], [253], [254], [255], [256], [257], [258], [259], [260], [261], [262], [263], [264] is not straightforward. Nevertheless, there is a subset of sensors devoted to the measurement of the volume fraction of alcohols in DI water [17], [24], [255], [256], or to the measurement of electrolyte concentration in very diluted solutions of DI water [25], [253], [264]. Thus, Table 3 reports a comparison of such sensors to the light of the maximum sensitivity and resolution, the key performance parameters in these sensors. Note that for the sensors devoted to the measurement of volume fraction of alcohol in DI water, the sensitivity is given in units of dB/ %, whereas the resolution is given in % (of alcohol in DI water), and the value given in the table corresponds to the minimum volume fraction that can be resolved. The output variable of these sensors is the magnitude of the cross-mode transmission or reflection coefficient (typically expressed in dB). For the sensors focused on the determination of the electrolyte content in DI water solutions, the output variable is also the
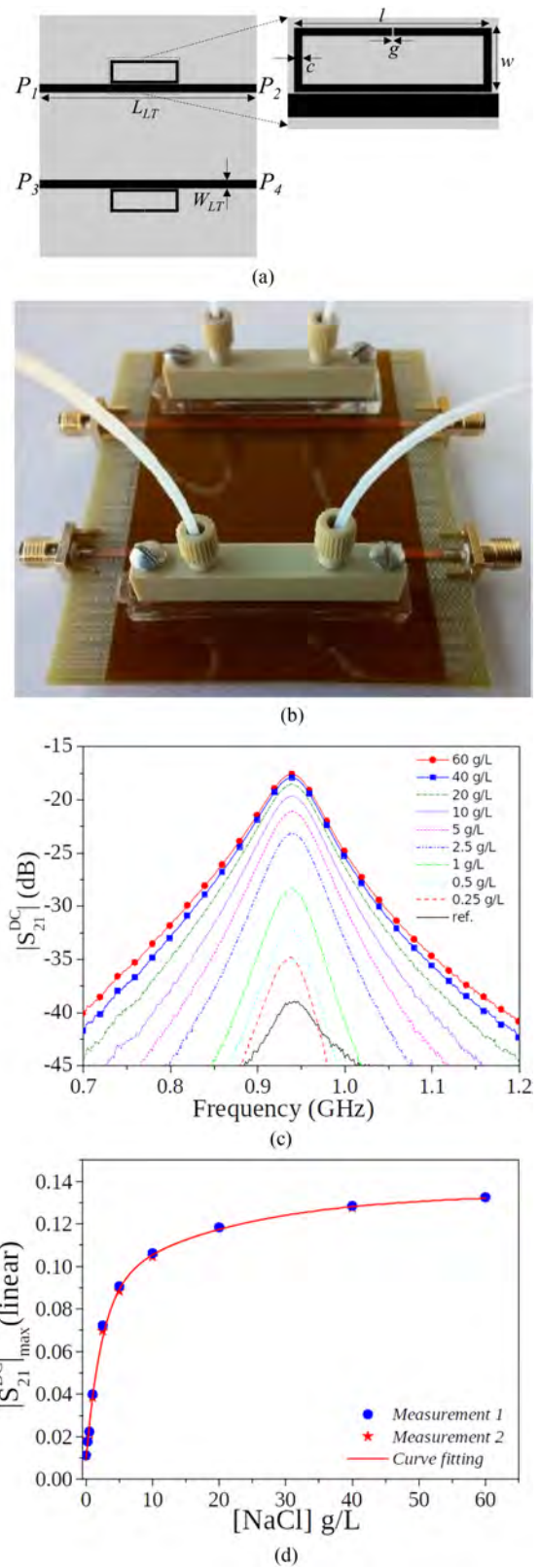

FIGURE 54. (a) Layout of the SRR-based differential-mode microfluidic sensor. (b) photograph. (c) cross-mode transmission coefficient for different concentrations of NaCl. (d) dependence of the maximum value of the cross-mode transmission coefficient with the concentration of NaCl. Reprinted from [253] with permission.

TABLE 3. Comparison of Differential-Mode Microfluidic Sensors

Ref.	Mode	Max. Sensitivity	Resolution
[17]	Non. Res. / T	11.52 dB/ %	1.0 %
[24]	Res. / T	0.70 dB/ %	5.0 %
[25]	Res. / T	10.08 dB/(g/L)	0.25 g/L
[253]	Res. / T	12.27 dB/(g/L)	0.25 g/L
[255]	Res. / R	0.45 dB/ %	10.0 %
[256]	Res. / R	1.60 dB/ %	2.5 %
[264]	Res. / T	10.40 dB/(g/L)	0.125 g/L

cross-mode transmission coefficient. However, the input variable is the concentration of electrolytes, expressed in g/L, and this explains the units of the sensitivity and resolution for these sensors in Table 3. The table includes the information relative to the operation mode of the sensors, indicating whether the sensors is resonant (Res.) or non-resonant (Non-Res.), and whether it operates in transmission (T) or in reflection (R). According to the table, the devices reported in [17] and [253] exhibit very good sensitivity and resolution for each subset of sensors, i.e., volume fraction of alcohol in DI water and concentration of electrolytes in DI water, respectively.

VII. CONCLUSION

In conclusion, this review paper has pointed out the progressively increasing research activity, especially in recent years, in the topic of balanced microwave systems, including transmission lines, filters, circuits, and sensors. The superior immunity of differential systems against EMI and noise, as compared to their single-ended counterparts is the main cause of the progressive penetration of balanced circuits and filters in modern communication systems. Let us also mention that integrated circuits (CMOS, BiCMOS) operating in the millimeter-wave band (for frequencies above 100 GHz) also pull the systems towards differential-mode implementations, with the benefit of potentially higher power generation. Concerning sensors, differential mode structures exhibit an inherent robustness against cross-sensitivities caused by (inevitable) common mode stimuli, such as ambient temperature, humidity and pressure. The main design strategies for the different types of devices have been briefly discussed in the paper, and illustrative examples have been reported. It has been the purpose of the authors in writing this paper to combine in a single document the fundamentals of balanced transmission lines, circuits, and sensors, with the canonical approaches or design strategies of the different considered devices, yet presenting some state-of-the-art specific implementations of the latest trends in the topic (e.g., advanced balanced circuits, or reflection-less balanced filters, among others).

REFERENCES

[1] J. F. White, *High Frequency Techniques: An Introduction to RF and Microwave Engineering*. Hoboken, NJ, USA: Wiley, 2004.

[2] C. H. Tsai and T. L. Wu, "A broadband and miniaturized common-mode filter for gigahertz differential signals based on negative permittivity metamaterials," *IEEE Trans. Microw. Theory. Techn.*, vol. 58, no. 1, pp. 195–202, Jan. 2010.

[3] S. H. Hall, G. W. Hall, and J. A. McCall, *High-Speed Digital System Design: A Handbook of Interconnect Theory and Design Practices*. Hoboken, NJ, USA: Wiley, 2000.

[4] E. Fronbarg, M. Kanda, C. Lasek, M. Piket-May, and S. H. Hall, "The impact of a non-ideal return path on differential signal integrity," *IEEE Trans. Electromagn. Compat.*, vol. 44, no. 1, pp. 11–15, Feb. 2002.

[5] R. Schmitt, *Electromagnetic Explained: A Handbook for Wireless/RF, EMC, and High-Speed Electronics*. Oxford, U.K.: Newness, 2002.

[6] S. Caniggia and F. Maradei, *Signal Integrity and Radiated Emission of High-Speed Digital Systems*. Hoboken, NJ, USA: Wiley, 2008.

[7] D. E. Bockelman and W. R. Eisenstadt, "Combined differential and common-mode scattering parameters: Theory and simulation," *IEEE Trans. Microw. Theory Techn.*, vol. 43, no. 7, pp. 1530–1539, Jul. 1995.

[8] G. D. Vendelin, A. M. Pavio, and U. L. Rodhe, *Microwave Circuit Design Using Linear and Nonlinear Techniques*, 2nd ed. Hoboken, NJ, USA: Wiley, 2005.

[9] K. C. Gupta, R. Garg, I. Bahl, and P. Barthia, *Microstrip Lines and Slotlines*, 2nd ed. Norwood, MA, USA: Artech House, 1996.

[10] F. Martín, L. Zhu, J. Hong, and F. Medina, *Balanced Microwave Filters*. Hoboken, NJ, USA: Wiley, 2018.

[11] F. Martín, P. Vélez, J. Muñoz-Enano, and L. Su, *Planar Microwave Sensors*. Hoboken, NJ, USA: Wiley, 2022.

[12] T. Chretiennot, D. Dubuc, and K. Grenier, "A microwave and microfluidic planar resonator for efficient and accurate complex permittivity characterization of aqueous solutions," *IEEE Trans. Microw. Theory Techn.*, vol. 61, no. 2, pp. 972–978, Feb. 2013.

[13] P. Vélez, F. Martín, R. Fernández-García, and I. Gil, "Embroidered textile frequency-splitting sensor based on stepped-impedance resonators," *IEEE Sensors J.*, vol. 22, no. 9, pp. 8596–8603, May 2022.

[14] J. Muñoz-Enano, P. Vélez, M. Gil, and F. Martín, "Planar microwave resonant sensors: A review and recent developments," *Appl. Sci.*, vol. 10, 2020, Art. no. 2615.

[15] J. Muñoz-Enano et al., "Planar phase-variation microwave sensors for material characterization: A review and comparison of various approaches," *Sensors*, vol. 21, 2021, Art. no 1542.

[16] J. Muñoz-Enano, P. Vélez, L. Su, M. Gil, P. Casacuberta, and F. Martín, "On the sensitivity of reflective-mode phase-variation sensors based on open-ended stepped-impedance transmission lines: Theoretical analysis and experimental validation," *IEEE Trans. Microw. Theory Techn.*, vol. 69, no. 1, pp. 308–324, Jan. 2021.

[17] J. Muñoz-Enano, P. Vélez, M. Gil, J. Mata-Contreras, and F. Martín, "Differential-mode to common-mode conversion detector based on rat-race hybrid couplers: Analysis and application to differential sensors and comparators," *IEEE Trans. Microw. Theory Techn.*, vol. 68, no. 4, pp. 1312–1325, Apr. 2020.

[18] T. C. Edwards and M. B. Steer, *Foundations of Interconnect and Microstrip Design*, 3rd ed. Hoboken, NJ, USA: Wiley, 2000.

[19] R. Mongia, I. Bahl, and P. Bhartia, *RF and Microwave Coupled Line Circuits*. Boston, MA, USA: Artech House, 1999.

[20] J. C. Freeman, *Fundamentals of Microwave Transmission Lines*. New York, NY, USA: Wiley, 1996.

[21] D. M. Pozar, *Microwave Engineering*. Hoboken, NJ, USA: Wiley, 2012.

[22] A. Ferrero and M. Pirola, "Generalized mixed-mode S-parameters," *IEEE Trans. Microw. Theory Techn.*, vol. 54, no. 1, pp. 458–463, Jan. 2006.

[23] W. R. Eisenstadt, B. Stengel, and B. M. Thompson, *Microwave Differential Circuit Design Using Mixed-Mode S-Parameters*. Norwood, MA, USA: Artech House, 2006.

[24] P. Vélez, K. Grenier, J. Mata-Contreras, D. Dubuc, and F. Martín, "Highly-sensitive microwave sensors based on open complementary split ring resonators (OCSRRs) for dielectric characterization and solute concentration measurements in liquids," *IEEE Access*, vol. 6, pp. 48324–48338, 2018.

[25] P. Vélez, J. Muñoz-Enano, M. Gil, J. Mata-Contreras, and F. Martín, "Differential microfluidic sensors based on dumbbell-shaped defect ground structures in microstrip technology: Analysis, optimization, and applications," *Sensors*, vol. 19, no. 14, 2019, Art. no. 3189.

[26] C. R. Paul, "A comparison of the contributions of common-mode and differential-mode currents in radiated emissions," *IEEE Trans. Electromagn. Compat.*, vol. 31, no. 2, pp. 189–193, May 1989.

[27] W. T. Liu, C.-H. Tsai, T.-W. Han, and T.-L. Wu, "An embedded common-mode suppression filter for GHz differential signals using periodic defected ground plane," *IEEE Microw. Wireless Compon. Lett.*, vol. 18, no. 4, pp. 248–250, Apr. 2008.

[28] S. J. Wu, C. H. Tsai, T. L. Wu, and T. Itoh, "A novel wideband common-mode suppression filter for gigahertz differential signals using coupled patterned ground structure," *IEEE Trans. Microw. Theory Techn.*, vol. 57, no. 4, pp. 848–855, Apr. 2009.

[29] J. Naqui et al., "Split rings-based differential transmission lines with common-mode suppression," in *Proc. IEEE MTT-S Int. Microw. Symp.*, 2011, pp. 1–4.

[30] J. Naqui et al., "Common mode suppression in microstrip differential lines by means of complementary split ring resonators: Theory and applications," *IEEE Trans. Microw. Theory Techn.*, vol. 60, no. 10, pp. 3023–3034, Oct. 2012.

[31] A. Fernández-Prieto et al., "Dual-band differential filter using broadband common-mode rejection artificial transmission line," *Prog. Electromagn. Res.*, vol. 139, pp. 779–797, 2013.

[32] J. Naqui, M. Durán-Sindreu, and F. Martín, "Selective mode suppression in microstrip differential lines by means of electric-LC (ELC) and magnetic-LC (MLC) resonators," *Appl. Phys. A*, vol. 115, pp. 637–643, 2014.

[33] T. W. Weng, C. H. Tsai, C. H. Chen, D. H. Han, and T. L. Wu, "Synthesis model and design of a common-mode bandstop filter (CM-BSF) with an all-pass characteristic for high-speed differential signals," *IEEE Trans. Microw. Theory Techn.*, vol. 62, no. 8, pp. 1647–1656, Aug. 2014.

[34] F. X. Yang, M. Tang, L. S. Wu, and J. F. Mao, "A novel wideband common-mode suppression filter for differential signal transmission," in *Proc. IEEE Elect. Des. Adv. Packag. Syst. Symp.*, 2014, pp. 129–132.

[35] Z. Zeng, Y. Yao, and Y. Zhuang, "A wideband common-mode suppression filter with compact-defected ground structure pattern," *IEEE Trans. Electromagn. Compat.*, vol. 57, no. 5, pp. 1277–1280, Oct. 2015.

[36] A. Ebrahimi, T. C. Baum, K. Wang, J. Scott, and K. Ghorbani, "Differential transmission lines loaded with magnetic LC resonators and application in common mode suppression," *IEEE Trans. Circuits Syst. I, Reg. Papers*, vol. 66, no. 10, pp. 3811–3821, Oct. 2019.

[37] F. de Paulis, L. Raimondo, S. Connor, B. Archambeault, and A. Orlandi, "Design of a common mode filter by using planar electromagnetic bandgap structures," *IEEE Trans. Adv. Packag.*, vol. 33, no. 4, pp. 994–1002, Nov. 2010.

[38] F. de Paulis, L. Raimondo, S. Connor, B. Archambeault, and A. Orlandi, "Compact configuration for common mode filter design based on planar electromagnetic bandgap structures," *IEEE Trans. Electromagn. Compat.*, vol. 54, no. 3, pp. 646–654, Jun. 2012.

[39] J. H. Choi, P. W. C. Hon, and T. Itoh, "Dispersion analysis and design of planar electromagnetic bandgap ground plane for broadband common-mode suppression," *IEEE Microw. Wireless Compon. Lett.*, vol. 24, no. 11, pp. 772–774, Nov. 2014.

[40] P. Vélez, J. Bonache, and F. Martín, "Differential microstrip lines with common-mode suppression based on electromagnetic bandgaps (EBGs)," *IEEE Antennas Wireless Propag. Lett.*, vol. 14, pp. 40–43, 2015.

[41] P. Vélez et al., "Enhancing common-mode suppression in microstrip differential lines by means of chirped electromagnetic bandgaps (EBGs)," *Microw. Opt. Technol. Lett.*, vol. 58, pp. 328–332, Feb. 2016.

[42] B. C. Tseng and L. K. Wu, "Design of miniaturized common-mode filter by multilayer low-temperature co-fired ceramic," *IEEE Trans. Electromagn. Compat.*, vol. 46, no. 4, pp. 571–579, Nov. 2004.

[43] C. Y. Hsiao, C. H. Tsai, C. N. Chiu, and T. L. Wu, "Radiation suppression for cable-attached packages utilizing a compact embedded common-mode filter," *IEEE Trans. Compon. Packag. Manuf. Technol.*, vol. 2, no. 10, pp. 1696–1703, Oct. 2012.

[44] G. H. Shiue, C. M. Hsu, C. L. Yeh, and C. F. Hsu, "A comprehensive investigation of a common-mode filter for gigahertz differential signals using quarter-wavelength resonators," *IEEE Trans. Compon. Packag., Manuf. Technol.*, vol. 4, no. 1, pp. 134–144, Jan. 2014.

[45] S. G. Kang, G. Shaffer, C. Kodama, C. O'Daniel, and E. Wheeler, "CSRR common-mode filtering structures in multilayer printed circuit boards," in *Proc. IEEE Int. Symp. Electromagn. Compat.*, 2015, pp. 1300–1303.

[46] C. H. Cheng and T. L. Wu, "A compact dual-band common-mode filtering component for EMC in wireless communication," in *Proc. Asia-Pacific Int. EMC Symp.*, 2015, pp. 349–351.

[47] C. Y. Hsiao, Y. C. Huang, and T. L. Wu, "An ultra-compact common-mode bandstop filter with modified-T circuits in integrated passive device (IPD) process," *IEEE Trans. Microw. Theory Techn.*, vol. 63, no 11, pp. 3624–3631, Nov. 2015.

[48] A. Fernández-Prieto et al., "Common-mode suppression for balanced bandpass filters in multilayer liquid crystal polymer technology," *IET Microw. Antennas Propag.*, vol. 9, pp. 1249–1253, Sep. 2015.

[49] B.-F. Su and T.-G. Ma, "Miniaturized common-mode filter using coupled synthetsized lines and mushroom resonators for high-speed differential signals," *IEEE Microw. Wireless Compon. Lett.*, vol. 25, no. 2, pp. 112–114, Feb. 2015.

[50] B. A. Mouris et al., "Glide symmetry applied to printed common-mode rejection filters," *IEEE Trans. Microw. Theory Techn.*, vol. 70, no. 2, pp. 1198–1210, Feb. 2022.

[51] C.-Y. Hsiao, C.-H. Cheng, and T.-L. Wu, "A new broadband common-mode noise absorption circuit for high-speed differential digital systems," *IEEE Trans. Microw. Theory Techn.*, vol. 63, no. 6, pp. 1894–1901, Jun. 2015.

[52] C. Chan and T. Wu, "A high-performance common-mode noise absorption circuit based on phase modification technique," *IEEE Trans. Microw. Theory Techn.*, vol. 67, no. 11, pp. 4394–4403, Nov. 2019.

[53] P.-J. Li and T.-L. Wu, "A novel circuit architecture of bidirectional common-mode noise absorption circuit," *IEEE Trans. Microw. Theory Techn.*, vol. 68, no. 4, pp. 1476–1486, Apr. 2020.

[54] J. D. Gavenda, "Measured effectiveness of a toroid choke in reducing common-mode current," in *Proc. IEEE Nat. Symp. Electromagn. Compat. Symp.*, 1989, pp. 208–210.

[55] K. Yanagisawa, F. Zhang, T. Sato, and Y. Miura, "A new wideband common-mode noise filter consisting of Mn–Zn ferrite core and copper/polyimide tape wound coil," *IEEE Trans. Magn.*, vol. 41, no. 10, pp. 3571–3573, Oct. 2005.

[56] J. Deng and K. Y. See, "In-circuit characterization of common-mode chokes," *IEEE Trans. Electromagn. Compat.*, vol. 49, no. 5, pp. 451–454, May 2007.

[57] F. Martín, *Artificial Transmission Lines for RF and Microwave Applications*. Hoboken, NJ, USA: Wiley, 2015.

[58] J. Naqui, *Symmetry Properties in Transmission Lines Loaded With Electrically Small Resonators: Circuit Modeling and Applications*. Heidelberg, Germany: Springer, 2016.

[59] J. Naqui, M. Durán-Sindreu, and F. Martín, "Selective mode suppression in coplanar waveguides using metamaterial resonators," *Appl. Phys. A, Mater. Sci. Process.*, vol. 109, pp. 1053–1058, Dec. 2012.

[60] J. Naqui, M. Durán-Sindreu, and F. Martín, "Differential and single-ended microstrip lines loaded with slotted magnetic-LC (MLC) resonators," *Int. J. Antennas Propag.*, vol. 2013, 2013, Art. no. 640514.

[61] F. Falcone, T. Lopetegi, J. D. Baena, R. Marqués, F. Martín, and M. Sorolla, "Effective negative-ε stop-band microstrip lines based on complementary split ring resonators," *IEEE Microw. Wireless Compon. Lett.*, vol. 14, pp. 280–282, Jun. 2004.

[62] C. S. Kim, J. S. Park, D. Ahn, and J. B. Lim, "A novel 1-D periodic defected ground structure for planar circuits," *IEEE Microw. Guided Wave Lett.*, vol. 10, no. 4, pp. 131–133, Apr. 2000.

[63] D. Schurig, J. J. Mock, and D. R. Smith, "Electric-field-coupled resonators for negative permittivity metamaterials," *Appl. Phys. Lett.*, vol. 88, 2006, Art. no. 041109.

[64] L. Su, J. Muñoz-Enano, P. Vélez, J. Martel, F. Medina, and F. Martín, "On the modeling of microstrip lines loaded with dumbbell defect-ground-structure (DB-DGS) and folded DB-DGS resonators," *IEEE Access*, vol. 9, pp. 150878–150888, 2021.

[65] B. A. Mouris, A. Fernández-Prieto, R. Thobaben, J. Martel, F. Mesa, and O. Quevedo-Teruel, "On the increment of the bandwidth of mushroom type EBG structures with glide symmetry," *IEEE Trans. Microw. Theory Techn.*, vol. 68, no. 4, pp. 1365–1375, Apr. 2020.

[66] J. D. Joannopoulos, R. D. Meade, and J. N. Winn, *Photonic Crystals: Molding the Flow of Light*. Princeton, NJ, USA: Princeton Univ. Press, 1995.

[67] E. Yablonovitch, "Photonic band gap structures," *J. Opt. Soc. Amer. B*, vol. 10, pp. 283–295, 1993.

[68] Y. Qian, V. Radistic, and T. Itoh, "Simulation and experiment of photonic band-gap structures for microstrip circuits," in *Proc. Asia-Pacific Microw. Conf.*, 1997, pp. 585–588.

[69] F. Falcone, T. Lopetegi, M. Irisarri, M. A. G. Laso, M. J. Erro, and M. Sorolla, "Compact photonic bandgap microstrip structures," *Microw. Opt. Technol. Lett.*, vol 23, pp. 233–236, 1999.

[70] M. A. G. Laso, T. Lopetegi, M. J. Erro, D. Benito, M. J. Garde, and M. Sorolla, "Multiple-frequency-tuned photonic bandgap microstrip structures," *IEEE Microw. Guided Wave Lett.*, vol. 10, no. 6, pp. 220–222, Jun. 2000.

[71] Q. Liu et al., "Reduction of EMI due to common-mode currents using a surface-mount EBG-based filter," *IEEE Trans. Electromagn. Compat.*, vol. 58, no. 5, pp. 1440–1447, Oct. 2016.

[72] C.-K. Chan, C.-H. Cheng, and T.-L. Wu, "Design of a broadband common-mode filter with four transmission zeros," *IEEE Trans. Electromagn. Compat.*, vol. 61, no. 4, pp. 1052–1060, Aug. 2019.

[73] C.-H. Cheng and T.-L. Wu, "An ultra-compact TSV-based common-mode filter (TSV-CMF) in three-dimensional integrated circuits (3-D ICs)," *IEEE Trans. Electromagn. Compat.*, vol. 58, no. 4, pp. 1128–1135, Aug. 2016.

[74] P.-J. Li, Y.-C. Tseng, C.-H. Cheng, and T.-L. Wu, "A novel absorptive common-mode filter for cable radiation reduction," *IEEE Trans. Compon., Packag., Manuf. Technol.*, vol. 7, no. 4, pp. 511–518, Apr. 2017.

[75] P.-J. Li, C.-H. Cheng, and T.-L. Wu, "A resistor-free absorptive common-mode filter using gap-coupled resonator," *IEEE Microw. Wireless Compon. Lett.*, vol. 28, no. 10, pp. 885–887, Oct. 2018.

[76] P.-J. Li and T.-L. Wu, "Synthesized method of dual-band common-mode noise absorption circuits," *IEEE Trans. Microw. Theory Techn.*, vol. 67, no. 4, pp. 1392–1401, Apr. 2019.

[77] C.-H. Cheng and T.-L. Wu, "Analysis and design method of a novel absorptive common-mode filter," *IEEE Trans. Microw. Theory Techn.*, vol. 67, no. 5, pp. 1826–1835, May 2019.

[78] Y. Guan, Y. Wu, and M. M. Tentzeris, "A bidirectional absorptive common-mode filter based on interdigitated microstrip coupled lines for 5G "Green" communications," *IEEE Access*, vol. 8, pp. 20759–20769, 2020.

[79] S.-K. Tseng, C.-N. Chiu, Y.-C. Tsao, and Y.-P. Chiou, "A novel ultra-wideband absorptive common-mode filter design using a miniaturized and resistive defected ground structure," *IEEE Trans. Electromagn. Compat.*, vol. 63, no. 1, pp. 66–73, Feb. 2021.

[80] Y. Zhu, K. Song, M. Fan, S. Guo, Y. Zhou, and Y. Fan, "Common-mode noise absorption circuit using double-sided parallel-strip line," *IEEE Microw. Wireless Compon. Lett.*, vol. 31, no. 1, pp. 25–28, Jan. 2021.

[81] H.-W. Liu, C.-H. Cheng, and T.-L. Wu, "A compact symmetrical single-cell bidirectional absorption common-mode filter," *IEEE Trans. Compon. Packag. Manuf. Technol.*, vol. 12, no. 4, pp. 655–664, Apr. 2022.

[82] Y.-H. Chen and C.-N. Chiu, "An ultrawideband bidirectional absorptive common-mode filter with all-pass signal transmission," *IEEE Access*, vol. 10, pp. 50000–50007, 2022.

[83] H.-W. Liu, C.-H. Cheng, P.-J. Li, and T.-L. Wu, "A novel compact single-stage absorption common-mode filter," *IEEE Trans. Electromagn. Compat.*, vol. 64, no. 1, pp. 111–118, Feb. 2022.

[84] P. Zhou, H. Zhao, Z. Xu, S. Li, Y. Shi, and X. Yin, "Analysis and modeling of wideband common-mode absorption with lossy complementary split-ring resonator chain in resistor-free differential microstrip lines," *IEEE Trans. Microw. Theory Techn.*, vol. 70, no. 2, pp. 1048–1058, Feb. 2022.

[85] T. Adiprabowo, D.-B. Lin, Y.-H. Zheng, Y.-H. Chen, C.-Y. Zhuang, and B.-H. Tsai, "Dual-band high absorbing and broadband suppressing common-mode noise filter," *IEEE Trans. Electromagn. Compat.*, vol. 64, no. 2, pp. 386–395, Apr. 2022.

[86] T. B. Lim and L. Zhu, "A differential-mode wideband bandpass filter on microstrip line for UWB application," *IEEE Microw. Wireless Compon. Lett.*, vol 19, no. 10, pp. 632–634, Oct. 2009.

[87] T. B. Lim and L. Zhu, "Differential-mode ultra-wideband bandpass filter on microstrip line," *Electron. Lett.*, vol. 45, no. 22, pp. 1124–1125, Oct. 2009.

[88] T. B. Lim and L. Zhu, "Differential-mode wideband bandpass filter with three transmission zeros under common-mode operation," in *Proc. Asia-Pacific Microw. Conf.*, 2009, pp. 159–162.

[89] T. B. Lim and L. Zhu, "Highly selective differential-mode wideband bandpass filter for UWB application," *IEEE Microw. Wireless Compon. Lett.*, vol. 21, no. 3, pp. 133–135, Mar. 2011.

[90] K. Aliqab and J. Hong, "Wideband differential-mode bandpass filters with stopband and common-mode suppression," *IEEE Microw. Wireless Compon. Lett.*, vol. 30, no. 3, pp. 233–236, Mar. 2020.

[91] W. Chen, Y. Wu, and W. Wang, "Planar wideband high-selectivity impedance-transforming differential bandpass filter with deep common-mode suppression," *IEEE Trans. Circuits Syst. II, Exp. Briefs*, vol. 67, no. 10, pp. 1914–1918, Oct. 2020.

[92] W. Zhang, Y. Wu, Y. Liu, C. Yu, A. Hasan, and F. M. Ghannouchi, "Planar wideband differential-mode bandpass filter with common-mode noise absorption," *IEEE Microw. Wireless Compon. Lett.*, vol. 27, no. 5, pp. 458–460, May 2017.

[93] J. S. Hong and M. J. Lancaster, *Microstrip Filters for RF/Microwave Applications*. New York, NY, USA: Wiley, 2001.

[94] J.-S. Hong and H. Shaman, "An optimum ultra-wideband microstrip filter," *Microw. Opt. Technol. Lett.*, vol. 47, no. 3, pp. 230–233, Nov. 2005.

[95] P. Vélez et al., "Differential bandpass filters with common-mode suppression based on stepped impedance resonators (SIRs)," in *Proc. IEEE MTT-S Int. Microw. Symp.*, 2013, pp. 1–4.

[96] P. Vélez, J. Selga, M. Sans, J. Bonache, and F. Martín, "Design of differential-mode wideband bandpass filters with wide stop band and common-mode suppression by means of multisection mirrored stepped impedance resonators (SIRs)," in *Proc. IEEE MTT-S Int. Microw. Symp.*, 2015, pp. 1–4.

[97] M. Sans et al., "Automated design of common-mode suppressed balanced wideband bandpass filters by means of agressive space mapping (ASM)," *IEEE Trans. Microw. Theory Techn.*, vol. 63, no. 12, pp. 3896–3908, Dec. 2015.

[98] P. Vélez et al., "Ultra-compact (80mm^2) differential-mode ultra-wideband (UWB) bandpass filters with common-mode noise suppression," *IEEE Trans. Microw. Theory Techn.*, vol. 63, no. 4, pp. 1272–1280, Apr. 2015.

[99] M. Sans et al., "Automated design of balanced wideband bandpass filters based on mirrored stepped impedance resonators (SIRs) and interdigital capacitors," *Int. J. Microw. Wireless Technol.*, vol. 8, no. 4–5, pp. 731–740, Jun. 2016.

[100] M. Sans et al., "Compact wideband balanced bandpass filters with very broad common-mode and differential-mode stopbands," *IEEE Trans. Microw. Theory Techn.*, vol. 66, no. 2, pp. 737–750, Feb. 2018.

[101] C.-H. Wu, C.-H. Wang, and C.-H. Chen, "Novel balanced coupled-line bandpass filters with common mode noise suppression," *IEEE Trans. Microw. Theory Techn.*, vol. 55, no. 2, pp. 287–295, Feb. 2007.

[102] X.-H. Wu and Q.-X. Chu, "Compact differential ultra-wideband bandpass filter with common-mode suppression," *IEEE Microw. Wireless Compon. Lett.*, vol. 22, no. 9, pp. 456–458, Sep. 2012.

[103] X.-H. Wu and Q.-X. Chu, "Differential wideband bandpass filter with high-selectivity and common-mode suppression," *IEEE Microw. Wireless Compon. Lett.*, vol. 23, no. 12, pp. 644–646, Dec. 2013.

[104] H. Wang, L.-M. Gao, K.-W. Tam, W. Kang, and W. Wu, "A wideband differential BPF with multiple differential- and common-mode transmission zeros using cross-shaped resonator," *IEEE Microw. Wireless Compon. Lett.*, vol. 24, no. 12, pp. 854–856, Dec. 2014.

[105] Z.-A. Ouyang and Q.-X. Chu, "An improved wideband balanced filter using internal cross-coupling and 3/4λ stepped-impedance resonator," *IEEE Microw. Wireless Compon. Lett.*, vol. 26, no. 3, pp. 156–158, Mar. 2016.

[106] L.-L. Qiu and Q.-X. Chu, "Balanced bandpass filter using stub-loaded ring resonator and loaded coupled feed-line," *IEEE Microw. Wireless Compon. Lett.*, vol. 25, no. 10, pp. 654–656, Oct. 2015.

[107] Q.-X. Chu and L.-L. Qiu, "Wideband balanced filters with high selectivity and common-mode suppression," *IEEE Trans. Microw. Theory Techn.*, vol. 63, no. 10, pp. 3462–3468, Oct. 2015.

[108] M. A. Sánchez-Soriano, G. Torregrosa-Penalva, and E. Bronchalo, "Compact wideband bandstop filter with four transmission zeros," *IEEE Microw. Wireless Compon. Lett.*, vol. 20, no. 6, pp. 313–315, Jun. 2010.

[109] W. J. Feng and W. Q. Che, "Novel wideband differential bandpass filters based on T-shaped structure," *IEEE Trans. Microw. Theory Techn.*, vol. 60, no. 6, pp. 1560–1568, Jun. 2012.

[110] W. J. Feng, W. Q. Che, and Q. Xue, "Compact ultra-wideband bandpass filters with notched bands based on transversal signal-interaction concepts," *IET Microw. Antennas Propag.*, vol. 7, no. 12, pp. 961–969, Nov. 2013.

[111] W. J. Feng, W. Q. Che, Y. L. Ma, and Q. Xue, "Compact wideband differential bandpass filter using half-wavelength ring resonator," *IEEE Microw. Wireless Compon. Lett.*, vol. 23, no. 2, pp. 81–83, Feb. 2013.

[112] W. J. Feng and W. Q. Che, "Ultra-wideband bandpass filter using broadband planar Marchand Balun," *IET Electron. Lett.*, vol. 47 no. 3, pp. 198–199, Feb. 2011.

[113] A. M. Abbosh, "Ultrawideband balanced bandpass filter," *IEEE Microw. Wireless Compon. Lett.*, vol. 21, no. 9, pp. 480–482, Sep. 2011.

[114] Y.-J. Lu, S.-Y. Chen, and P. Hsu, "A differential-mode wideband bandpass filter with enhanced common-mode suppression using slotline resonator," *IEEE Microw. Wireless Compon. Lett.*, vol. 22, no. 10, pp. 503–505, Oct. 2012.

[115] C.-H. Lee, C. I. G. Hsu, and C.-J. Chen, "Band-notched balanced UWB BPF with stepped-impedance slotline multi-mode resonator," *IEEE Microw. Wireless Compon. Lett.*, vol. 22, no. 4, pp. 182–184, Apr. 2012.

[116] J. Shi et al., "Compact low-loss wideband differential bandpass filter with high common-mode suppression," *IEEE Microw. Wireless Compon. Lett.*, vol. 23, no. 9, pp. 480–482, Sep. 2013.

[117] P. Vélez et al., "Differential bandpass filter with common mode suppression based on open split ring resonators and open complementary split ring resonators," *IEEE Microw. Wireless Compon. Lett.*, vol. 23, no. 1, pp. 22–24, Jan. 2013.

[118] A. K. Horestani, M. Durán-Sindreu, J. Naqui, C. Fumeaux, and F. Martín, "S-shaped complementary split ring resonators and application to compact differential bandpass filters with common-mode suppression," *IEEE Microw. Wireless Compon. Lett.*, vol. 24, no. 3, pp. 149–151, Mar. 2014.

[119] X. Guo, L. Zhu, K.-W. Tam, and W. Wu, "Wideband differential bandpass filters on multimode slotline resonator with intrinsic common-mode rejection," *IEEE Trans. Microw. Theory Techn.*, vol. 63, no. 5, pp. 1587–1594, May 2015.

[120] X. Guo, W. Wu, and L. Zhu, "A novel design method of wideband differential bandpass filters on the multimode slotline resonator," in *Proc. Asia-Pacific Microw. Conf.*, 2015, pp. 1–3.

[121] D. Chen, H. Bu, L. Zhu, and C. Cheng, "A DM wideband bandpass filter on slotline multi-mode resonator with controllable bandwidth," *IEEE Microw. Wireless Compon. Lett.*, vol. 25, no. 1, pp. 28–30, Jan. 2015.

[122] X. Guo, L. Zhu, and W. Wu, "Strip-loaded slotline resonators for differential wideband bandpass filters with intrinsic common-mode rejection," *IEEE Trans. Microw. Theory Techn.*, vol. 64, no. 2, pp. 450–458, Feb. 2016.

[123] X. Guo, W. Wu, and L. Zhu, "Research on slotline stub-loaded resonator and hybrid stub-loaded resonator for differential wideband filters," in *Proc. IEEE Int. Workshop Electromagn., Appl. Student Innov. Competition*, 2016, pp. 1–3.

[124] X. Guo, L. Zhu, and W. Wu, "Balanced wide-/dual-band BPFs on a hybrid multimode resonator with intrinsic common-mode rejection," *IEEE Trans. Microw. Theory Techn.*, vol. 64, no. 7, pp. 1997–2005, Jul. 2016.

[125] H. T. Zhu, W. J. Feng, W. Q. Che, and Q. Xue, "Ultra-wideband differential bandpass filter based on transversal signal-interference concept," *Electron. Lett.*, vol. 47, no. 18, pp. 1033–1035, Sep. 2011.

[126] X. H. Wang, H. Zhang, and B. Z. Wang, "A novel ultra-wideband differential filter based on microstrip line structures," *IEEE Microw. Wireless Compon. Lett.*, vol. 23, no. 3, pp. 128–130, Mar. 2013.

[127] W. J. Feng, W. Q. Che, T. F. Eibert, and Q. Xue, "Compact wideband differential bandpass filter based on the double-sided parallel-strip line and transversal signal-interaction concepts," *IET Microw. Antennas Propag.*, vol. 6, no. 2, pp. 186–195, Apr. 2012.

[128] B. Pan, H. Zhu, W. Feng, W. Che, and Q. Xue, "Compact balanced bandpass filter with wideband common mode suppression," in *Proc. IEEE Asia-Pacific Microw. Conf.*, 2020, pp. 935–937.

[129] W. Feng, B. Pan, H. Zhu, X. Y. Zhou, W. Che, and Q. Xue, "High performance balanced bandpass filters with wideband common mode suppression," *IEEE Trans. Circuits Syst. II, Exp. Briefs*, vol. 68, no. 6, pp. 1897–1901, Jun. 2021.

[130] Y. Zhu, K. Song, M. Fan, S. Guo, Y. Zhou, and Y. Fan, "Wideband balanced bandpass filter with common-mode noise absorption using double-sided parallel-strip line," *IEEE Microw. Wireless Compon. Lett.*, vol. 30, no. 4, pp. 359–362, Apr. 2020.

[131] L.-P. Feng, L. Zhu, S. Zhang, and X. Zhang, "Compact Chebyshev differential-mode bandpass filter on $\lambda/4$ CPS resonator with intrinsic common-mode rejection," *IEEE Trans. Microw. Theory Techn.*, vol. 66, no. 9, pp. 4047–4056, Sep. 2018.

[132] L.-P. Feng, L. Zhu, and S. Zhang, "Differential-mode low-pass filter using hybrid CPS and G-CPS with intrinsic common-mode rejection," *IEEE Trans. Microw. Theory Techn.*, vol. 67, no. 5, pp. 1836–1843, May 2019.

[133] Z.-A. Ouyang, L. Zhu, and L.-L. Qiu, "Wideband balanced filters with intrinsic common-mode suppression using coplanar strip double-sided shunt-stub structures," *IEEE Trans. Microw. Theory Techn.*, vol. 69, no. 8, pp. 3770–3782, Aug. 2021.

[134] Z.-A. Ouyang, L. Zhu, and L.-L. Qiu, "Wideband balanced filters with intrinsic common-mode suppression on coplanar stripline-based multimode resonators," *IEEE Trans. Circuits Syst. I, Regular Papers*, vol. 69, no. 6, pp. 2263–2275, Jun. 2022.

[135] J. L. Olvera-Cervantes and A. Corona-Chávez, "Microstrip balanced bandpass filter with compact size, extended-stopband and common-mode noise suppression," *IEEE Microw. Wireless Compon. Lett.*, vol. 23, no. 10, pp. 530–532, Oct. 2013.

[136] A. Fernández-Prieto, A. Lujambio, J. Martel, F. Medina, F. Mesa, and R. R. Boix, "Simple and compact balanced bandpass filters based on magnetically coupled resonators," *IEEE Trans. Microw. Theory Techn.*, vol. 63, no. 6, pp. 1843–1853, Jun. 2015.

[137] J. Shi and Q. Xue, "Balanced bandpass filters using center-loaded half-wavelength resonators," *IEEE Trans. Microw. Theory Techn.*, vol. 58, no. 4, pp. 970–977, Apr. 2010.

[138] C. H. Wu, C. H. Wang, and C. H. Chen, "Stopband-extended balanced bandpass filter using coupled stepped-impedance resonators," *IEEE Microw. Wireless Compon. Lett.*, vol. 17, no. 7, pp. 507–509, Jul. 2007.

[139] C. H. Wu, C. H. Wang, and C. H. Chen, "Balanced coupled-resonator bandpass filters using multisection resonators for common-mode suppression and stopband extension," *IEEE Trans. Microw. Theory Techn.*, vol. 55, no. 8, pp. 1756–1763, Aug. 2007.

[140] S.-C. Lin and C.-Y. Yeh, "Stopband-extended balanced filters using both $\lambda/4$ and $\lambda/2$ SIRs with common-mode suppression and improved passband selectivity," *Prog. Electromagn. Res.*, vol. 128, pp. 215–228, May 2012.

[141] T. Yan, D. Lu, J. Wang, and X. H. Tang, "High-selectivity balanced bandpass filter with mixed electric and magnetic coupling," *IEEE Microw. Wireless Compon. Lett.*, vol. 26, no. 6, pp. 398–400, Jun. 2016.

[142] J. Shi and Q. Xue, "Dual-band and wide-stopband single-band balanced bandpass filters with high selectivity and common-mode suppression," *IEEE Trans. Microw. Theory Techn.*, vol. 58, no. 8, pp. 2204–2212, Aug. 2010.

[143] J. Shi, J. Chen, H. Tang, and L. Zhou, "Differential bandpass filter with high common mode rejection ratio inside the differential-mode passband using controllable common mode transmission zero," in *Proc. IEEE Int. Wireless Symp.*, 2013, pp. 1–4.

[144] A. Fernández-Prieto, J. Martel, F. Medina, F. Mesa, and R. R. Boix, "Compact balanced FSIR bandpass filter modified for enhancing common-mode suppression," *IEEE Microw. Wireless Compon. Lett.*, vol. 25, no. 3, pp. 154–156, Mar. 2015.

[145] A. Fernández-Prieto, J. Bhatker, A. Lujambio, J. Martel, F. Medina, and R. R. Boix, "Balanced bandpass filter based on magnetically coupled coplanar waveguide folded-stepped impedance resonators," *Electron. Lett.*, vol. 52, pp. 1229–1231, Jul. 2016.

[146] J. Z. Chen and J. Chen, "Compact balanced bandpass filter using interdigital line resonator with high common-mode noise suppression," *Microw. Opt. Technol. Lett.*, vol. 54, pp. 918–920, Apr. 2012.

[147] J. Shi, J.-X. Chen, and Q. Xue, "A novel differential bandpass filter based on double-sided parallel-strip line dual-mode resonator," *Microw. Opt. Technol. Lett.*, vol. 50, pp. 1733–1735, Jul. 2008.

[148] X. Gao, W. Feng, and W. Che, "High selectivity differential bandpass filter using dual behavior resonators," *Prog. Electromagn. Res. Lett.*, vol. 53, pp. 89–94, May 2015.

[149] J. X. Chen, C. Shao, Q. Y. Lu, H. Tang, and Z. H. Bao, "Compact LTCC balanced bandpass filter using distributed-element resonator," *Electron. Lett.*, vol. 49, pp. 354–356, Feb. 2013.

[150] M. Li, H. Lee, J. G. Park, and J. C. Lee, "A narrow bandpass balanced filter with back-to-back structure," in *Proc. IEEE 5th Glob. Symp. Millimeter Waves*, 2012, pp. 295–298.

[151] N. Jankovic and V. Crnojevic-Bengin, "Balanced bandpass filter based on square patch resonators," in *Proc. 12th Int. Conf. Telecommun. Modern Satell., Cable Broadcast. Serv.*, 2015, pp. 189–192.

[152] Y. X. Zhou, J. D. Ye, D. X. Qu, X. J. Zhong, and J. F. Zhang, "A balanced bandpass filter with open stubs centrally loaded," in *Proc. IEEE Int. Conf. Commun. Problem-Solving*, 2014, pp. 429–430.

[153] Q. Zhang, C. Chen, and W. Chen, "High common-mode suppression balanced bandpass filter using isosceles right-angled triangular resonator," *Electron. Lett.*, vol. 55, no. 18, pp. 1000–1002, Sep. 2019.

[154] A. Arbelaez, J.-L. Olvera, A. Corona, and C. Saavedra, "Compact closed-loop resonator filters with wide spurious free band and extended common-mode noise suppression," *IET Microw. Antennas Propag.*, vol. 14, no. 9, pp. 860–866, Jun. 2020.

[155] J. X. Chen, Y. Zhan, W. Qin, Z. H. Bao, and Q. Xue, "Novel narrowband balanced bandpass filter using rectangular dielectric resonator," *IEEE Microw. Wireless Compon. Lett.*, vol. 25, no. 5, pp. 289–291, May 2015.

[156] Y. Zhan, J. Li, W. Qin, and J. X. Chen, "Low-loss differential bandpass filter using $TE_{01\delta}$-mode dielectric resonators," *Electron. Lett.*, vol. 51, no. 13, pp. 1001–1003, Jun. 2015.

[157] J.-X. Chen, Y. Zhan, W. Qin, Z.-H. Bao, and Q. Xue, "Analysis and design of balanced dielectric resonator bandpass filters," *IEEE Trans. Microw. Theory Techn.*, vol. 64, no. 5, pp. 1476–1483, May 2016.

[158] A. K. Horestani and M. Shahabadi, "Balanced filter with wideband common-mode suppression in groove gap waveguide technology," *IEEE Microw. Wireless Compon. Lett.*, vol. 28, no. 2, pp. 132–134, Feb. 2018.

[159] F. Wei, Y. J. Guo, P. Y. Qin, and X. W. Shi, "Compact balanced dual- and tri-band bandpass filters based on stub loaded resonators," *IEEE Microw. Wireless Compon. Lett.*, vol. 25, no. 2, pp. 76–78, Feb. 2015.

[160] C. H. Lee, C. I. G. Hsu, and C. C. Hsu, "Balanced dual-band BPF with stub-loaded SIRs for common-mode suppression," *IEEE Microw. Wireless Compon. Lett.*, vol. 20, no. 2, pp. 70–72, Feb. 2010.

[161] J. Shi and Q. Xue, "Novel balanced dual-band bandpass filter using coupled stepped-impedance resonators," *IEEE Microw. Wireless Compon. Lett.*, vol. 20, no. 1, pp. 19–21, Jan. 2010.

[162] L. Yang, W. W. Choi, K. W. Tam, and L. Zhu, "Balanced dual-band bandpass filter with multiple transmission zeros using doubly short-ended resonator coupled line," *IEEE Trans. Microw. Theory Techn.*, vol. 63, no. 7, pp. 2225–2232, Jul. 2015.

[163] X. Xu, J. P. Wang, G. Zhang, and J. X. Chen, "Design of balanced dual-band bandpass filter based on substrate integrated waveguide," *Electron. Lett.*, vol. 49, no. 20, pp. 1278–1280, Sep. 2013.

[164] Y. J. Shen, H. Wang, W. Kang, and W. Wu, "Dual-band SIW differential bandpass filter with improved common-mode suppression," *IEEE Microw. Wireless Compon. Lett.*, vol. 25, no. 2, pp. 100–102, Feb. 2015.

[165] F. Bagci, A. Fernández-Prieto, A. Lujambio, J. Martel, J. Bernal, and F. Medina, "Compact balanced dual-band bandpass filter based on modified coupled-embedded resonators," *IEEE Microw. Wireless Compon. Lett.*, vol. 27, no. 1, pp. 31–33, Jan. 2017.

[166] P. J. Ugarte-Parrado et al., "Compact balanced dual-band band-pass filter with magnetically coupled embedded resonators," *IET Microw. Antennas Propag.*, vol. 13, pp. 492–497, Mar. 2019.

[167] J. L. Medrán-del-Río, A. Lujambio, A. Fernández-Prieto, A. J. Martínez-Ros, J. Martel, and F. Medina, "Multilayered balanced dual-band bandpass filter based on magnetically coupled open-loop resonators with intrinsic common-mode rejection," *Appl. Sci.*, vol. 10, no. 9, 2020, Art. no. 3113.

[168] F. Wei, J. H. Yu, C. Y. Zhang, C. Zeng, and X. W. Shi, "Compact balanced dual-band BPFs based on short and open stub loaded resonators with wide common-mode suppression," *IEEE Trans. Circuits Syst. II, Exp. Briefs*, vol. 67, no. 12, pp. 3043–3047, Dec. 2020.

[169] X. Guan, B. Zhao, and B. Ren, "Dual-band differential bandpass filters using quadruple-mode stubs-loaded ring resonator with intrinsic common-mode suppression for 5G," *IEEE Access*, vol. 8, pp. 205550–205557, 2020.

[170] H. Liu, Z. Wang, S. Hu, H.-X. Xu, and B. Ren, "Design of tri-band balanced filter with wideband common-mode suppression and upper stopband using square ring loaded resonator," *IEEE Trans. Circuits Syst. II, Exp. Briefs*, vol. 67, no. 10, pp. 1760–1764, Oct. 2020.

[171] Y.-K. Han, H.-W. Deng, J.-M. Zhu, S.-B. Xing, and W. Han, "Compact dual-band dual-mode SIW balanced BPF with intrinsic common-mode suppression," *IEEE Microw. Wireless Compon. Lett.*, vol. 31, no. 2, pp. 101–104, Feb. 2021.

[172] D. Simpson and D. Psychogiou, "Multi-band differential bandpass filters with quasi-elliptic-type passbands and multi-transmission zero common-mode suppression," in *Proc. IEEE MTT-S Int. Microw. Symp.*, 2019, pp. 1027–1030.

[173] C.-H. Lee, C.-I. G. Hsu, and P.-H. Wen, "Balanced and balun diplexers designed using center-grounded uniform-impedance resonators," *Microw. Opt. Technol. Lett.*, vol. 56, no. 3, pp. 555–559, 2014.

[174] P.-H. Wen, C.-I. G. Hsu, C.-H. Lee, and H.-H. Chen, "Design of balanced and balun diplexers using stepped-impedance slot-line resonators," *J. Electromagn. Waves Appl.*, vol. 28, no. 6, pp. 700–715, 2014.

[175] C. H. Wu, C. H. Wang, and C. H. Chen, "A novel balanced-to-unbalanced diplexer based on four-port balanced-to-balanced bandpass filter," in *Proc. 38th Eur. Microw. Conf.*, 2008, pp. 28–31.

[176] Z. H. Bao, J. X. Chen, E. H. Lim, and Q. Xue, "Compact microstrip diplexer with differential outputs," *Electron. Lett.*, vol. 46, pp. 766–768, May 2010.

[177] Q. Xue, J. Shi, and J. X. Chen, "Unbalanced-to-balanced and balanced-to-unbalanced diplexer with high selectivity and common-mode suppression," *IEEE Trans. Microw. Theory Techn.*, vol. 59, no. 11, pp. 2848–2855, Nov. 2011.

[178] Y. Zhou, H. W. Deng, and Y. Zhao, "Compact balanced-to-balanced microstrip diplexer with high isolation and common-mode suppression," *IEEE Microw. Wireless Compon. Lett.*, vol. 24, no. 3, pp. 143–145, Mar. 2014.

[179] H. L. Chan, C. H. Lee, and C. I. G. Hsu, "Balanced dual-band diplexer design using microstrip and slot-line resonators," in *Proc. Asia-Pacific Microw. Conf.*, 2015, pp. 1–3.

[180] C. H. Lee, C. I. G. Hsu, S. X. Wu, and P. H. Wen, "Balanced quad-band diplexer with wide common-mode suppression and high differential-mode isolation," *IET Microw. Antennas Propag.*, vol. 10, no. 6, pp. 599–603, 2016.

[181] H. Deng, Y. Zhao, Y. Fu, Y. He, and X. Zhao, "High selectivity and CM suppression microstrip balanced BPF and balanced-to-balanced diplexer," *J. Electromagn. Waves Appl.*, vol. 27, no. 8, pp. 1047–1058, 2013.

[182] W. Jiang, Y. Huang, T. Wang, Y. Peng, and G. Wang, "Microstrip balanced quad-channel diplexer using dual-open/short-stub loaded resonator," in *Proc. IEEE MTT-S Int. Microw. Symp.*, 2016, pp. 1–3.

[183] A. Fernández-Prieto, A. Lujambio, J. Martel, F. Medina, F. Martín, and R. R. Boix, "Balanced-to-balanced microstrip diplexer based on magnetically coupled resonators," *IEEE Access*, vol. 6, pp. 18536–18547, 2018.

[184] A. Fernández-Prieto, A. Lujambio, F. Martín, J. Martel, F. Medina, and R. R. Boix, "Compact balanced-to-balanced diplexer based on split-ring resonators balanced bandpass filters," *IEEE Microw. Wireless Compon. Lett.*, vol. 28, no. 3, pp. 218–220, Mar. 2018.

[185] Y. C. Li and Q. Xue, "Tunable balanced bandpass filter with constant bandwidth and high common-mode suppression," *IEEE Trans. Microw. Theory Techn.*, vol. 59, no. 10, pp. 2452–2460, Oct. 2011.

[186] H. Zhu and A. M. Abbosh, "Tunable balanced bandpass filter with wide tuning range of center frequency and bandwidth using compact coupledline resonator," *IEEE Microw. Wireless Compon. Lett.*, vol. 26, no. 1, pp. 7–9, Jan. 2016.

[187] M. Fan, K. Song, and Y. Zhu, "Reconfigurable differential filter with constant absolute bandwidth and high common-mode suppression," *IEEE Microw. Wireless Compon. Lett.*, vol. 28, no. 10, pp. 894–896, Oct. 2018.

[188] T.-Y. Lin and T. -L. Wu, "Balanced bandpass filter with reflectionless common-mode suppression," in *Proc. IEEE Elect. Des. Adv. Packag. Syst.*, 2016, pp. 17–19.

[189] M. Kong, Y. Wu, Z. Zhuang, and Y. Liu, "Narrowband balanced absorptive bandstop filter integrated with wideband bandpass response," *Electron. Lett.*, vol. 54, pp. 225–227, 2018.

[190] R. Gómez-García, J.-M. Munoz-Ferreras, W. Feng, and D. Psychogiou, "Balanced symmetrical quasi-reflectionless single-and dual-band bandpass planar filters," *IEEE Microw. Wireless Compon. Lett.*, vol. 28, no. 9, pp. 798–800, Sep. 2018.

[191] T.-Y. Lin, Y.-C. Huang, and T.-L. Wu, "Novel absorptive balanced bandpass filters using resistive loaded transmission lines," *IEEE Trans. Compon., Packag. Manuf. Technol.*, vol. 9, no. 4, pp. 745–753, Apr. 2019.

[192] T.-Y. Lin and T.-L. Wu, "Balanced bandpass filter with common-mode reflectionless feature by terminated coupled lines," *IEEE Trans. Electromagn. Compat.*, vol. 62, no. 4, pp. 1090–1097, Aug. 2020.

[193] L. Yang, R. Gómez-García, and M. Fan, "Input-reflectionless balanced wideband bandpass filter using multilayered vertical transitions," in *Proc. IEEE Asia-Pacific Microw. Conf.*, 2020, pp. 418–420.

[194] X. Chen, T. Yang, and P. -L. Chi, "Arbitrary-order balanced filter with reflectionless characteristics for both common- and differential-mode signals," *IEEE Microw. Wireless Compon. Lett.*, vol. 31, no. 6, pp. 553–556, Jun. 2021.

[195] Y. Zhang, Y. Wu, Y. Wei, and W. Wang, "Novel planar balanced bandpass filter with wideband common-mode suppression and in-band common-mode noise absorption," *Int. J. RF Microw. Comput. Aided Eng.*, vol. 31, 2021, Art. no. e22483.

[196] Y. Zhang, Y. Wu, W. Wang, and J. Yan, "High-performance common-and differential-mode reflectionless balanced band-pass filter using coupled ring resonator," *IEEE Trans. Circuits Syst. II, Exp. Briefs*, vol. 69, no. 3, pp. 974–978, Mar. 2022.

[197] W. Feng, W. Che, and Q. Xue, "The proper balance: Overview of microstrip wideband balance circuits with wideband common mode suppression," *IEEE Microw. Mag.*, vol. 16, no. 5, pp. 55–68, Jun. 2015, doi: 10.1109/MMM.2015.2408275.

[198] W. Feng, W. Che, Y. Shi, Q. Xue, X. Y. Zhang, and X. Y. Zhou, "Balanced to unbalanced: An overview of multifunctional wideband balanced-to-unbalanced four- and five-port filtering power dividers," *IEEE Microw. Mag.*, vol. 21, no. 11, pp. 50–57, Nov. 2020.

[199] J. Shi, K. Xu, W. Zhang, J. -X. Chen, and G. Zhai, "An approach to 1-to-2^n way microstrip balanced power divider," *IEEE Trans. Microw. Theory Techn.*, vol. 64, no. 12, pp. 4222–4231, Dec. 2016.

[200] J. W. May and G. M. Rebeiz, "A 40–50-GHz SiGe 1:8 differential power divider using shielded broadside-coupled striplines," *IEEE Trans. Microw. Theory Techn.*, vol. 56, no. 7, pp. 1575–1581, Jul. 2008.

[201] B. Xia, L.-S. Wu, and J. Mao, "A new balanced-to-balanced power divider/combiner," *IEEE Trans. Microw. Theory Techn.*, vol. 60, no. 9, pp. 2791–2798, Sep. 2012.

[202] B. Xia, L.-S. Wu, S.-W. Ren, and J.-F. Mao, "A balanced-to-balanced power divider with arbitrary power division," *IEEE Trans. Microw. Theory Techn.*, vol. 61, no. 8, pp. 2831–2840, Aug. 2013.

[203] W. Feng, C. Zhao, W. Che, and Q. Xue, "A balanced-to-balanced network with unequal power division and wideband common mode suppression," *IEEE Microw. Wireless Compon. Lett.*, vol. 26, no. 4, pp. 237–239, Apr. 2016.

[204] J. Shi, J. Wang, K. Xu, J.-X. Chen, and W. Liu, "A balanced-to-balanced power divider with wide bandwidth," *IEEE Microw. Wireless Compon. Lett.*, vol. 25, no. 9, pp. 573–575, Sep. 2015.

[205] L.-S. Wu, Y.-X. Guo, and J.-F. Mao, "Balanced-to-balanced Gysel power divider with bandpass filtering response," *IEEE Trans. Microw. Theory Techn.*, vol. 61, no. 12, pp. 4052–4062, Dec. 2013.

[206] M. Luo, X. Xu, X.-H. Tang, and Y.-H. Zhang, "A compact balanced-to-balanced filtering Gysel power divider using $\lambda_g/2$ resonators and short-stub-loaded resonator," *IEEE Microw. Wireless Compon. Lett.*, vol. 27, no. 7, pp. 645–647, Jul. 2017.

[207] M. Luo et al., "Balanced-to-balanced Gysel filtering power divider with arbitrary power division," *IEEE Access*, vol. 8, pp. 36454–36463, 2020.

[208] Q. Liu, J. Wang, L. Zhu, G. Zhang, and W. Wu, "Design of a new balanced-to-balanced filtering power divider based on square patch resonator," *IEEE Trans. Microw. Theory Techn.*, vol. 66, no. 12, pp. 5280–5289, Dec. 2018.

[209] Q. Liu, J. Wang, L. Zhu, and W. Wu, "Design of balanced-to-balanced filtering power divider with arbitrary power division ratio based on circular patch resonator," *IET Microw. Antennas Propag.*, vol. 14, no. 4, pp. 253–259, Jan. 2020.

[210] G. Zhang, Q. Zhang, Q. Liu, W. Tang, and J. Yang, "Design of a new dual-band balanced-to-balanced filtering power divider based on the circular microstrip patch resonator," *IEEE Trans Circuits Syst. II, Exp. Briefs*, vol. 68, no. 12, pp. 3542–3546, Dec. 2021.

[211] F. Wei, Z.-J. Yang, P.-Y. Qin, Y. J. Guo, B. Li, and X.-W. Shi, "A balanced-to-balanced in-phase filtering power divider with high selectivity and isolation," *IEEE Trans. Microw. Theory Techn.*, vol. 67, no. 2, pp. 683–694, Feb. 2019.

[212] F. Yang, F. Wei, S.-F. Liu, and X.-W. Shi, "A novel balanced wideband power divider based on microstrip-slot transitions," *Int. J. RF Microw. Comput. Aided Eng.*, vol. 24, no. 4, pp. 437–442, Jul. 2014.

[213] X. Guo, L. Zhu, J. Wang, and W. Wu, "Wideband microstrip-to-microstrip vertical transitions via multiresonant modes in a slotline resonator," *IEEE Trans. Microw. Theory Techn.*, vol. 63, no. 6, pp. 1902–1909, Jun. 2015.

[214] L. Chen, F. Wei, X. Y. Cheng, and Q. K. Xiao, "A dual-band balanced-to-balanced power divider with high selectivity and wide stopband," *IEEE Access*, vol. 7, pp. 40114–40119, 2019.

[215] F. Wei, Z.-J. Yang, B. Li, and X.-W. Shi, "A balanced UWB power divider based on parallel coupling slotlines with improved isolation," *Int. J. RF Microw. Comput. Aided Eng.*, vol. 29, 2019, Art. no. e21510.

[216] M. Li, Y. Wu, L. Jiao, L. Ma, W. Wang, and Y. Liu, "A planar balanced-to-balanced power divider with wideband filtering responses and common-mode suppressions," *IEEE Access*, vol. 6, pp. 42057–42065, 2018.

[217] P. Vélez, M. Durán-Sindreu, A. Fernández-Prieto, J. Bonache, F. Medina, and F. Martín, "Compact dual-band differential power splitter with common-mode suppression and filtering capability based on differential-mode composite right/left-handed transmission-line metamaterials," *IEEE Antennas Wireless Propag. Lett.*, vol. 13, pp. 536–539, 2014.

[218] K. W. Hamed, A. P. Freundorfer, and Y. M. M. Antar, "A new broadband monolithic passive differential coupler for K/ka-band applications," *IEEE Trans. Microw. Theory Techn.*, vol. 54, no. 6, pp. 2527–2533, Jun. 2006.

[219] K. Staszek, K. Wincza, and S. Gruszczynski, "Rigorous approach for design of differential coupled-line directional couplers applicable in integrated circuits and substrate-embedded networks," *Sci. Rep.*, vol. 6, no. 11, pp. 1–12, 2016.

[220] I. Piekarz, J. Sorocki, K. Janisz, K. Wincza, and S. Gruszczynski, "Wideband three-section symmetrical coupled-line directional coupler operating in differential mode," *IEEE Microw. Wireless Compon. Lett.*, vol. 28, no. 6, pp. 488–490, Jun. 2018.

[221] K. Janisz, I. Piekarz, K. Staszek, K. Wincza, and S. Gruszczynski, "Differentially fed directional couplers with coupled-conductors of unequal widths," *IEEE Microw. Wireless Compon. Lett.*, vol. 28, no. 9, pp. 759–761, Sep. 2018.

[222] J. Martel, A. Fernández-Prieto, J. L. Medrán-del-Río, F. Martín, and F. Medina, "Design of a differential coupled-line directional coupler using a double-side coplanar waveguide structure with common-signal suppression," *IEEE Trans. Microw. Theory Techn.*, vol. 69, no. 2, pp. 1273–1281, Feb. 2021.

[223] I. Piekarz, J. Sorocki, K. Wincza, S. Gruszczynski, and J. Papapolymerou, "High-performance differentially fed coupled-line directional couplers realised in inhomogeneous medium," *IET Microw. Antennas Propag.*, vol. 13, no. 12, pp. 2005–2012, 2019.

[224] S. Gruszczynski, R. Smolarz, and K. Wincza, "Differential bi-level microstrip directional coupler with equalized coupling coefficients for directivity improvement," *Electronics*, vol. 9, 2020, Art. no. 547.

[225] J. Shi, J. Qiang, K. Xu, and J.-X. Chen, "A balanced branch-line coupler with arbitrary power division ratio," *IEEE Trans. Microw. Theory Techn.*, vol. 65, no. 1, pp. 78–85, Jan. 2017.

[226] J. Shi et al., "A balanced filtering branch-line coupler," *IEEE Microw. Wireless Compon. Lett.*, vol. 26, no. 2, pp. 119–121, Feb. 2016.

[227] W. Feng, Y. Zhao, W. Che, R. Gómez-García, and Q. Xue, "Multi-band balanced couplers with broadband common-mode suppression," *IEEE Trans. Circuits Syst. II, Exp. Briefs*, vol. 65, no. 12, pp. 1964–1968, Dec. 2018.

[228] W. Feng, X. Duan, Y. Shi, and S. Shi, "Dual-band balanced coupler with wideband common-mode suppression," *Int. J. RF Microw. Comput. Aided Eng.*, vol. 30, 2020, Art. no. e22077.

[229] L. Qiao et al., "A balanced filtering directional coupler with wide common-mode suppression based on slotline structure," *Electronics*, vol. 10, 2021, Art. no. 2254.

[230] F. Wei et al., "A balanced filtering directional coupler based on slotline using asymmetric parallel loaded branches," *IEEE Trans. Compon., Packag., Manuf. Technol*, vol. 12, no. 7, pp. 1222–1231, Jul. 2022.

[231] Y. Wang, M. Yu, and K. Ma, "Substrate integrated suspended slot line and its application to differential coupler," *IEEE Trans. Microw. Theory Techn.*, vol. 68, no. 12, pp. 5178–5189, Dec. 2020.

[232] Y. Liu, F. Wei, X. Shi, and C. Zeng, "A balanced-to-balanced directional coupler based on branch-slotline coupled structure," *Frequenz*, vol. 74, no. 11–12, pp. 427–433, 2020.

[233] M. H. A. Elsawaf and A. M. E. Safwat, "Wideband high-CMRR fully differential couplers using multimode star-junction," *IEEE Trans. Microw. Theory Techn.*, vol. 69, no. 6, pp. 3015–3022, Jun. 2021.

[234] M. H. A. Elsawaf, A. M. H. Nasr, and A. M. E. Safwat, "Miniaturized couplers using multi-mode star-junction," in *Proc. IEEE/MTT-S Int. Microw. Symp.*, 2020, pp. 739–742.

[235] H. J. Ng, M. Jahn, R. Feger, C. Wagner, and A. Stelzer, "An efficient SiGe double-balanced mixer with a differential rat-race coupler," in *Proc. 8th Eur. Microw. Integr. Circuits Conf.*, 2013, pp. 580–583.

[236] L. Li, L.-S. Wu, J. Mao, M. Tang, and X.-W. Gu, "A balanced-to-balanced rat-race coupling network based on defected slots," *IEEE Microw. Wireless Compon. Lett.*, vol. 29, no. 7, pp. 459–461, Jul. 2019.

[237] W. Feng et al., "Balanced rat-race couplers with wideband common-mode suppression," *IEEE Trans. Microw. Theory Techn.*, vol. 67, no. 12, pp. 4724–4732, Dec. 2019.

[238] A. Amini, H. Shahi, and M. Mehri, "A single-layer balanced directional coupler design based on crossover structures," *IEEE Trans. Microw. Theory Techn.*, vol. 68, no. 8, pp. 3298–3307, Aug. 2020.

[239] S. Chen, W.-C. Lee, and T.-L. Wu, "A balanced-to-balanced power divider with common-mode noise absorption," in *Proc. IEEE MTT-S Int. Microw. Symp.*, 2016, pp. 1–4.

[240] B. Xia, L.-S. Wu, and J.-F. Mao, "An absorptive balanced-to-balanced power divider," *IEEE Access*, vol. 6, pp. 14613–14619, 2018.

[241] S. Chen, W.-C. Lee, and T.-L. Wu, "Balanced-to-balanced and balanced-to-unbalanced power dividers with ultra-wideband common-mode rejection and absorption based on mode-conversion approach," *IEEE Trans. Compon. Packag. Manuf. Technol.*, vol. 9, no. 2, pp. 306–316, Feb. 2019.

[242] F. Lin, W. Feng, and X. Tan, "Tunable balanced power dividers: An overview of recently developed balanced power dividers and couplers with fixed and tunable functions," *IEEE Microw. Mag.*, vol. 22, no. 2, pp. 46–56, Feb. 2021.

[243] Y.-W. Lin, Y.-C. Chou, and C.-Y. Chang, "A balanced digital phase shifter by a novel switching-mode topology," *IEEE Trans. Microw. Theory Techn.*, vol. 61, no. 6, pp. 2361–2370, Jun. 2013.

[244] W. Zhang and J. Shi, "A balanced phase shifter with common-mode suppression," *IEEE Trans. Ind. Electron.*, vol. 66, no. 1, pp. 378–386, Jan. 2019.

[245] L.-L. Qiu and L. Zhu, "Balanced wideband phase shifters with good filtering property and common-mode suppression," *IEEE Trans. Microw. Theory Techn.*, vol. 67, no. 6, pp. 2313–2321, Jun. 2019.

[246] Y. Han, R. Li, L. Qiao, and F. Wei, "Balanced wideband quasi-Schiffman phase shifters based on slotlines," *IEEE Trans. Circuits Syst. II, Exp. Briefs*, vol. 69, no. 11, pp. 4283–4287, Nov. 2022.

[247] F. J. Ferrández-Pastor, J. M. García-Chamizo, and M. Nieto-Hidalgo, "Electromagnetic differential measuring method: Application in microstrip sensors developing," *Sensors*, vol. 17, no. 7, 2017, Art. no. 1650.

[248] J. Muñoz-Enano, P. Vélez, M. Gil, and F. Martín, "An analytical method to implement high sensitivity transmission line differential sensors for dielectric constant measurements," *IEEE Sensors J.*, vol. 20, no. 1, pp. 178–184, Jan. 2020.

[249] C. Damm, M. Schussler, M. Puentes, H. Maune, M. Maasch, and R. Jakoby, "Artificial transmission lines for high sensitive microwave sensors," in *Proc. IEEE Sensors*, 2009, pp. 755–758.

[250] A. Ebrahimi et al., "Highly sensitive phase-variation dielectric constant sensor based on a capacitively-loaded slow-wave transmission line," *IEEE Trans. Circuits Syst. I, Regular Papers*, vol. 68, no. 7, pp. 2787–2799, Jul. 2021.

[251] M. Gil, P. Vélez, F. Aznar, J. Muñoz-Enano, and F. Martín, "Differential sensor based on electro-inductive wave (EIW) transmission lines for dielectric constant measurements and defect detection," *IEEE Trans. Antennas Propag.*, vol. 68, no. 3, pp. 1876–1886, Mar. 2020.

[252] C. Herrojo et al., "Highly sensitive defect detectors and comparators exploiting port imbalance in rat-race couplers loaded with step-impedance open-ended transmission lines," *IEEE Sensors J.*, vol. 21, no. 23, pp. 26731–26745, Dec. 2021.

[253] P. Vélez, J. Muñoz-Enano, K. Grenier, J. Mata-Contreras, D. Dubuc, and F. Martín, "Split ring resonator (SRR) based microwave fluidic sensor for electrolyte concentration measurements," *IEEE Sensors J.*, vol. 19, no. 7, pp. 2562–2569, Apr. 2019.

[254] J. Muñoz-Enano, P. Vélez, M. Gil, E. Jose-Cunilleras, A. Bassols, and F. Martín, "Characterization of electrolyte content in urine samples through a differential microfluidic sensor based on dumbbell-shaped defect ground structures," *Int. J. Microw. Wireless Technol.*, vol. 12, no. 9, pp. 817–824, 2020.

[255] A. Ebrahimi, F. J. Tovar-López, J. Scott, and K. Ghorbani, "Differential microwave sensor for characterization of glycerol-water solutions," *Sensors Actuators B, Chem.*, vol. 321, Oct. 2020, Art. no. 128561.

[256] J. Muñoz-Enano, P. Vélez, M. Gil, and F. Martín, "Microfluidic reflective-mode differential sensor based on open split ring resonators (OSRRs)," *Int. J. Microw. Wireless Technol.*, vol. 12, pp. 588–597, Sep. 2020.

[257] A. Ebrahimi, J. Scott, and K. Ghorbani, "Transmission lines terminated with LC resonators for differential permittivity sensing," *IEEE Microw. Wireless Compon. Lett.*, vol. 28, no. 12, pp. 1149–1151, Dec. 2018.

[258] H. Hallil et al., "Differential passive microwave planar resonator-based sensor for chemical particle detection in polluted environments," *IEEE Sensors J.*, vol. 19, no. 4, pp. 1346–1353, Feb. 2019.

[259] P. Vélez, J. Muñoz-Enano, and F. Martín, "Differential sensing based on quasi-microstrip-mode to slot-mode conversion," *IEEE Microw. Wireless Compon. Lett.*, vol. 29, no. 10, pp. 690–692, Oct. 2019.

[260] B. Camli, E. Altinagac, H. Kizil, H. Torun, G. Dundar, and A. D. Yalcinkaya, "Gold-on-glass microwave split-ring resonators with PDMS microchannels for differential measurement in microfluidic sensing," *Biomicrofluidics*, vol. 14, no. 5, Sep. 2020, Art. no. 054102.

[261] H. Y. Gan et al., "Differential microwave microfluidic sensor based on microstrip complementary split-ring resonator (MCSRR) structure," *IEEE Sensors J.*, vol. 20, no. 11, pp. 5876–5884, Jun. 2020.

[262] M. C. Jain, A. V. Nadaraja, B. M. Vizcaino, D. J. Roberts, and M. H. Zarifi, "Differential microwave resonator sensor reveals glucose-dependent growth profile of E. coli on solid agar," *IEEE Microw. Wireless Compon. Lett.*, vol. 30, no. 5, pp. 531–534, May 2020.

[263] S. Mohammadi and M. H. Zarifi, "Differential microwave resonator sensor for real-time monitoring of volatile organic compounds," *IEEE Sensors J.*, vol. 21, no. 5, pp. 6105–6114, Mar. 2021.

[264] P. Vélez, J. Muñoz-Enano, and F. Martín, "Electrolyte concentration measurements in DI water with 0.125 g/L resolution by means of CSRR-based structures," in *Proc. 49th Eur. Microw. Conf.*, 2019, pp. 340–343.

FERRAN MARTIN (Fellow, IEEE) was born in Barakaldo (Vizcaya), Spain, in 1965. He received the B.S. degree in physics from the Universitat Autònoma de Barcelona (UAB), Bellaterra, Spain, in 1988, and the Ph.D. degree in 1992. From 1994 to 2006, he was an Associate Professor of electronics with the Departament d'Enginyeria Electrònica, Universitat Autònoma de Barcelona, and since 2007, he has been a Full Professor of electronics. In recent years, he has been involved in different research activities, including modeling and simulation of electron devices for high frequency applications, millimeter wave and THz generation systems, and the application of electromagnetic bandgaps to microwave and millimeter wave circuits. He is currently the Head of the Microwave Engineering, Metamaterials and Antennas Group (GEMMA Group), UAB, and Director of CIMITEC, a research Center on Metamaterials supported by TECNIO (Generalitat de Catalunya). He has authored and coauthored more than 650 technical conference, letter, journal papers, and book chapters. He is the co-author of the book on metamaterials titled *Metamaterials With Negative Parameters: Theory, Design and Microwave Applications* (Wiley), the author of the book *Artificial Transmission Lines for RF and Microwave Applications* (Wiley), a Co-Editor of the book *Balanced Microwave Filters* (Wiley/IEEE Press), the co-author of the book *Time-Domain Signature Barcodes for Chipless-RFID and Sensing Applications* (Springer), and the coauthor of the book *Planar Microwave Sensors* (Wiley/IEEE Press). He has generated 22 Ph.D. students, has filed several patents on metamaterials, and has headed several development contracts. He is very active in the field of metamaterials and their application to the miniaturization and optimization of microwave circuits andantennas. His research interests include microwave sensors and RFID systems, with special emphasis on the development of high data capacity chipless-RFID tags. He has organized several international events related to metamaterials and related topics, including workshops at the IEEE International Microwave Symposium (years 2005 and 2007) and European Microwave Conference in 2009, 2015, and 2017, and the Fifth International Congress on Advanced Electromagnetic Materials in Microwaves and Optics (Metamaterials 2011), where he acted as the Chair of the Local Organizing Committee. He is a member of the IEEE Microwave Theory and Technology Society (IEEE MTT-S). He is also a member of the Technical Committees of the European Microwave Conference (EuMC) and the International Congress on Advanced Electromagnetic Materials in Microwaves and Optics (Metamaterials). He is a reviewer of IEEE TRANSACTIONS ON MICROWAVE THEORY AND TECHNIQUES and IEEE MICROWAVE AND WIRELESS COMPONENTS LETTERS, among many other journals. He is a member of the Editorial Board of *IET Microwaves, Antennas and Propagation*, *International Journal of RF and Microwave Computer-Aided Engineering*, and *Sensors*. Among his distinctions, he was the recipient of the 2006 Duran Farell Prize for Technological Research, he holds the Parcde Recerca UAB – Santander Technology Transfer Chair, and he has been the recipient of three ICREA ACADEMIA Awards (calls 2008, 2013 and 2018). He is a Fellow of IET. He has acted as guest editor of six special issues on metamaterials and sensors in five international journals.

FRANCISCO MEDINA (Fellow, IEEE) was born in Puerto Real (Cádiz), Spain, in 1960. He received the *Licenciado* degree in physics (electronics) and the Ph.D. degree in physics from the University of Seville, Seville, Spain, in 1983 and 1987, respectively. Afterwards, he spent one year with the group headed by Prof. Henri Baudrand with EN-SEEIHT, INP Toulouse, France, as a Postdoctoral Researcher. Then, he joined the Department of Electronics and Electromagnetism, Physics Faculty, University of Seville, where he became an Associate Professor in 1990 and a Full Professor in 2009. Since 1998, he has been the Head of the Microwave Group with the Department of Electronics and Electromagnetism. He was the recipient of a Salvador de Madariaga Fellowship during a four month visiting scholar stay at QMUL, London, U.K. He has been working on several topics related to applied electromagnetism and microwave engineering, including the modeling of planar transmission lines, antennas and circuits using optimized integral equation methods, (bi)anisotropic structures, metamaterials, and periodic electromagnetic structures. He has also contributed to the design of a variety of planar passive microwave printed devices. This research has mainly been reported in 12 book chapters, 170 JCR journal papers, and more than 350 conference contributions. He is currently the Editor-in-Chief of the *International Journal of Microwave and Wireless Technologies*. He also acts a reviewer of many journals, mainly in the fields of microwave and antenna engineering, optics, and applied physics. He co-organized the 2017 IEEE-MTT NEMO Symposium, Seville, Spain, and collaborates as a TPC member or reviewer with a number of main conferences in the aforementioned fields.